Morphology, Crystallization and Melting Behavior of Propylene-Ethylene Statistical Copolymers

Julie Tammy Uan-Zo-li

Dissertation submitted to the Faculty of the
Virginia Polytechnic Institute and State University
in partial fulfillment of the requirements for the degree of

Doctor of Philosophy
in
Materials Science and Engineering

Dr. Hervé Marand, Chairman

Dr. Brian J. Love	Dr. William Reynolds
Dr. Alan Esker	Dr. Richey Davis

September 2005
Blacksburg, Virginia

KEYWORDS: propylene-ethylene copolymers, ethylene inclusion, rigid amorphous fraction, thermodynamic heat of fusion, α and γ phases

Morphology, Crystallization and Melting Behavior of Propylene-Ethylene Statistical Copolymers

Julie T. Uan-Zo-li

Hervé Marand, Advisory Chairman

Abstract

In this work the morphology, crystallization and melting behavior of novel Dow Chemical propylene-ethylene copolymers were investigated.

The incorporation of ethylene units into a polypropylene chain resulted in the decrease in crystallization, melting and glass transition temperatures and overall crystallinity. Based on the shape of heat capacity curves and the dependence of the melting temperature offset on ethylene content, it was concluded that copolymers prepared using different catalyst systems exhibited different ethylene sequence length distributions.

The behavior of Dow Chemical propylene-ethylene copolymers was compared to that of copolymers prepared using traditional metallocene and Ziegler-Natta catalysts. The catalyst system used in the preparation of these new copolymers is similar to a metallocene catalyst system.

It was demonstrated that ethylene defects are partially included in the polypropylene crystal. The thermodynamic heat of fusion at the equilibrium melting temperature decreased by 44% with an increase in ethylene concentration from 0 mol% to 21.2 mol%. On the basis of calorimetric and density data, the inclusion model based on the Sanchez-Eby crystallization theory was shown to be applicable for the evaluation of the degree of crystallinity. At the same time, inadequacies were found in application of the rigid amorphous fraction model to these copolymers.

The formation of γ-phase crystals was shown to be favored by both an increase in the ethylene content and a decrease in the crystallization rate. Increase in the ethylene content was shown to lead to a decrease in the density, length and thickness of α-phase crystals. It was also demonstrated that the cross-hatching morphology is present in all propylene-ethylene copolymers.

ACKNOWLEDGEMENTS

I would like to express my sincere gratitude to my advisor, Dr. Hervé Marand, for his help and guidance over the past several years.

I would like to thank Dr. Brian J. Love, Dr. Alan Esker, Dr. Bill Reynolds and Dr. Richey Davis for serving on my committee and for their useful remarks on my original proposal.

I would like to thank Dow Chemical and GE scholarship program for providing the financial support for this research project.

My gratitude to the following people for the help with this dissertation. Vickie Long and Dr. Marek Pyda (University of Tennessee) for the use of their DSC equipment. Steve McCartney for the help performing SEM experiments. My colleagues and friends Chris Fratini, Brian Okerberg and Zhenyu Huang for their technical advice, for their tremendous help with my experiments (especially when I was pregnant) and just for the great time that we have shared.

Thank you to my friends, Ksenia Tcheslavskaia, Ksenia Pronina, Gleb Tcheslavski, Alexey Pronin and Phil Papush for keeping me company and being there when I needed them.

I would like to thank my family: my parents, Tamara and Mike, Rima, my brother Joe, my sisters, Anna and Rachel, and my extended family: Svetlana and Boris for their love and encouragement.

My special thank you to my mother, Tamara, and my mother-in-law, Svetlana, who took months out of their busy schedules to help me to take care of my son Sean.

Thank you to my husband Alex for sharing with me all the ups and downs of our life, for his support and love.

Finally, thank you to my wonderful son Sean, the joy of my life and my biggest accomplishment.

To my family…

TABLE OF CONTENTS

LIST OF FIGURES

LIST OF TABLES

1 INTRODUCTION

Polypropylenes and polyethylenes belong to the commodity thermoplastics which account for the majority (about two thirds) of plastic materials consumed.[1] Both of these materials are commonly used in a number of applications ranging from flexible bottles and toys to TV cabinets and luggage.[2] In order to improve the properties of these materials and widen the spectrum of their uses, scientists copolymerize their monomers to form ethylene-propylene and propylene-ethylene copolymers. Copolymerization of ethylene and propylene results in increased clarity, toughness and flexibility[3] of the final product.

Initially, polyethylenes were synthesized by radical polymerization. However, the resulting materials had high degrees of branching and low densities and the process itself was carried out at high pressures and temperatures.[4] Polypropylenes were initially synthesized by several cationic initiators, but the resulting materials, which were atactic low molecular weight polymers, did not have any commercial value.[4] The discovery in the fifties of Ziegler-Natta catalysts, which allowed the stereospecific polymerization at low pressures and temperatures close to ambient, revolutionized the production of polypropylene, polyethylene and their copolymers.[3,4] The resulting materials were linear and had fairly wide molecular mass distributions. The recent development of metallocene catalysts has led to further improvements in polypropylene and polyethylene chemistry, since it is now possible to obtain materials with high stereoregularity and narrow molecular mass distribution. The polypropylenes, polyethylenes and ethylene-propylene copolymers are now produced in vast quantities. The commercial production of propylene-ethylene copolymers with high ethylene content has, however, remained challenging.

Recently, the Dow Chemical Company has developed a novel catalyst system that allows for the copolymerization of propylene with ethylene and alpha-olefin monomers in solution over a wide compositional range. These materials have unusual

crystallization and melting behavior and are claimed to have superior mechanical and optical properties.[5]

The purpose of this study is to establish structure-property relationships for these new propylene-ethylene systems and to compare these materials to those synthesized using the traditional Ziegler-Natta and metallocene catalysts. In this work, the effect of comonomer content on the overall crystallinity, thermal properties and thermodynamic heat of fusion will be addressed. The studies of the development of crystallinity and morphology as a function of comonomer content and processing conditions will also be conducted. Since the level of inclusion of ethylene units into the propylene crystal phase is still debated, this study will also need to focus on the fundamental understanding of the effects of ethylene copolymerization with propylene. Finally, the studies of heterogeneous nucleation effects on these copolymers will be presented.

2 BACKGROUND

2.1 Stereochemistry of Polypropylene

Polypropylenes belong to the group of polymers that exhibit isomers. There are two kinds of the isomerism that will be discussed here: structural isomerism and configurational isomerism.[6]

Structural isomerism deals with the orientation of the monomer units as they are incorporated into the growing polymer chain. There are three possible options of connecting monomer units: head-to-tail, head-to-head and tail-to-tail. Head-to-tail isomers are called regio-regular. The other isomers are considered as defects in the polymerization process and their presence leads to a decrease in the overall crystallinity of the material.

Configurational isomerism deals with the spatial arrangements of the side-groups in the polymer molecule. Since polypropylenes have pseudochiral centers, they possess an ability to form different spatial arrangements or in other words to exhibit different tacticity. In the case of polypropylene, the polymer is said to be isotactic when the methyl-side groups lay on the same side of the pseudochiral centers. Conversely, the polymer is said to be syndiotactic when the side groups are on alternating sides of the polymer chain. Finally, the polymer is said to be atactic when the side groups are distributed randomly on either sides of the pseudochiral centers[7](Figure 2.1.1). The placement of methyl groups in the isotactic fashion on one side of the pseudochiral center is called meso-placement and is designated by *m*. On the other hand, placement of the group on the opposite sides of the pseudochiral center is called racemic placement and is designated by *r*. This way, an atactic polymer will have a random sequence of *r*'s and *m*'s, since it has a random distribution of side groups on both sides of the pseudochiral center.

Both structural and configurational isomerisms are controlled by the polymerization process. Different catalyst systems favor the formation of one type of isomers and inhibit the formation of the others.[8] Polymerization conditions can also

affect the isomer distribution along the polymer backbone. Since stereochemistry plays an important role in the ability of a polymer to crystallize and in defining the properties of the resulting crystals,[9] both structural and configurational isomerism will be discussed in more details in the next chapters as we talk specifically about their role in the crystallization of polypropylene.

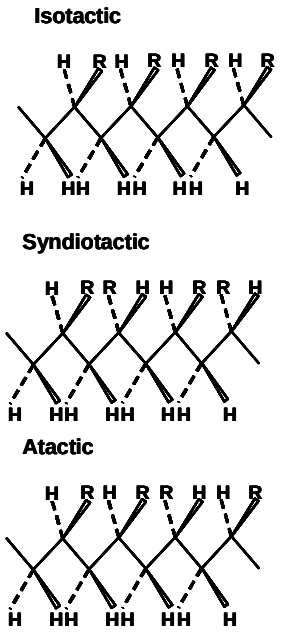

Figure 2.1.1 Tacticity in poly(α-olefin)[*]

2.2 Crystallization

Since polymers can crystallize in a number of ways (melt, solution, quiescent, flow-induced, etc…), an exhaustive discussion is beyond the scope of this work. We will focus here on crystallization from the melt under quiescent conditions.

Polymer crystallization from the melt takes place in two stages: primary crystallization and secondary crystallization.

[*] Adapted from Sperling L.H., *Introduction to Physical Polymer Science*, 2nd ed., John Wiley & Sons Inc., New York, 1992, ch.2

Primary crystallization consists of the nucleation and the growth of spherulites, up to the point of spherulite impingement. Nucleation is believed to be heterogeneous and require the presence of impurities in the polymer melt which serve as sites for the formation of nuclei. After the onset of nucleation, growth of the spherulite proceeds in the radial direction from the nucleus and results in the formation of crystalline fibrils of approximately constant width.[10] Each fibril is, in fact, constituted by chain-folded lamellae, where the fold surfaces are in general parallel to the spherulite radius (Figure 2.2.1[11]).

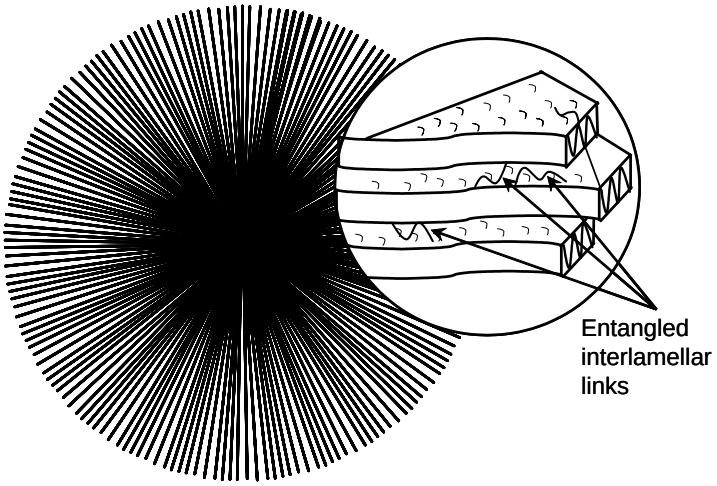

Figure 2.2.1 Polymer Spherulite with Chain-folded Lamellae*

The most important feature of a lamella is its thickness which is related to the fold length. The lamellar thickness (l) varies with crystallization conditions and is inversely proportional to the supercooling. If K_l is a constant related to polymer characteristics, such as the end surface free energy and the enthalpy of fusion, and ΔT is the difference between the equilibrium melting and crystallization temperatures, then,

$$l \propto \frac{K_l}{\Delta T}$$ **Equation 2.2.1[12]**

Entangled interlamellar links between chain-folded lamellae that are shown in Figure 2.2.1, consist of tie molecules that start in one of the lamella and end up in the neighboring lamella. The tie molecules formed during primary crystallization are

* Adapted from Hoffman J., Davis G., Lauritzen J., *Treatise on Solid State Chemistry,* Vol 3, *Crystalline and Noncrystalline Solids*, Hannay N., Ed. Plenum Press, New York., 1976, ch.7

believed to be shorter than several times the dimension of a random coil.[13] The interlamellar links account for the incidence of plastic deformation of semicrystalline materials by providing the mechanism for stress transfer between crystalline lamellar regions.

According to the Keith, the spherulite goes through several developmental stages during its growth (Figure 2.2.2).[14] At first, a chain-folded precursor forms and serves as a basis for the formation of sheaf-like structures (hedrites or axialites[15]), the intermediate stages of the spherulite development. After lamellae splay outward, the familiar spherical shape of the spherulitic structure appears.[16] The spherulite texture changes with crystallization temperature from compact and open at low temperature to coarse and fine at high temperature[10]. Under isothermal conditions the rate of spherulitic growth is constant in the radial direction[17] and the growth continues until impingement with other spherulites. As mentioned earlier, the impingement marks the end of the primary crystallization.

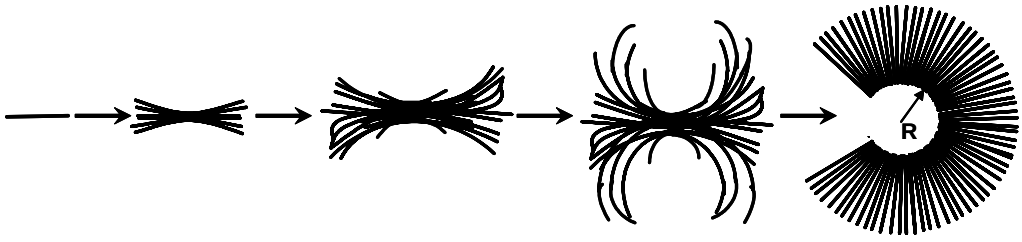

Figure 2.2.2 Developmental Stages of a Spherulite*

Depending on the chain structure, the secondary crystallization may involve the processes of lamellar thickening and/or the formation of new lamellae in gaps between existing lamellae.[13,18] Since the lamellae formed during the primary crystallization have high surface-to-volume ratios, they have high free energies. The process of thickening leads to a decrease in free energy and the formation of a more stable crystal; it is then, by definition, thermodynamically driven and can be explained mathematically as follows. If the lateral dimension of a crystal is *x*, the thickness of the crystal is *l*, and the surface free

* Adapted from Khoury F., Passaglia E., *Treatise on Solid State Chemistry*, Vol 3, *Crystalline and Noncrystalline Solids*, Hannay N., Ed. Plenum Press, New York, 1976, ch.6

energies of the basal surfaces and the lateral surfaces are σ and σ_e ($\sigma_e > \sigma$) respectively, then the surface free energy of the lamellar crystal is

$$G_s = 4xl\sigma + 2x^2\sigma_e \qquad \textbf{Equation 2.2.2}$$

The thickening leads to a decrease in *x*, an increase in *l* and, consequently a decrease in G_s.[19]

The formation of new crystals in-between existing lamellae is possible because of the presence of amorphous material consisting of interlamellar links, loose folds, etc.... Some of the variables that define the ease of formation of these crystals are the crystallization conditions, the amount of entanglements, which is, in turn, a function of the molecular weight and the amount of regio- and stereo-defects present in the chains, which controls the amount of interlamellar links. [18,20]

Over the years a number of theories have been proposed to describe lamellar and spherulitic growth: among them the Keith-Padden theory[10,15] Sadler's entropic barrier (rough surface) model,[21,22] and the Lauritzen-Hoffman (LH) nucleation theory.[*,23,24,25,26]

The LH nucleation theory accounts for the dependence of lamellar thickness on supercooling and the dependence of growth rate on crystallization temperature. It provides an explanation for the observation of chain-folding and predicts the dependence of growth rate on molecular weight. It views the growth of a crystal as a two-step kinetically controlled mechanism: the critical deposition of a first stem on a lateral surface and the subsequent chain-folding to complete a new layer of the substrate. The LH theory defines three regimes of crystallization kinetics which are shown schematically in Figure 2.2.3.

As defined by the LH theory, deposition of a stem occurs at the rate *i*, whereas substrate completion associated with chain folding occurs at the rate *g*. Regime I, which takes place at high temperatures, is characterized by a superior rate of substrate completion as compared to the rate of deposition on the crystal substrate *i* ($g >> i$). Regime II, which occurs at intermediate temperatures, is characterized by the competition between stem deposition and lateral growth ($g \approx i$). Finally, regime III, typically at large supercoolings, is characterized by a superior rate of stem deposition leading to multiple secondary nuclei formed on the substrate ($i >> g$). Regime III is observed when the niche

separation between crystalline stems is comparable with the stem width. The crystal growth rate predicted by the LH theory is expressed as

$$G = G_0 \exp\left[-U^* / R(T - T_\infty)\right]\exp\left[-K_g / T\Delta T\right] \qquad \textbf{Equation 2.2.3}^{24}$$

where G_0 is pre-exponential factor that contains quantities not strongly dependent on temperature, U^* is the activation energy for chain reptation in the melt, R is the gas constant, T is crystallization temperature, T_∞ is the temperature at which reptation motions stop, K_g is a nucleation constant and ΔT is the undercooling.

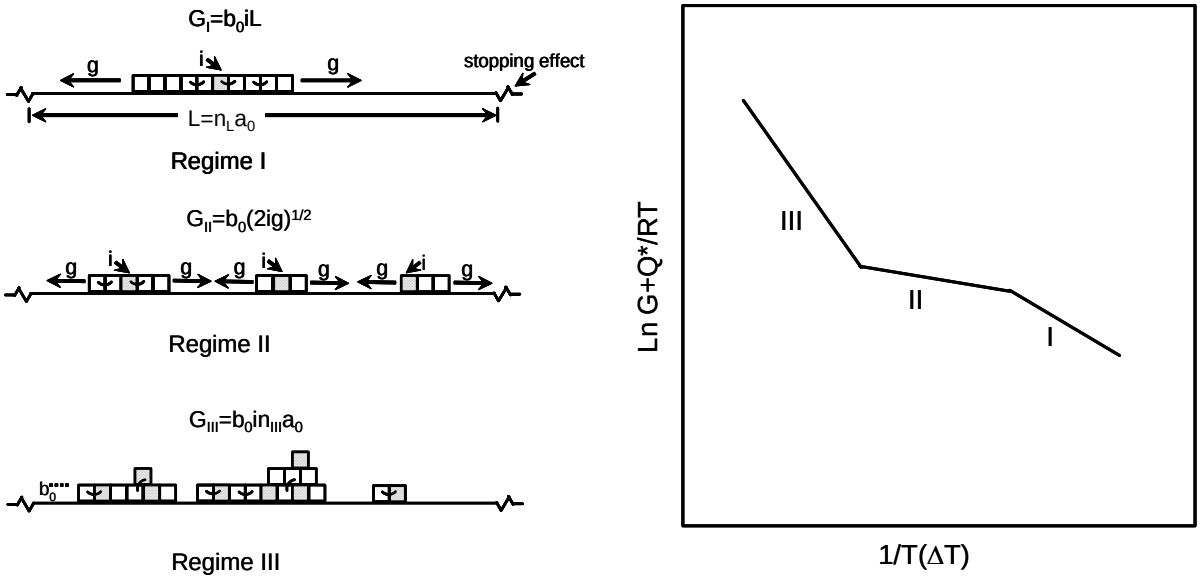

Figure 2.2.3 Crystal Growth Regimes*

2.3 Copolymer Crystallization

Copolymers result from the polymerization of several chemically or structurally different types of monomeric units (mers). Depending on the distribution of mers along the polymer chain, different types of copolymers can be formed. When the mers are statistically distributed, the resulting copolymer is called statistical; in the case, when the sequence of unit distribution is mathematically indefinable, the copolymer is called

*Adapted from Hoffman J., Miller R., *Polymer*, **1997**, *38* , 3151-3212

unspecified[7]. Statistical copolymers include block, random and alternating copolymers. In the case of block copolymers, long sequences of mers of one type are followed by long sequences of mers of another type. In the case of alternating copolymers, the mers of different types are distributed in alternating sequences. Finally, in the case of random copolymers, the monomeric units of each type are distributed randomly throughout the chain so that the probability of finding a mer of either type is independent of the nature of its neighboring unit. Depending on the overall composition, random copolymers may have a short order periodicity in the unit distribution and may have relatively long sequences of either mer.

Repeat unit distribution is extremely important from the stand-point of copolymer properties, in general, and copolymer crystallization, in particular. For example, in the case of a block copolymer, if the mer-sequences are sufficiently long, the entropy of mixing of the individual blocks is relatively low. If the block enthalpy of mixing is sufficiently positive, an excess of free energy contribution may lead to microphase separation. In this case, different phases would be present, with each phase exhibiting its own glass transition temperature (T_g), melting temperature (T_m) and crystallization temperature (T_c)[27]. On the other hand, chemically identical materials having shorter blocks will be less susceptible to microphase separation and exhibit single T_g, T_m and T_c intermediate between the values of the corresponding homopolymers. One can also imagine that the properties of crystallizable copolymers will be greatly affected by the "minority" comonomer inclusion in or exclusion from the "majority" comonomer crystal as well as by the presence of stereo defects. Since there is considerable ongoing debate on this topic, the review of prominent but extreme random copolymer crystallization theories is presented here.

Flory's thermodynamic equilibrium theory[28,29,30] of copolymer crystallization assumes that monomer B is excluded from the crystallites formed by A. The ability of a sequence of A units to crystallize is dependent on its length ξ and on the crystallization temperature: at a given temperature, if ξ is larger than a critical value, ξ^*, then crystallization takes place. At high temperatures, units of length ξ larger than ξ^* crystallize to form thick crystallites that in turn melt at high temperatures. As the crystallization temperature decreases, the critical value of ξ^* decreases as well and shorter

sequences are able to crystallize forming thinner crystals. As a result, copolymers exhibit a significantly wider melting range than corresponding homopolymers whose chemical structure consists entirely of units A. According to Flory, the equilibrium melting temperature of a copolymer, T_m, is defined by the following relationship:

$$1/T_m - 1/T_m^0 = -(R/\Delta H_u)\ln p \qquad \textbf{Equation 2.3.1}^{30}$$

where T_m^0 is the melting point of the pure polymer, R is a gas constant, ΔH_u is the heat of fusion per unit and p is a probability that unit A is succeeded by unit A regardless of the preceding units. As evident from Equation 2.3.1, the melting temperature in Flory's model is independent of the chemical nature of unit B. The same is true of the degree of crystallinity: the universal decrease in crystallinity due to copolymerization is solely a function of the amount of units B and not of their chemical nature.

Based on the kinetic theory employed by Lauritzen, DiMarzio and Passaglia,[31] Helfand and Lauritzen[32] proposed a kinetic theory of copolymer crystallization that accounts for both the incorporation of B units into A crystals and their exclusion. The likelihood of inclusion of B units is considered from the perspective of energetic cost of adding and detaching a stem during lamellar substrate formation and the energy differences between the two processes. In the case of addition of an A unit, the crystal free energy is lowered by ΔF_0; however, in the case of insertion of a B unit, a free-energy price ε is paid. The temperature dependence of ΔF_0 is given as

$$\Delta F_0 = (\Delta H_f / T_m^0)(T_m^0 - T) \qquad \textbf{Equation 2.3.2}^{32}$$

where T_m^0 is the melting point of a pure crystal and ΔH_f is the heat of fusion of a pure crystal. A decrease in temperature leads to a decrease in the crystal free energy and a subsequent increase in the non-equilibrium inclusion of B units. This theory also accounts for a lower copolymer melting temperature than that predicted by the exclusion equilibrium model. This theory also predicts an increase in lamellar thickness due to B unit incorporation. The model does not explicitly address the chemical nature of B.

Sanchez and Eby[33,34,35] developed a kinetic theory of random copolymer crystallization that accounts for both complete inclusion and exclusion as well as the

partial inclusion of units B into a crystalline matrix. These extreme models of inclusion and exclusion are shown schematically in Figure 2.3.1.

The Sanchez-Eby model asserts that the crystalline morphology is kinetically determined and the inclusion of B units into a crystal can lead to a thermodynamically more stable system. In the inclusion model, the depression of the crystal melting point is due to the decrease in the heat of fusion. Conversely, in the exclusion model, the melting point depression is due to an increase in the entropy of fusion. Under isothermal conditions, the Sanchez-Eby theory predicts an increase in lamellar thickness with concentration of non-crystallizable B units, for both inclusion and exclusion models. However, for a quenched system or for a system cooled at a constant rate, the crystal thickness decreases with an increase in B concentration.[35]

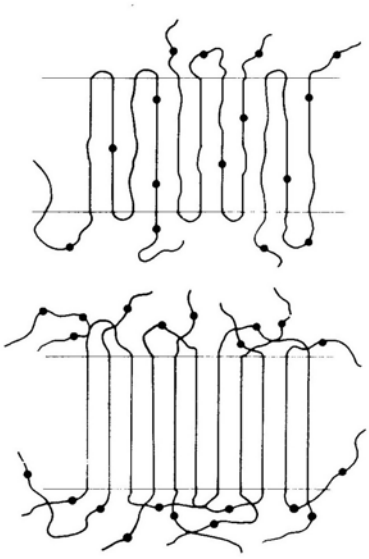

Figure 2.3.1 Inclusion (top) and Exclusion (bottom) Models[35] [*]

After thermodynamic and kinetic theories were published, numerous studies were conducted and a large amount of evidence was collected to support both theories.[36]

Zimmerman[37] studied the structural properties of Ziegler-Natta propylene-ethylene copolymers with ethylene content up to 11%. He found that neither the normalized heat of fusion nor the unit cell dimensions changed as a function of

[*] Reprinted with permission from Sanchez I., Eby R., *Macromolecules*, **1975**, *8*, 638-641. Copyright 1975 American Chemical Society

comonomer content. On the basis of these observations, Zimmerman concluded that ethylene is excluded from polypropylene crystals.

Studies by Bruckner et al.[38] and Feng et al.[39,40] supported Zimmerman's findings. However, when Lahonen et al.[41,42] studied propylene-ethylene copolymers in the same ethylene concentration range as Zimmerman, their findings were opposite to those of Zimmerman. They suggested a small decrease in the normalized enthalpy of fusion with an increase in ethylene content and a slight expansion of the unit cell along the *b* direction measured for propylene homopolymer and propylene-ethylene copolymers. They concluded that ethylene is partially included in the propylene crystal. The same conclusion was also reached in the number of other studies by De Rosa et al.,[43,44,4546],Starkweather et al.,[47] Busico et al.,[48] Hosier et al.[49] and others.

A study conducted by Alamo et al.[50] looked at the morphological partitioning of ethylene defects in the random metallocene-based propylene-ethylene copolymers using the solid state NMR spectroscopy. They have found that 42% of the ethylene units were included in the propylene crystal for copolymers with ethylene concentration of 0.8-7.5 mol%. Furthermore, Alamo et al. demonstrated that the included ethylene units were distributed equally through the whole crystal region and were not concentrated on the crystal side of the interphase. They have also demonstrated the decrease in the normalized heat of fusion associated with the ethylene inclusion in a polypropylene crystal. The authors believe that the rate of ethylene unit incorporation in PP crystal should stay at 42% or possibly higher for the copolymers with ethylene concentrations above 7.5 mol % for the materials crystallized at the same undercoolings.

As will be demonstrated in the following chapters, we believe that the Sanchez-Eby kinetic theory should apply in the case of propylene-ethylene copolymers, Ethylene units can in fact enter the polypropylene crystal; however, the inclusion is limited to single ethylene (E) units. The included single ethylene units will serve as defects in the polypropylene crystal formation. For the PP crystallized non-isothermally, the inclusion of ethylene will result in decrease in the lamellar thickness and will lead to decrease in the crystallization and melting temperatures and overall crystallinity.[49,51,52,53] EE, EEE or larger sequences will be effectively excluded from the propylene crystal as predicted by both Sanchez-Eby and Flory's theories.

The inclusion of single copolymer units in a polypropylene crystal is not limited to ethylene units. In the series of studies by De Rosa et al,[43,54,55] butene, a bulkier comonomer unit, was found to be included in the crystals of syndiotactic polypropylene as well. However, comonomers such as hexene and higher alpha-olefins were excluded from the polypropylene crystal in all instances.[49]

From the standpoint of previous discussions, it follows that both the chemical nature and the unit distribution play a crucial role in determining the extent of comonomer inclusion or exclusion and the resulting properties.

2.4 Morphology

Since it has been established that ethylene units can enter polypropylene crystals as defects, it is now essential to take a look at the morphology of polypropylene and propylene-ethylene copolymers in order to understand what happens to ethylene and other defects as they enter the crystal.

It has been determined that polypropylene exhibits polymorphism. Depending on the crystallization conditions and the regio and stereochemistry, polypropylene can form α, β, γ or smectic phases, all of which are based on the 3_1 helical conformation[56] characterized by a 6.5 A repeat distance.[57,58]

The β crystal phase of polypropylene has a trigonal unit cell with cell dimensions of a = b = 11.03 A, c = 6.49 A and contains three isochiral helices as reported by Meille et al.[59] The β phase morphology exhibits significant screw dislocations,[57] a density lower than that of the γ and α phases,[70,60] higher static disorder,[60,61] higher spherulitic growth rates and lower stability.[70] The conditions[59] favoring the β phase formation in isotactic propylene are crystallization with the help of certain nucleating agents,[62] directional solidification in a temperature gradient and oriented crystallization under shear. Upon heating, β phase crystals transform into α phase crystals.[70]

The smectic phase is an unstable, partially ordered phase of iPP that transforms to α phase if annealed at temperatures above 70-80°C.[63] Conditions favoring the smectic phase formation are quenching, casting of both iPP and low ethylene content propylene-ethylene copolymers[63] and drawing at room temperature.[57]

Both β and smectic phases are not of a large significance for the present discussion and will not be mentioned any further in this manuscript. Instead the focus will shift to α and γ phase crystals since they are the subject of this work.

The α phase crystal of polypropylene shown in Figure 2.4.1 has a monoclinic unit cell with cell dimensions a = 6.65 A, b= 20.96 A, c = 6.5 A, β = 99.8°.

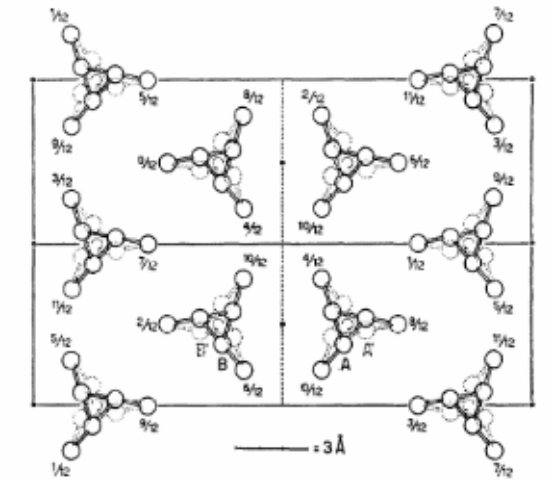

Figure 2.4.1 Two Unit Cells of iPP α-Phase Crystal[64*]

As a result of steric repulsion effects between methyl groups, α phase crystals are made up of sheets of alternating right handed (R) and left handed (L) helices.[64] As a result, regular packing in the α phase can be described as follows[56]

RL RL RL RL RL

However, if the chirality of two consecutive sheets happens to be the same due to a "local accident", the packing becomes[56]

RL RL RL + LR LR LR

This local accident gives rise to epitaxial lamellar branching which leads to the cross-hatched morphology which is unique to polypropylene. In this case the helices are parallel to different cell edges because of chain axis rotation by angle β with the *a* and *c* axes of one unit cell parallel to the respective *c* and *a* axis of the other.[65] As a result of

[*] Reprinted from *Polymer, 37(22),* Lotz B., Wittmann J.C., Lovinger A.J., *Structure and morphology of poly(propylenes): A molecular analysis* , 4979-4992, Copyright 1996 with permission from Elsevier

this rotation, daughter lamellae nucleate at angles of 100° and 80° from the parent lamella. It is possible to obtain two distinct forms of α phase crystals: α_1 and α_2 which differ by the degree of disorder.[66] Transition from the less ordered α_1 to the more ordered α_2 can be achieved by annealing with partial melting and subsequent recrystallization.[67,48]

The γ crystal phase of polypropylene has an orthorhombic unit cell with the cell dimensions a = 8.54 A, b = 9.93 A, c = 42.41 A as reported by Brückner and Meille.[68]The alternating right and left handed helices form bilayers of the following structure:[56]

RL + LR + RL + LR + RL + LR

As first determined by Brückner et al.,[68,69] polymer chains in γ phase crystals are not parallel to each other: polymer chains are parallel to one of two diagonals of the (*a, b*) plane and are, therefore, at 80° angle from each other and at a 40° angle from the parent lamella (Figure 2.4.2). It is important to note that γ phase crystals grow on the *ac* lateral faces of α phase lamellae[70] and that γ phase crystals do not branch since they usually grow by a process that is similar to the one leading to the formation of branches in α phase. It has been shown that α and γ phase crystals can co-exist under a number of experimental conditions and that this coexistence is a fundamental property of the system;[71,72] however, the γ crystals form much thinner lamellae than do α phase crystals.[73] It was reported by Campbell et al.[73] that the lamellar thickness in iPP samples containing only γ crystals is about half that found in samples containing only α phase crystals formed at the same supercoolings. The transformation of γ phase crystals into α phase crystals is possible for oriented systems obtained by drawing.[70]

The conditions favoring the formation of γ phase in isotactic polypropylene are crystallization at high pressures,[74,75,76] slow crystallization at high temperatures,[57,77] crystallization of short chains,[78] presence of ethylene units[51,77,79] and other defects affecting the stereo or regioregularity.[71, 80, 81]

Alamo et al.[82] conducted a study aimed at determining whether the nature of the defects, (i.e. regio vs. stereo) play a role in the formation of γ phase crystals. It was found that materials containing identical amounts of defects but of different nature have identical γ phase contents over the whole range of crystallization temperatures. The same

study examined the effect of isotactic sequence length on γ phase formation. The conclusion was reached that γ phase formation becomes less favorable with increasing PP sequence length. Yamada et al.[83] studied the effects of tacticity (stereo defects) on the cross-hatching morphology of polypropylene. They determined that the cross-hatching density increases with a decrease in isotacticity. In the study by Burfield and Doi,[84] it was determined that tacticity also affects the glass transition behavior of polypropylene: T_g of syndiotactic PP is 14°C higher than that of isotactic PP. VanderHart et al[85,86] used solid-state NMR spectroscopy to study how different types of defects in iPP partition between the crystal and amorphous regions. They determined that about half of the common stereo-defects (i.e. defects of the *mrrm* type) are included in the iPP α-crystal phase as opposed to about a quarter of 2,1 erythro defects (regio defects from head-to-head insertion). Since the propylene-ethylene copolymers used in this work contain both types of defects, these findings are extremely important for our study.

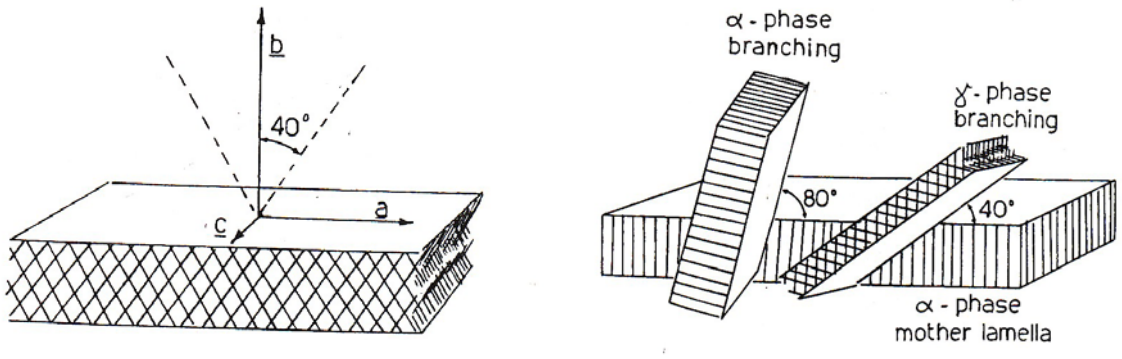

Figure 2.4.2 γ iPP Crystal (left); α and γ Branching (right)[57*]

[*] Reprinted from *Prog. Polym. Sci., 16(2-3),* Bruckner S., Meille S.V., Petraccone V., Pirozzi B., *Polymorphism in isotactic polypropylene* , 361-404, Copyright 1991 with permission from Elsevier

2.5 Two and Three Phase Models

In the preceding sections, the discussion was mainly focused on the crystalline region; however, the amorphous and interfacial regions are equally important in the material properties determination. There are two prominent models that are commonly used in the semicrystalline material analysis: two-phase and three-phase models. Both of them will be briefly described in this section since they will play an important part in the discussion in the following chapters.

2.5.1 Two-Phase Model

The two-phase model depicts a semicrystalline polymer as having only two phases: crystalline phase and amorphous phase (Figure 2.5.1).

The main assumption of the two-phase model is insignificance of the transitional region between the crystalline and amorphous phases. It is assumed that the interphase region is so thin that it does not contribute significantly to the overall material properties and the system as treated as if the sharp transition exists between the crystalline and amorphous regions. The overall crystallinity of such system is then expressed by Equation 2.5.1:

$$X^c(T) = 1 - X^a(T) \qquad \textbf{Equation 2.5.1}$$

where $X^c(T)$ is the mass fraction of the crystalline material and $X^a(T)$ is the mass fraction of the amorphous material.

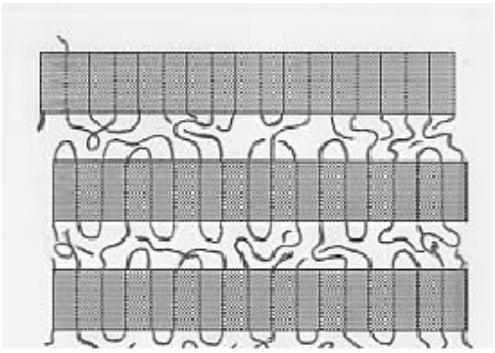

Figure 2.5.1 Two-Phase Model

This model is routinely utilized in order to calculate the crystallinities of the semicrystalline materials, especially as a part of the differential scanning calorimetry analysis (Equation 2.5.2).

$$X^{c}(T) = \frac{\Delta H_f}{\Delta H_f^0} \qquad \textbf{Equation 2.5.2}$$

where ΔH_f is the measured sample enthalpy change during melting and ΔH^0_f is the thermodynamic heat of fusion at the melting point.

The crystallinity of the semicrystalline polymer can also be calculated by evaluating the change in the heat capacity of the material measured at the glass transition temperature (T_g). T_g is defined as the temperature at which large range coordinated molecular motions (10-50 atoms) occur. Below the T_g the amorphous polymer chains are frozen with only vibrational motion and short range rotations present.[87] As the temperature is raised the chains start gaining mobility. The change in the heat capacity during T_g serves as the measure of the fraction of the relaxing amorphous material. If the only contributors to the heat capacity are amorphous and crystalline regions and all polymer chains in the amorphous region undergo the relaxation during the glass transition, then the crystallinity of the polymer can be expressed by Equation 2.5.3

$$X^{c}(T) = 1 - \frac{\Delta C_p^{sc}}{\Delta C_p^{liq}} \qquad \textbf{Equation 2.5.3}$$

where ΔC_p^{sc} is the change in the heat capacity at T_g of the semicrystalline material and ΔC_p^{liq} is the change in the heat capacity at T_g of the fully amorphous material. The quantity $\frac{\Delta C_p^{sc}}{\Delta C_p^{liq}}$ is also called mobile amorphous fraction and is commonly denoted as f_{maf}.

Finally, by employing the two-phase model, the weight percent crystallinities of the semicrystalline polymers can be determined using density measurements. The

density is assumed to be a function of the densities of the crystalline and amorphous regions and the crystallinities are calculated using Equation 2.5.4.

$$X^c = \frac{\rho_c(\rho - \rho_a)}{\rho(\rho_c - \rho_a)} \qquad \textbf{Equation 2.5.4}$$

The two-phase model is capable of predicting material behavior in the systems where the contribution of the interphase region is negligible as in the case of linear polymers without bulky side-groups. Its usage beyond these materials is a subject to limitations and should be used only if approximate property predictions are sufficient.

2.5.2 Three-Phase Model

The three-phase model is considered more advanced by comparison to a two-phase model. It takes into an account the interfacial region between the crystalline and the amorphous phases which is comprised of high fraction of non-crystallizable units and stereo and regio defects that might be excluded from the crystal structure. It also holds the chains folds of varying loop length that are the by-product of the chain-folding mechanism of the crystal growth. The interfacial region is characterized by high interfacial free energy.[88] The three-phase model is shown schematically in Figure 2.5.2.

The interesting concept introduced in the scope of the three-phase model is that of the rigid amorphous fraction (RAF). RAF consists of the non-crystalline amorphous portion of material constrained by the crystalline region. These constraints result from frequent crossing of the interface by long folded polymer chains.[89] In most cases RAF does not participate in the relaxation that occurs as a result of passing through a T_g. It is believed that the relaxation of RAF occurs somewhere between the T_g(amorphous) and T_m and in some cases, as was claimed for poly(oxy-2,6-dimethyl-1,4-phenylene), can even occur above T_m.[90] The separate from T_g (amorphous) relaxation attributed to RAF was shown for polypropylene,[91] PEEK,[92] poly(oxymethylene),[93,94] poly(phenylene sulfide)[95] and several others polymer systems.[89]

In the study conducted by Grebowicz et al.,[91] three-phase model was applied in the analysis of the thermal properties of isotactic polypropylene. It was found that the

material crystallized at 0.5K/min, reached 47% crystallinity. According to the authors, it also contained 22% of the mobile amorphous fraction and 31% of the rigid amorphous fraction that contributed to non-crystalline region.

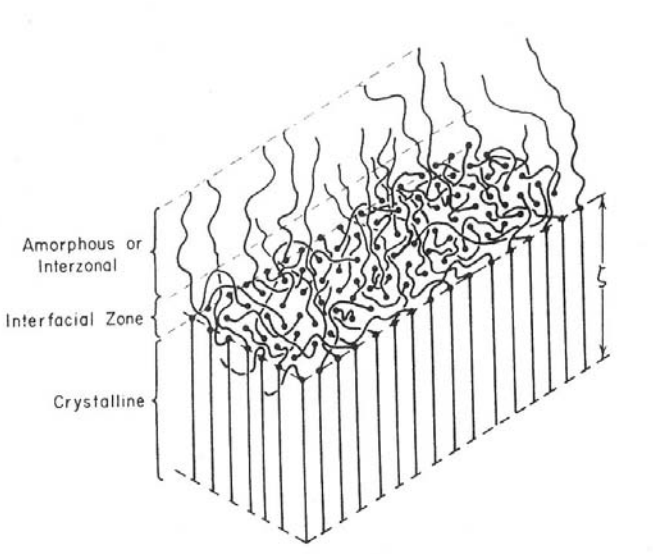

Figure 2.5.2 Schematic representation of the semicrystalline material[96*]

Some polymers such as polyethylene and polyethylene-propylene copolymers do not show a separate T_g for RAF and the effect of the crystal is displayed only in the broadening of the glass transition region.[97,89,90] However, according to Wunderlich[89] the RAF-like structure is present in HDPE as well as demonstrated by Electron Spectroscopic Imaging (ESI) conducted by Kunz et al.[98,99]

The existence of RAF was further supported by considering its effect on the overall heat capacity of the system. If a RAF is present, but does not participate in the relaxation at T_g, then the sum of the mass fractions of crystallinity and mobile amorphous phase should be less than 1. The magnitude of the heat capacity step at T_g should decrease because the amount of chains relaxing at T_g has been decreased by the amount corresponding to RAF. Hence, the right side of Equation 2.5.3 should be higher than the

[*] Reprinted with permission from Mandelkern L., *J. Phys. Chem.*, **1971**, *75*, 3909-3920. Copyright 1971 American Chemical Society

left side. This deficiency in ΔC_p at T_g was first shown by Menczel and Wunderlich[100] and later demonstrated in other studies.[91,92,94]

In order to take into account the RAF contribution to an overall heat capacity, Equation 2.5.3 has to be adjusted to include the mass fraction of RAF. The three-phase model then defines material crystallinity, X_c as

$$X^c(T) = 1 - f_{MAF} - f_{RAF} = 1 - \frac{\Delta C_p^{sc}}{\Delta C_p^{liq}} - f_{RAF} \qquad \textbf{Equation 2.5.5}$$

where f_{MAF} is the mass fraction of mobile amorphous phase and f_{RAF} is the mass fraction of rigid amorphous phase.

If the three-phase model is used, then the crystallinity calculations from the density measurements should include the RAF contribution as well. The RAF density should fall between the densities of the fully amorphous and full crystalline materials. Only a few studies discussed the RAF densities. Huo and Cebe[101] calculated the density of RAF in poly(phenylene sulfide). They suggested that the RAF density was only slightly higher than that of the mobile amorphous fraction and much lower than the PPS crystal density. The studies by Fischer and Fakirov[102] and Bornschlegl and Bonart[103] of the structure and properties of poly(ethylene terephthalate) and poly(butylene terephthalate) did not specifically address the issue of RAF. However, both studies looked at the changes in the amorphous density with the degree of crystallinity. It was found that the constrained amorphous phase density of semicrystalline materials was higher than the density of the fully amorphous materials and that the amorphous density increased with the increase in crystallinity.

These results as well as the applicability of the two-phase and three-phase models to the Dow propylene-ethylene copolymer system will be discussed in details in the latter chapters of this work.

2.6 Nucleating Agents

It had been discussed in Section 2.2 that the nucleation is one of the processes that controls the primary crystallization. The nucleation for polymeric materials is heterogeneous and requires the presence of a nucleation site for the formation of nucleus. One of the methods that are used to increase the polymer nucleation efficiency is the addition to the polymer melt of a foreign surface in the form of a nucleating agent. The introduction of a foreign surface reduces the free-energy barrier to a primary nucleation leading to a decrease in the critical nucleus size. The result of lowering a free enthalpy of nucleation is the decrease in the crystallization induction time, which, in turn, results in the increase in the nucleation rates.[104,105] In the bulk polymer, as the heterogeneous nucleation is initiated, the growth spreads through the whole material in a very short time period.[106]

Since the addition of the nucleating agents leads to an increase in the nucleation rates, the number of spherulites appearing simultaneously increases. The spherulite impingement then takes place at the smaller spherulite radii leading to a finer morphology[107] than would have been resulted in the absence of a nucleating agent. The mechanism for the heterogeneous nucleation is believed to be epitaxial.[108,109]

The addition of a nucleating agent changes the mechanical and optical properties of the modified materials. The reported improvement in the optical properties and impact resistance, commonly reported as an outcome of this type of heterogeneous crystallization, result from the decrease in the size of the spherulites[110]. The reported improvement in the tensile strength and flexural modulus result from the increase in the overall crystallinity of the materials.[111, 112]

The nucleating agents commonly used to enhance polymer crystallization are low molecular weight compounds. These compounds are divided into mineral and organic nucleating agents. In the past years, the organic nucleating agents have been used extensively to increase the nucleation efficiency of the polymers and improve their optical and mechanical properties.[113] One of the most common and well studied groups of the polypropylene organic nucleators consists of the sorbitol derivatives.[113,114,115] The efficiency of sorbitols in promoting the polypropylene nucleation has been linked to their

superior dispersion in the polymer matrix reached through the formation of thermoreversible gels.[116]

Macromolecular nucleating agents can also be used to enhance the nucleation of the polypropylene. In this case the resulting system can be treated as a blend with a low concentration of the nucleating agent. In this work macromolecular additives, both miscible and immiscible in the polypropylene matrix, will be used to enhance the nucleation efficiency of the propylene-ethylene copolymers.

3 PROPOSAL AND THESIS STATEMENT

Although a number of published studies have been aimed at the determination of structure-property relationships for propylene-ethylene copolymers, few, if any of the previous researchers have had access to a series of materials displaying such a wide range of ethylene concentrations as has been available in this study. The new catalyst system developed by the Dow Chemical Company provided the means of preparing propylene-ethylene copolymers of unique stereo- and regio-chemistry, where the regio and stereo errors are believed to be at the origin of the much improved mechanical and optical properties. At the same time this catalyst system made it possible to copolymerize propylene and ethylene containing up to 30 mol % ethylene. Synthesis of these materials has set the stage for a systematic study of the effects of ethylene content and other defects on the morphology and properties of propylene-ethylene copolymers over a wide compositional range. Since these materials exhibit some unusual characteristics such as good optical and mechanical properties and, as will be demonstrated further, unusual crystallization and melting behavior, it is beneficial to compare these novel copolymers with copolymers prepared by traditional metallocene and Ziegler-Natta catalysts in order to understand the source of these material improvements.

As was noted in the previous sections, there is an ongoing debate in the scientific community on the issue of inclusion vs. exclusion of ethylene units from polypropylene crystal. This question is important because it deals with the fundamental understanding of copolymer crystallization and crystal perfection. It is also essential in correctly determining the degree of crystallinity for copolymers and consequently for making further material behavior predictions since these are often based on the knowledge of the overall degree of crystallinity. In this work the degrees of crystallinity will be determined by two different methods. In the first method, the inclusion of the ethylene into the propylene crystal will be taken into the account and the two-phase model will be applied to the Dow propylene-ethylene system. In the second method, the RAF will be

taken into the account. The details of crystallinity calculations and Calorimetry data analysis will be presented in Chapter 5.

It has generally been assumed in the literature that even if ethylene units enter the polypropylene crystal lattice, the theoretical heat of fusion of the resulting crystal does not change. However, some evidence of unit cell expansion that exists in the literature[42] suggests that ethylene incorporation may lead to a decrease in crystal density and to a decrease in crystal cohesive forces.

This study is set to accomplish the following primary goals:

- Establish structure-property relationships for the new "Dow Chemical" copolymers focusing on the effect of comonomer content on the overall crystallinity and thermal properties (Chapter 6).

- Study the development of crystallinity as a function of the comonomer content and processing conditions (Chapter 6).

- Study the morphology of these materials as a function of commoner content and processing conditions focusing on the formation of α and γ crystal phases (Chapter 6).

- Compare the thermal properties of Dow Chemical materials to these of copolymers prepared by Ziegler-Natta and metallocene catalysts (Chapter 6).

- Study the effects of ethylene content on the thermodynamic heat of fusion to shed further light on the concept of crystal perfection and ethylene inclusion and determine the validity of the two and three phase models in respect to this propylene-ethylene system (Chapter 6).

As a secondary goal, this study will examine the behavior of nucleated propylene-ethylene copolymers in order to establish a nucleation efficiency scale for copolymer materials prepared with a small amount of macromolecular additives (Chapter 7).

Thesis Statement

Addition of ethylene to a propylene chain to form a statistical propylene-ethylene copolymer favors the formation of γ phase crystals and leads to a systematic depression of the melting, crystallization and glass transition temperatures as well as crystallinity. Ethylene units are partially included in isotactic polypropylene crystals as defects. Hence, the thermodynamic heat of fusion should be a function of the concentration of combined stereo, regio and comonomer defects.

4 EXPERIMENTAL

4.1 Materials

Statistical isotactic propylene-ethylene copolymers were supplied in the form of pellets by the Dow Chemical Company in several batches (series). The materials along with their composition, series number, catalyst type, molecular weights and polydispersity indexes (as determined by Dow) are listed in Table 4.1.1. The information on tacticity and regio-errors content, as supplied by Dow, is listed in Table 4.1.2.

Table 4.1.1 Dow Chemical Copolymers

Sample Name	Series	Ethylene Content, mol%	M_w, g/mol	M_w/M_n	Catalyst Type
PE-I (0.0, 320)	I	0.0	320,000	2.7	A
PE-I (8.2, 300)	I	8.2	300,000	2.2	A
PE-I (13.6, 290)	I	13.6	290,000	3.1	A
PE-I (15.7, 260)	I	15.7	260,000	2.2	A
PE-I (19.4, 260)	I	19.4	260,000	2.4	A
PE-II (4.4, 320)	II	4.4	320,000		A
PE-III (7.8, 160)	III	7.8	160,000	2.2	A
PE-III (12.3, 310)	III	12.3	310,000	2.6	A
PE-III (12.4, 160)	III	12.4	160,000	2.3	A
PE-III (14.8, 160)	III	14.8	160,000	2.3	A
PE-III (15.0, 120)	III	15.0	120,000	2.2	A
PE-VI (18.0, 320)	VI	18.0	320,000	3.4	B
PE-VII (3.3, 230)	VII	3.3	230,000	2.3	B
PE-VII (5.4, 160)	VII	5.4	160,000	2.4	B
PE-VII (6.7, 330)	VII	6.7	330,000	2.3	B
PE-VII (7.0, 170)	VII	7.0	170,000	2.3	B
PE-VII (12.3, 300)	VII	12.3	300,000	2.4	B
PE-VII (12.8, 150)	VII	12.8	150,000	2.2	B
PE-VII (16.6, 150)	VII	16.6	150,000	2.3	B
PE-VII (17.4, 290)	VII	17.4	290,000	2.4	B
PE-VII (21.2, 280)	VII	21.2	280,000	2.4	B
PE-VIII (4.8, 310)	VIII	4.8	310,000		B
PE-VIII (7.8, 220)	VIII	7.8	220,000		B
PE-VIII (13.3, 290)	VIII	13.3	290,000		B

Table 4.1.2 Tacticity and Regio-Error Content

Sample Name	Regio-Errors mol%	%mm	%mr	%rr
PE-I (0.0, 320)	1.18	93.7	4.6	1.6
PE-I (8.2, 300)	0.47	94.3	2.2	3.4
PE-I (13.6, 290)	0.34	96.4	0	3.6
PE-I (15.7, 260)	0.24	95.3	0	4.7
PE-I (19.4, 260)	0.18	95.2	0	4.8
PE-II (4.4, 320)	0.57	93.5	4.1	2.4
PE-III (7.8, 160)	0.41	95.0	2.8	2.2
PE-III (12.3, 310)	0.31	95.3	0.8	3.9
PE-III (12.4, 160)	0.21	97.3	0	2.7
PE-III (14.8, 160)	0.31	93.8	1.9	4.4
PE-III (15.0, 120)	0.3	97.2	0	2.8
PE-VI (18.0, 320)	0.26	95.7	0	4.3
PE-VII (3.3, 230)	0.87	92.8	5.3	1.8
PE-VII (5.4, 160)	0.89	93.6	4.7	1.8
PE-VII (6.7, 330)	0.52	95.4	2.6	2
PE-VII (7.0, 170)	0.46	95.3	2.7	2
PE-VII (12.3, 300)	0.37	97.3	0	2.7
PE-VII (12.8, 150)	0.32	97.7	0	2.3
PE-VII (16.6, 150)	0.24	97.3	0	2.7
PE-VII (17.4, 290)	0.41	91.7	0	8.3
PE-VII (21.2, 280)	0.2	96.2	0	3.8

For the comparison purposes, several metallocene and Ziegler-Natta propylene-ethylene copolymers, listed in Table 4.1.3 and Table 4.1.4 respectively were supplied by Dow Chemical in the form of pellets.

Table 4.1.3 Metallocene Copolymers

Sample Name	Ethylene Content, mol%	Molecular Weight, g/mol	M_w/M_n
Wintec WFX6	5.2	222,000	2.7
Wintec WFX4T	6.5	308,000	2.5
P/E 1	13.5	117,000	2
P/E 2	11.1	147,000	2.1

Table 4.1.4 Ziegler-Natta Copolymers

Sample Name	Ethylene Content, mol%	M_w g/mol	M_w/M_n
6D69	4.4		
DS6D82	8.3	255,000	3.5

The nucleated PE-I (8.2, 300) copolymers were supplied by Dow Chemical. The types and the concentrations of the commercial nucleating agents are listed in Table 4.1.5.

Table 4.1.5 Types and Concentrations of Nucleating Agents

Nucleating Agent	Concentration, Wt %
Vanilla iPP-low MFR (0.5)	1, 3
Vanilla iPP-high MFR (50)	1, 3, 10
Commercial HMS iPP	1, 3, 10
HDPE	1, 3, 10

4.2 Methodology

The different techniques used to analyze propylene-ethylene copolymers along with the sample preparation conditions will be briefly outlined in this section.

4.2.1 DSC Measurements

Heating and Cooling Scans

The TA Q 1000 Differential Scanning Calorimeter (DSC) was used to obtain heating and cooling traces of Dow, Ziegler-Natta and Metallocene copolymers. The materials were heated to 180 °C, held isothermally for 5 min, cooled at 10 °C/min to -55 °C, held isothermally for 5 min, heated to 180 °C and held isothermally for 5 min. The runs were conducted under helium atmosphere. The baseline run using two empty pans was carried out before the first sample run and was repeated after every 5 samples.

The Perkin Elmer Pyris 1 DSC was used to obtain heating and cooling traces of the nucleated copolymers. The materials were heated to 200 °C, held isothermally for 5 min, cooled at 10 °C/min to 25 °C, held isothermally for 5 min, heated to 200 °C and held isothermally for 5 min. The runs were conducted under nitrogen atmosphere. The baseline run using two empty pans was carried out before the first sample run and was repeated after every 5 samples.

The materials were prepared by pressing the pellets between two pieces of Kapton^{TM} in a Carver^{TM} hot press with nitrogen purge. Molds made of shims with a thickness of .39 mm were used to regulate the film thickness. The temperature of the press was set to 200°C. The samples were first allowed to melt for 5 min under low pressure; a load of 2.3 metric tons was then applied for 10 sec, followed by release of pressure for 10 sec. The last two steps were repeated 5 times in order to degas the melt and minimize the amount of bubbles in the final film. Finally the films were quenched in ice water.

In order to get a reliable signal in the low temperature region while introducing as little heat transfer variations between the materials as possible, the masses of DSC samples were kept between 10.500 and 11.500 mg.

The masses of sample and reference pans with lids were matched in order to minimize heat flow displacement between the two sample holders. The sum of masses of pans and lids was kept in the range from 27.680 mg to 27.760mg.

DSC scans were corrected for temperature lags for both cooling and heating scans. Cooling scans[117] were corrected by determining the temperature lag for the nematic-to-isotropic transition onset of 4,4-azoxyanisole which occurs at 136°C. Heating scans were corrected by determining the temperature lag during the melting of indium (using PP-indium sandwiched films) the onset of which occurs at 156.6°C.

The enthalpy calibration using the enthalpy of melting of Indium of 28.5 J/g and the initial melting Indium endotherm slope calibrations of the DSC machine were performed prior to the measurements. These were done to ensure the correct shape of the melting endotherm and the magnitude of the measured enthalpy change.

Specific heat capacities of the copolymers were calculated from the apparent heat capacities by using a correction factor determined from the DSC trace recorded for a 28.296 mg sapphire standard.

Isothermal Crystallization

Isothermal crystallization experiments were carried out using a Perkin Elmer Pyris 1 DSC.

The samples were prepared by the method described in the preceding section with the exception of the thickness of shims which in this case was 0.1mm.

The masses of DSC samples were kept between 3.000 and 4.000 mg: small enough to avoid heat transfer problems, but large enough to get a reliable stable signal. The appropriate sample sizes were determined in the preliminary experiments where the effect of mass (1.00 to 20.00 mg) on the reproducibility of the DSC signal was studied.

DSC scans were corrected for temperature lag during heating using the melting onset of Indium (using PP-Indium sandwich) which occurs at 156.6°C.

The lowest crystallization temperatures for each copolymer were chosen based on the crystallization onset temperature determined in independent heating/cooling experiments. The runs were conducted using the following program. The materials were melted at 200°C for 5 min, then cooled at 40 °C/min rate to the chosen crystallization temperature, held for 1min, then heated at the 10 °C/min rate to 200°C melted for 5 min, cooled at the 40 °C/min rate to the chosen crystallization temperature, held at this temperature for a specified time, then heated at the 10 °C/min rate to 200°C and the entire process (including 1min crystallization step used as a baseline) was repeated for the next length of crystallization time. The runs were conducted under nitrogen atmosphere.

The samples, crystallization temperatures and times are summarized in Table 4.2.1.

Table 4.2.1 Isothermal Crystallization Conditions

Sample Name	Crystallization Temperature °C	Crystallization Time min
PE-I (0.0, 320)	119.6	2, 4, 8, 16, 32, 64, 128
	120.1	2, 4, 8, 16, 32, 64, 128
	122.1	4, 8, 16, 32, 64, 128
	124.1	8, 16, 32, 64, 128
PE-I (8.2, 300)	78.6	2, 4, 8, 16, 32, 64, 128
	79.1	2, 4, 8, 16, 25, 32, 45, 64
	84.1	10, 16, 32, 64
	86.1	20, 32, 45, 64, 90
PE-I (13.6, 290)	64.6	2, 4, 8, 16, 32, 64, 128
	70.1	8, 16, 32, 45, 60, 90
	72.1	8, 16, 32, 45, 60, 90
PE-I (15.7, 260)	39.6	2, 8, 16, 32, 64, 128
	44.1	8, 16, 32, 60, 90, 120
	45.1	8, 16, 32, 60, 90, 120
PE-II (4.4, 320)	95.1	2, 4, 8, 16, 32, 64, 128, 256
	97.1	2, 4, 8, 16, 32, 64, 128
	99.1	4, 8, 16, 32, 64, 128
	101.1	4, 8, 16, 32, 64, 128
PE-III (7.8, 160)	83	2, 4, 8, 16, 32, 64, 128
	86	4, 8, 16, 32, 64, 128
	88	4, 8, 16, 32, 64, 128
PE-III (12.3, 310)	71	2, 4, 8, 16, 32, 64, 128
	73	4, 8, 16, 32, 64, 128
	75	8, 16, 32, 64, 128

Temperature Modulated DSC (TMDSC)

TMDSC (TA Q1000) in the saw-tooth mode was used in order to evaluate the reversible heat capacity of PE-VII (17.4, 290). A sample of 4.369 mg mass was prepared by the method outlined in the preceding section. The material was cooled under helium purge from 200°C to -90°C at 10°C/min overall rate with the temperature amplitude A of 1°C, period p of 60s and step rate q of 2°C/min.

4.2.2 Density Measurements*

Density measurements were obtained using a Techne™ density column filled with a mixture of isopropanol and water allowing a density gradient in the range of 0.81-0.93 g/cm^3. The water bath surrounding the column was kept at 23°C. The column was calibrated using 14 standardized calibration glass beads.

The materials were prepared by pressing the pellets between two pieces of Kapton™ in a Carver™ hot press with nitrogen purge. Molds made of shims with a thickness of .39 mm were used to regulate the film thickness. The temperature of the press was set to 200°C. The samples were first allowed to melt for 5 min under low pressure; a load of 2.3 metric tons was then applied for 10 sec, followed by release of pressure for 10 sec. The last two steps were repeated 5 times in order to degas the melt and minimize the amount of bubbles in the final film. Finally the films were quenched in ice water.

The samples were crystallized using Perkin Elmer Pyris 1 DSC. They were melted at 180°C for 3 min, cooled to -40°C at the rate of 10°C/min, held at this temperature for 5min and heated to 23°C at the rate of 10°C/min.

The materials were then cut in a variety of shapes with an approximate diameter of 5 mm. Before being dropped inside the density column, the samples were dipped in water in order to avoid creation of bubbles on the material surfaces.

4.2.3 Wide-Angle X-ray Measurements

Wide angle X-ray diffraction experiments were carried out using a Scintag XDS 2000 powder diffractometer operated at room temperature using a CuKα radiation. The diffraction pattern was obtained with a step size of 0.04° and a step duration of 10s. In order to capture the peaks associated with α and γ phases, the measurements were taken for the 2θ angles of 17° to 21°[118].

The materials were prepared by pressing the pellets in a Carver™ hot press with nitrogen purge between two pieces of Kapton™. A mold with a circular opening of 25

* Density column was prepared by Chris Fratini

mm in diameter and with a thickness of 2.53 mm was used to regulate the sample size. The molding temperature was set to 200°C. The samples were first allowed to melt for 5 min under low pressure; a load of 2.3 metric tons was then applied for 10 sec, followed by release of pressure for 10 sec. The last two steps were repeated 10 times in order to degas the melt to minimize the amount of bubbles in the final sample. Finally, the samples were cooled by one of three methods. In the first case, the materials were quenched in ice water. In the second case, they were cooled on the bench top. In the third case, they were slowly cooled to room temperature in the press. The recorded temperature profile for the slowly cooled samples is shown in Table 4.2.2.

Table 4.2.2 X-ray Samples Cooling Profile

Temperature °C	Cooling Rate, °C/min
150 to 100	~ 1.0
100 to 50	1.0-0.1
50 to 25	<0.1

4.2.4 Atomic Force Microscopy (AFM)

AFM experiments were carried out using Digital Instrument, Dimension 3000 multi-mode atomic force microscope operated in the tapping mode at room temperature.

The materials were prepared by first dissolution of the polymer in boiling xylene at 140°C. Then the samples were obtained by spin-coating onto a silanized silicon wafer.

4.2.5 Scanning Electron Microscopy (SEM)

SEM experiments were carried out using a LEO 1550 scanning electron microscope with accelerating voltage of 5kV. Prior to the analysis, the materials were coated with gold using BAL-TEC SCD 05 sputter coater to minimize charging.

The scanning was complicated by the fact that the propylene-ethylene copolymers were easily damaged by the electron beam. In order to minimize the surface damage, the

sample sweeping time was kept as small as was possible for obtaining a good quality image.

The SEM samples were prepared from the films pressed by the same method as the one outlined in the material preparation section for the isothermal crystallization studies. Samples of a variety of shapes were then cut out of the films and recrystallized under nitrogen atmosphere on a glass cover slip in a TC 91/ THMS 600 Linkam hot stage by melting at 200°C for 2min followed by cooling to room temperature at 1°C/min rate.

In order to obtain the SEM images with better resolution, the first batch of samples was etched. The etching was carried out in a solution containing 60 ml of concentrated H_2SO_4, 0.454g of $KMnO_4$ and 30ml of 85 v/v %H_3PO_4. The etching removed some of the amorphous material from the samples; however, it did not significantly improve the SEM image quality (due to staining by the $KMnO_4$ solution). As a result, the etching was not used for the other batches of SEM samples. The images obtained from etched samples will be specified when the SEM results will be presented.

5 CALORIMETRY ANALYSIS

5.1 Heat Capacity Calculations

A Differential Scanning Calorimeter measures the difference in the heat flow between the sample pan and the empty reference pan as the temperature changes linearly with time or under isothermal conditions as time elapses. For the illustration, the *raw sample DSC* output for the data collected during cooling of PE-I (0.0, 320) is shown as a function of temperature and time in Figure 5.1.1 and Figure 5.1.2 respectively.

In order to convert this data into a heat capacity curves, it is necessary to obtain the *heat displacement curves* for the sample, the sapphire and the baseline (if the baseline is not already subtracted from the sample and the sapphire scans). The initial displacement curves (D') (shown in Figure 5.1.3 for PP sample) are obtained by fitting the stable part of the isotherm at both ends of the scan, drawing the displacement baseline (shown in red) through the red points and finally subtracting the baseline from the sample curve (Equation 5.1.1, Equation 5.1.2 and Equation 5.1.3).

$$D'_{sample} = Heatflow_{sample} - Baseline_{displacement(sample)} \quad \textbf{Equation 5.1.1}$$

$$D'_{sapphire} = Heatflow_{sapphire} - Baseline_{displacement(sapphire)} \quad \textbf{Equation 5.1.2}$$

$$D_{baseline} = Heatflow_{baselin} - Baseline_{displacement(baseline)} \quad \textbf{Equation 5.1.3}$$

If the sample baseline has been already subtracted by the DSC program, then the true displacement curve is equal to the initial displacement curve:

$$D_{sample} = D'_{sample} \quad \textbf{Equation 5.1.4}$$

$$D_{sapphire} = D'_{sapphire} \quad \textbf{Equation 5.1.5}$$

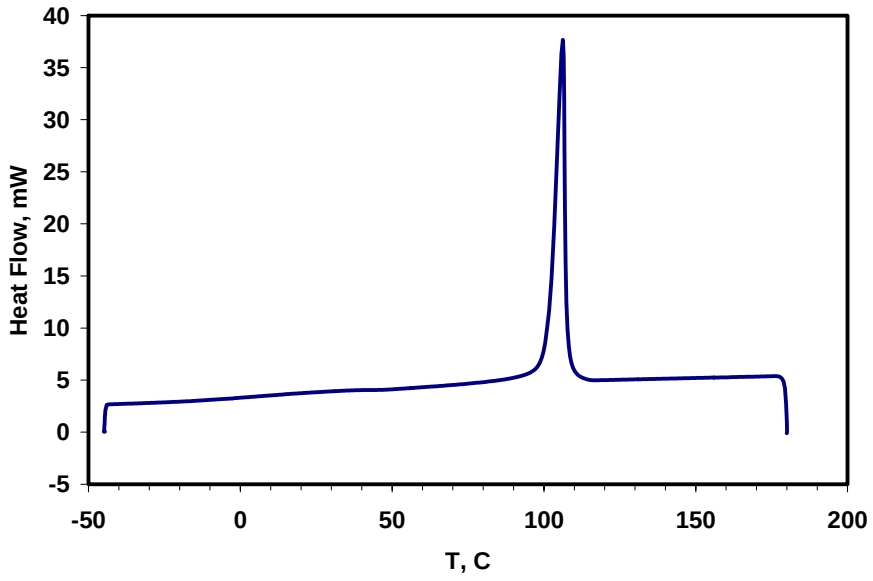

Figure 5.1.1 Raw DSC cooling curve of PE-I (0.0, 320) as a function of temperature

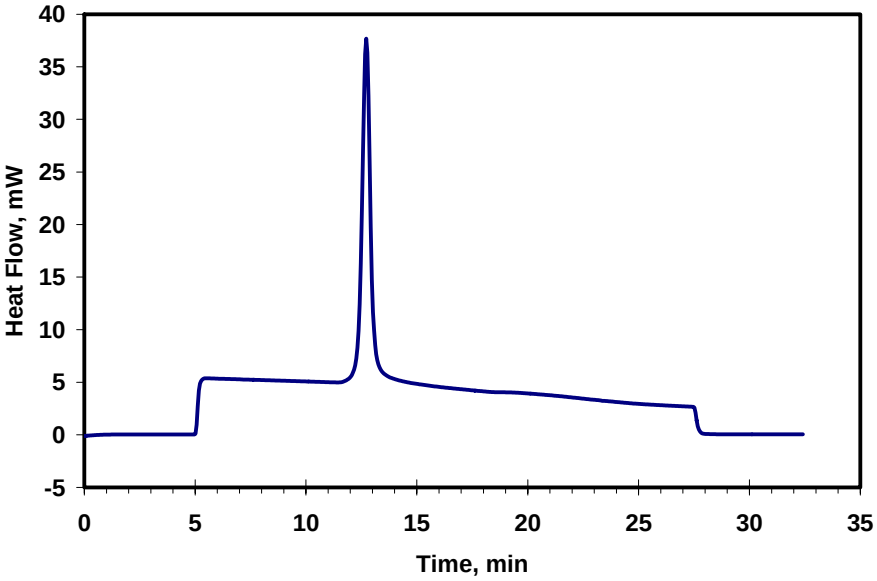

Figure 5.1.2 Raw DSC cooling curve of PE-I (0.0, 320) as a function of time

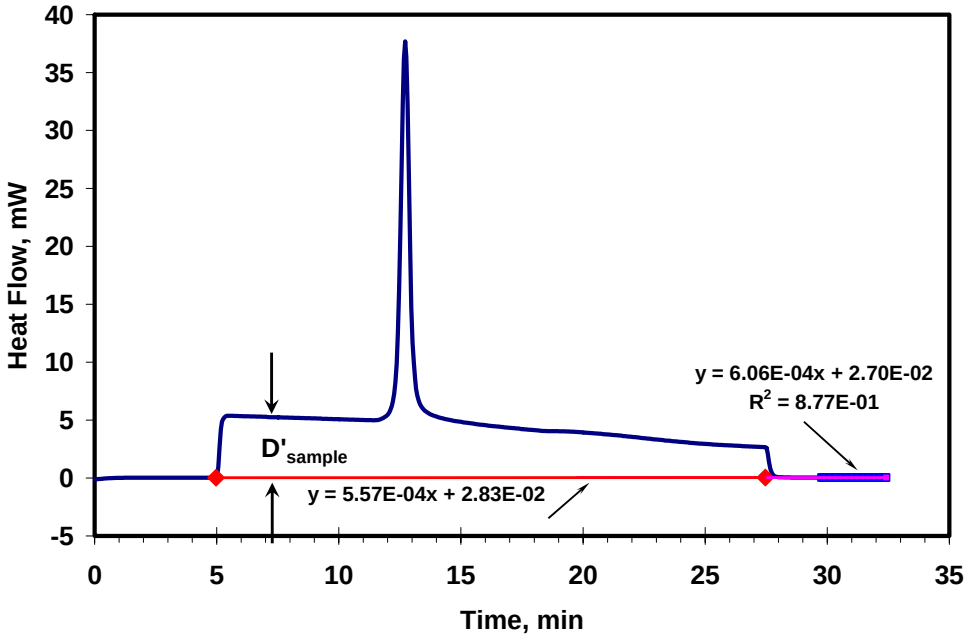

Figure 5.1.3 Calculation of the Heat Displacement Curve

Otherwise, the true displacement curve is determined by subtracting the baseline displacement from the sapphire and the sample initial displacements:

$$D_{sample} = D'_{sample} - D_{baseline} \qquad \textbf{Equation 5.1.6}$$

$$D_{sapphire} = D'_{sapphire} - D_{baseline} \qquad \textbf{Equation 5.1.7}$$

The heat displacement in mW is then converted to an apparent heat capacity in J/g*K (Figure 5.1.4) by taking into account the heating/cooling rate (R) and the masses of the samples (W):

$$Cp_{apparent}(sample) = \frac{D_{sample}}{R_{scanning} * W_{sample}} \qquad \textbf{Equation 5.1.8}$$

$$Cp_{apparent}(sapphire) = \frac{D_{sapphire}}{R_{scanning} * W_{sapphire}} \qquad \textbf{Equation 5.1.9}$$

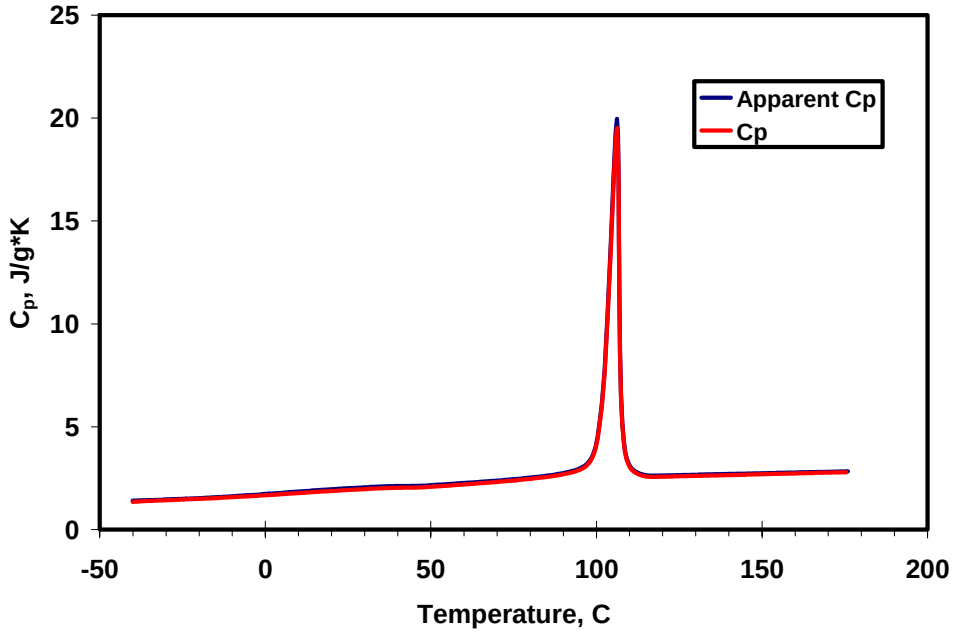

Figure 5.1.4 PP Heat Capacities

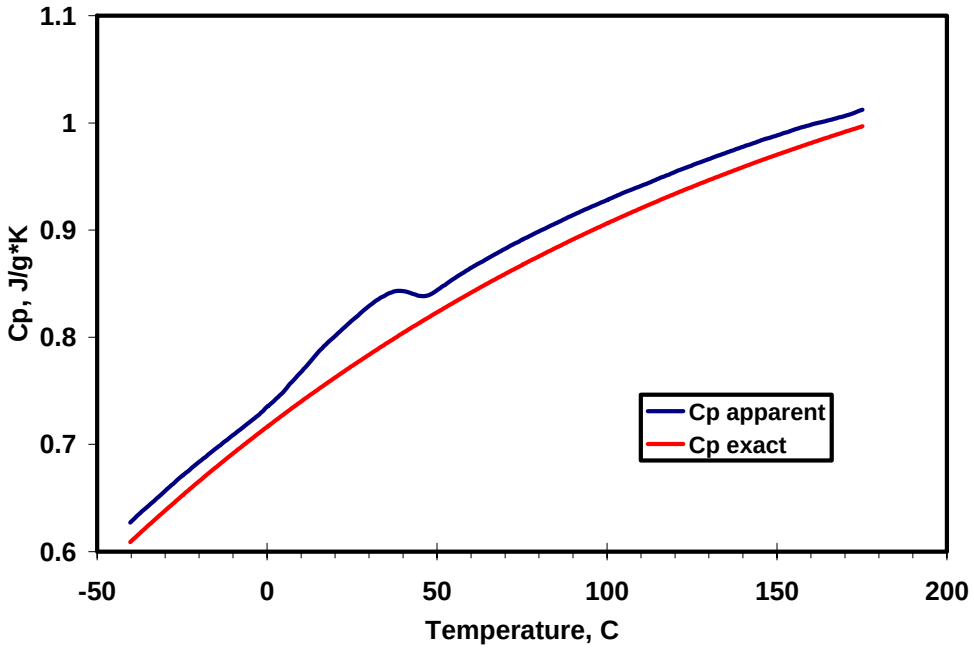

Figure 5.1.5 Sapphire C_p Apparent and C_p Exact

The correction factor (F_c) is obtained by dividing the exact heat capacity of sapphire standard[119] by the measured apparent sapphire standard heat capacity (Equation 5.1.10).

$$F_c = \frac{Cp_{exact}(sapphire)}{Cp_{apparent}(sapphire)} \qquad \textbf{Equation 5.1.10}$$

Sapphire standard exact and apparent heat C_p's as well as F_c are shown in Figure 5.1.5 and Figure 5.1.6 respectively. The heat capacities of the samples are then calculated by multiplying the apparent heat capacities by the correction factor F_c (Figure 5.1.4):

$$Cp(sample) = Cp_{apparent}(sapphire) * F_c \qquad \textbf{Equation 5.1.11}$$

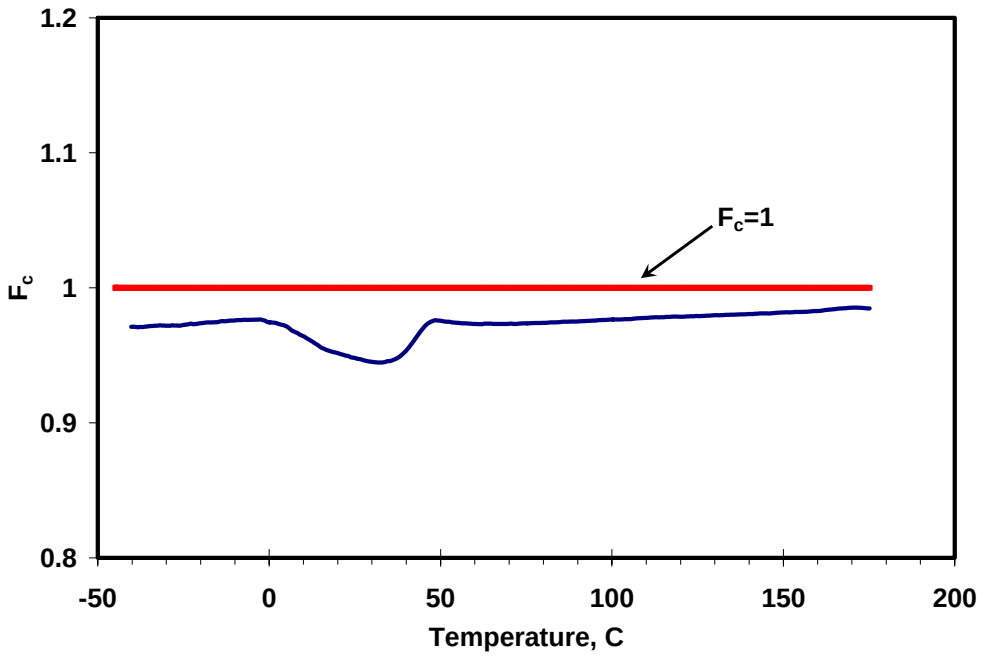

Figure 5.1.6 Correction Factor (F_c)

5.2 Crystallinity Analysis

Crystallinity measurements are routinely performed in order to characterize and compare materials as well as predict their properties. There are several methods to analyze DSC data to find the crystallinity. The easiest and most commonly used approach is to integrate the area under the crystallization or melting curve to get the enthalpy and divide it by the thermodynamic heat of fusion (ΔH_f^0) of a 100% crystalline material at melting (value generally found in the literature). While this approach is straight forward and convenient and gives a "back of the envelope" estimate of the degree of crystallinity, it lacks accuracy. First, it does not take into consideration the temperature dependence of ΔH_f^0, which, on the basis of heat capacity measurements[120], is expected to change for PP from 207 J/g at 188°C to 150 J/g at 0°C. Second, it uses an arbitrarily drawn heat capacity baseline from an arbitrary temperature at the beginning of the crystallization or melting curve to an equally arbitrary temperature at the end of that curve. A more accurate approach[117] for determination of crystallinity involves the use of the true specific heat capacity curve, based on specific heat capacities of fully crystalline (C_{pc}) and fully amorphous (C_{pliq}) PP and considering the temperature dependence of ΔH_f^0. This approach assumes a two phase morphological model consisting of amorphous and crystalline regions. This method is used in this work for crystallinity calculations on propylene-ethylene copolymers. The values for C_{pc}, C_{pliq} and ΔH_f^0 are derived using the empirical rule of mixture for random copolymers from the ATHAS database composed by Wunderlich.[120]

In theory, if the correction using the sapphire standard is done correctly and the C_{pliq} and C_{pc} curves are representative of the material behavior in the melt and glass regions respectively, no further data manipulation is necessary. However, often, when the measurements are performed using the DSC equipment, there is a mismatch between the C_{pliq} and C_{pc} curves and the measured heat capacity curves. In some cases a complete match of the glassy and melt baselines can be achieved by simply shifting the experimental heat capacity curves up or down. In other cases, a choice must be made between matching the experimental and theoretical heat capacity baselines in the melt or in the glass region. In this latter case, the remaining unmatched baseline is artificially

raised or lowered until the theoretical and experimental baselines coincide. (Note that uncertainties of about 2-3 % in the baseline heat capacities are expected.) In this work, when such a mismatch was encountered, the sample heat capacity curves were matched in the glass region with a C_{pc} curve and the data points in the melt were raised or lowered to match a C_{pliq} curve. The implications of different shifting procedures as well as the logic behind matching the curves in the glassy region will be discussed in Section 5.3.

An example of two-phase model analysis is shown in Figure 5.2.1. It is assumed that the specific heat capacity of a material (C_{pb}) in the absence of thermal transitions lies between the specific heat capacities of the fully crystalline and the fully amorphous materials[117]:

$$C_{pb}(T) = X^{c}(T)C_{pc}(T) + X^{a}(T)C_{pliq}(T) \qquad \textbf{Equation 5.2.1}$$

with

$$X^{c}(T) + X^{a}(T) = 1 \qquad \textbf{Equation 5.2.2}$$

where X_c is mass fraction crystallinity. The crystallinity X_c is then calculated at each small temperature interval by using C_p, ΔH_f^o, C_{pb}, C_{pc}, and C_{pliq}. The exact algorithm involved in this calculation is shown in the Appendix 1.

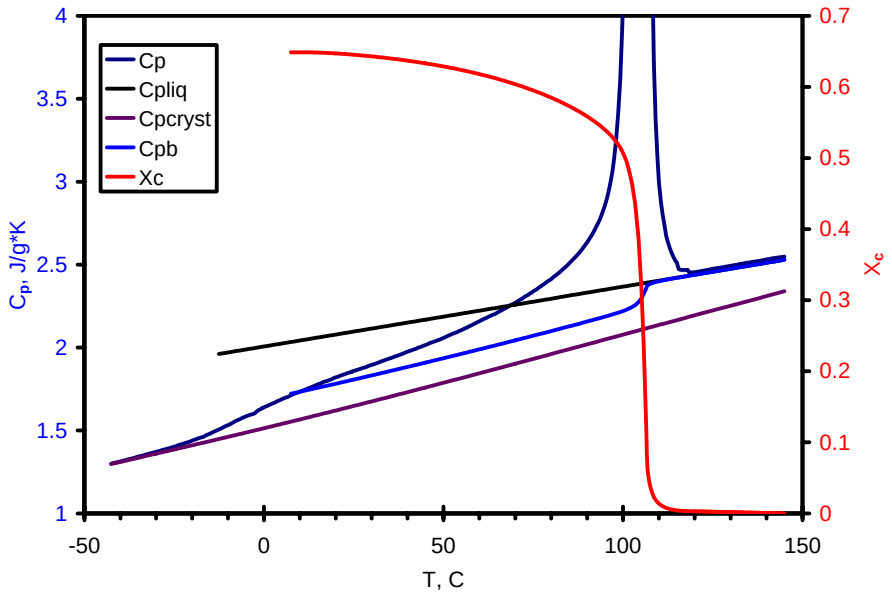

Figure 5.2.1 Sample Crystallization Analysis Trace of PP

According to a two-phase model, the crystallinity values obtained from the area calculation and from the value of C_p just above T_g (based on its position between C_{pc}, and C_{pliq}) have to be the same (Equation 5.2.3).

$$\Delta H_f^0(T) = \Delta H_f^0(T_m) + \int_{T_m}^{T} \left[C_{p_c}(T) - C_{p_{liq}}(T) \right] dT \qquad \textbf{Equation 5.2.3}$$

Propylene-ethylene copolymers were analyzed by the method outlined above with the ΔH_f^0 value of 207 J/g taken from the ATHAS database[120]. It was assumed that the C_{pliq} values for the copolymers are the weight average values of the propylene and ethylene homopolymers. Using the rule of mixture, they were calculated by Equation 5.2.4.

$$C_{p_{liq}}^{P/E}(T) = \phi C_{p_{liq}}^{PE}(T) + (1-\phi) C_{pliq}^{PP}(T) \qquad \textbf{Equation 5.2.4}$$

where the P/E denotes propylene-ethylene copolymer, PE – polyethylene, PP – polypropylene and ϕ is the weight fraction of ethylene. The assumption of additivity of homopolymer heat capacities was tested by evaluating the reversible heat capacity of PE-VII (17.4, 290) using TMDSC (Figure 5.2.2). Since the calculated and measured heat capacities are in agreement, both in the melt and in the glassy state, this approximation should be satisfactory for further analysis.

The analysis of P/E (0.0, 330) is shown in Figure 5.2.3. In this sample, the crystallinity determined from the area calculation is 48% and the crystallinity determined from the C_p value just above T_g (marked by point A) is 65%. Clearly, this result is in a direct disagreement with the Equation 5.2.3. Identical problems were encountered during the analysis of all propylene-ethylene copolymers.

The following sections described two possible approaches for resolution of the crystallinity mismatch dilemma. Application of these approaches for Dow Chemical copolymers will be discussed in Chapter 6.

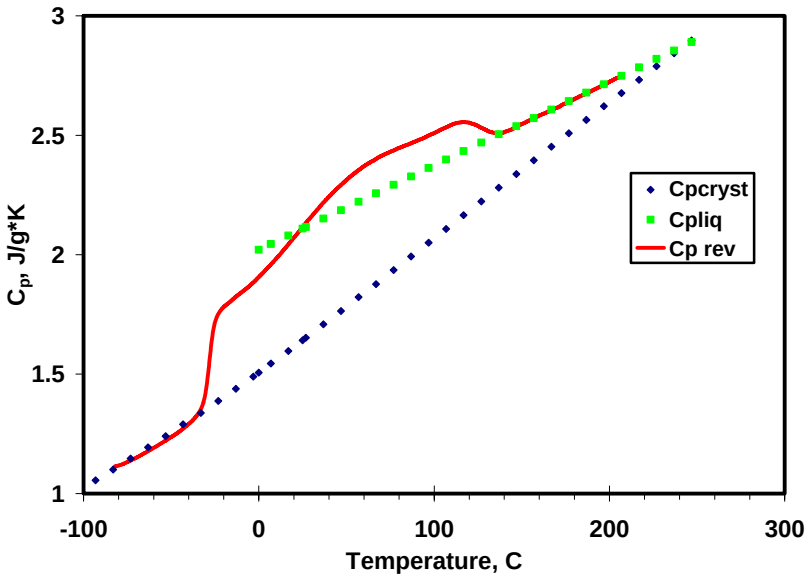

Figure 5.2.2 Reversible Heat Capacity of PE-VII (17.4, 290)

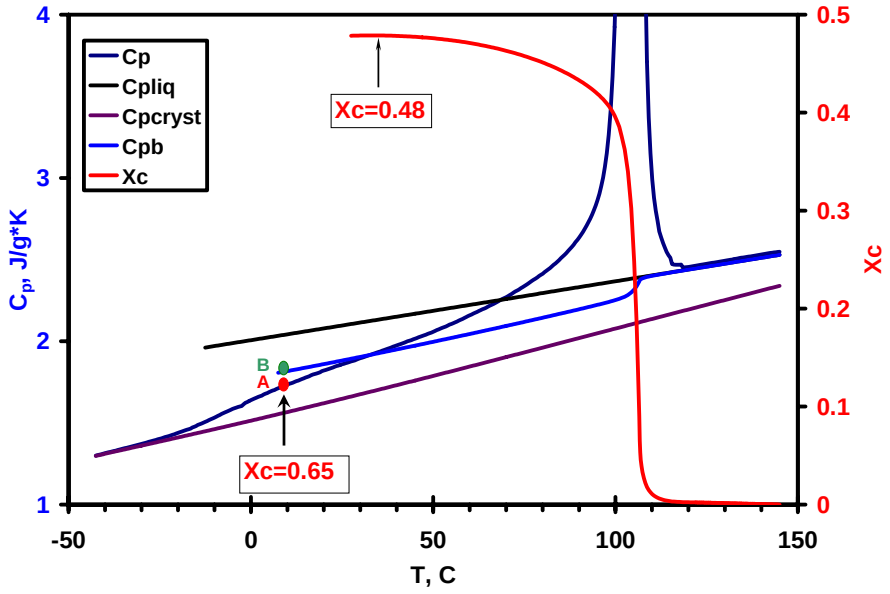

Figure 5.2.3 Crystallization of P/E (0.0, 330), ΔH_f^0 =207 J/g

5.2.1 Ethylene Inclusion Analysis

The two-phase model analysis of crystallinity outlined in the previous section does not specifically address the issue of copolymer inclusion and exclusion from the crystal. The thermodynamic constants used to calculate the thermal properties of the propylene-ethylene copolymer crystals were the equilibrium polypropylene thermodynamic heat of fusion ΔH_f^0 at melting temperature T_m^0 for pure polypropylene.

The Sanchez-Eby kinetic theory of random copolymers[34,35], discussed in Section 2.3, allows for the incorporation of comonomer units into the crystal. It also shows that as a result of such incorporation the equilibrium melting temperature and the thermodynamic heat of fusion of the equilibrium copolymer crystal decrease.

The following analysis assumes that as a result of defect incorporation, either in the form of copolymer units or of regio and stereo errors, the resulting crystal thermodynamic heat of fusion decreases. The validity of this analysis will be discussed in Chapter 6.

If the thermodynamic heat of fusion depression assumption is accepted, the mismatch in crystallinity between the ΔH and the C_p calculation can be explained by an overestimation in the ΔH_f^0 values. Use of an unreasonably high thermodynamic heat of fusion leads to the underestimation of the crystalline phase contribution to the overall specific heat capacity. As a result, the baseline C_{pb} is too large and the crystallinity determined by ΔH calculations is lower than determined from the baseline heat capacity.

If the P/E (0.0, 330) polymer is analyzed with the lower ΔH_f^0 of 165 J/g, an excellent consistency in the degrees of crystallinity from two calculations is observed (Figure 5.2.4).

In this analysis values of thermodynamic heat of fusion lower than 207 J/g ΔH_f^0 were used in the crystallinity calculations of all propylene-ethylene copolymers. ΔH_f^0 values were found iteratively by matching crystallinities obtained from the area calculation and from the magnitude of C_p just above T_g.

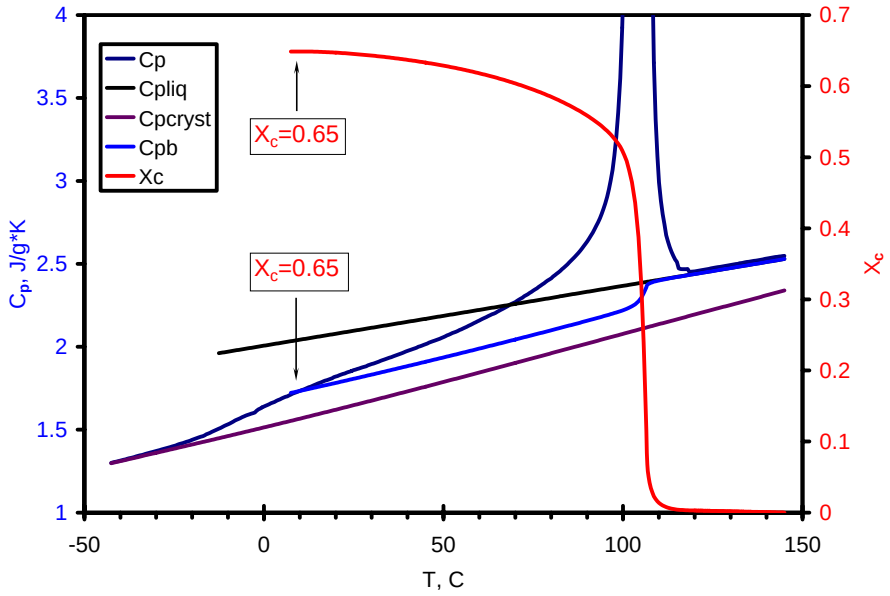

Figure 5.2.4 Crystallization of P/E (0.0, 330), ΔH_f^0 =165 J/g

5.2.2 RAF Based Analysis

The second analysis is based on the three-phase model that considers the contribution from the rigid amorphous heat capacity (RAF) to the overall heat capacity. The concept of RAF was developed by Wunderlich[89,91,92] and has been discussed in Section 2.5.2.

This analysis utilizes the same treatment of the crystallinity as was used in the polypropylene study by Grebowicz et al.[91] (Section 2.5.2). The mismatch in the crystallinity between ΔH and the C_p (T_g) calculations in Figure 5.2.3 is attributed to the presence of a RAF.

In this case, the thermodynamic heat of fusion of the equilibrium propylene-ethylene crystal is assumed to be the same as it was for the equilibrium propylene crystal. It is assumed that the measured heat capacity is underestimated due to the presence of a RAF. If a RAF were not there, the point A in Figure 5.2.3 would be moved to a point B resulting in the 48 % crystallinity calculated at C_p (T_g). As a result, the crystallinity from

ΔH and the C_p (T_g) calculations would match. The crystallinity is obtained from the area calculations and both amorphous and rigid fractions are calculated using Equation 2.5.5.

The applicability of this analysis to Dow propylene-ethylene copolymers will be discussed in Chapter 6.

5.3 Uncertainty Analysis

In this section the uncertainty in the thermodynamic heat of fusion calculations due to different procedures of matching the C_{pliq} and C_{pc} curves and the measured heat capacity curves will be discussed.

Two possible sources of uncertainty have been identified, namely the experimental error due to the instrument limitations and the error in the theoretical C_{pliq} and C_{pc} curves themselves.

It is generally accepted that TA Q1000 DSC is capable of measuring accurate heat capacities in the glassy region.[121] The possible inaccuracies of the melt region measurements can then be corrected by subsequent sapphire correction summarized in Section 5.1. Since in our case the mismatch between the measured and theoretical heat capacity curves for some samples is still present after sapphire calibration, this correction is not sufficient. In light of this, in order to use the theoretical C_{pliq} and C_{pc} curves in crystallinity calculations, the measured C_p is matched in the low temperature region by shifting C_p curves up or down. The remaining deviation from the C_{pliq} curve in the melt for both cooling and melting traces is demonstrated in Figure 5.3.1. Most of the differences between the measured and the theoretical melt heat capacities fall within 2% of the theoretical values. This deviation is corrected in the final step by raising or lowering the experimental data points corresponding to the melt region prior to the transition onset until they match with the C_{pliq} (Figure 5.3.2) (Method 1).

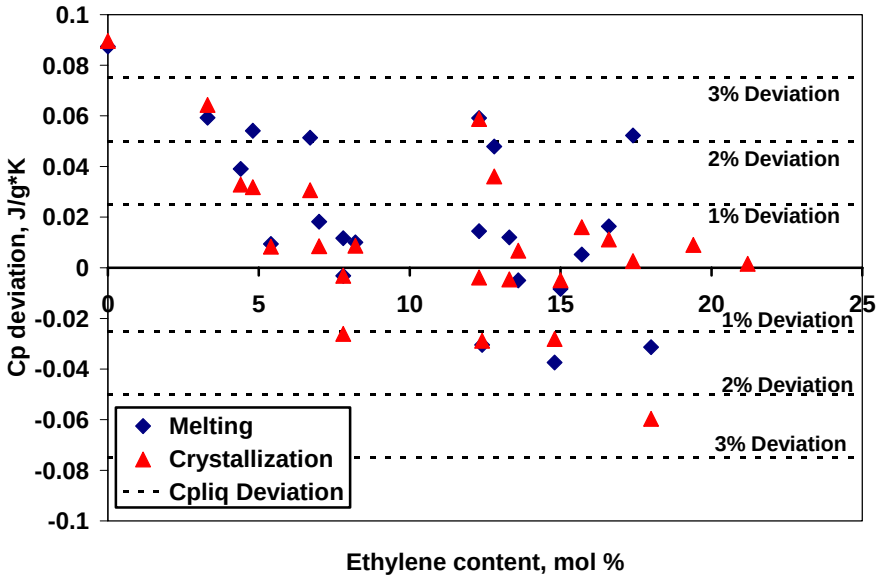

Figure 5.3.1 Deviation of C_p from the C_{pliq} in the Melt

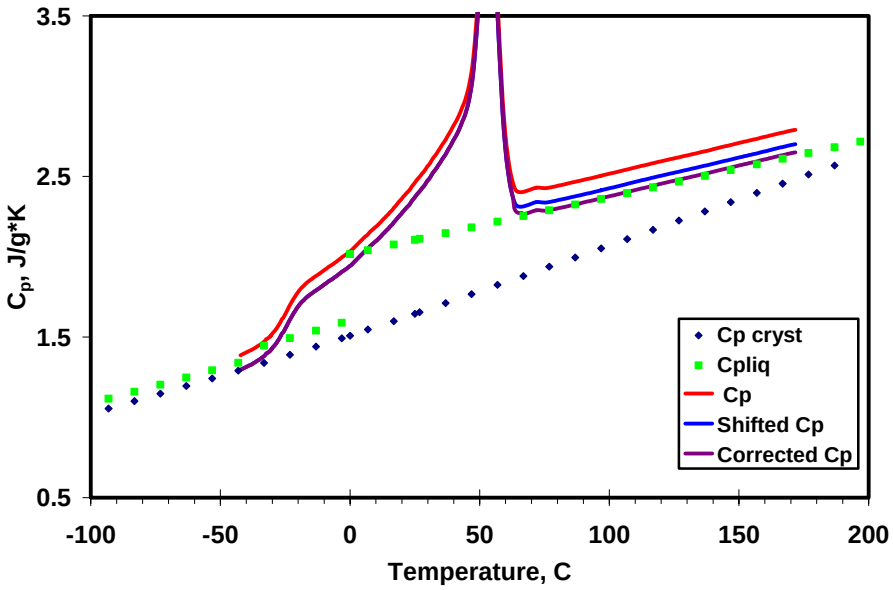

Figure 5.3.2 PE-III (12.3, 310) C_p Corrections

The theoretical C_{pliq} curves for the copolymers were calculated based on the weight average values of the propylene and ethylene homopolymers. While the rule of mixture assumption was tested using reversible heat capacity measurements for PE-VII (17.4, 290), the calculated amorphous and crystalline heat capacity curves might not be

representative of the real copolymer system. In this case the possible solution to the mismatch problem would be first matching the measured C_p curves either in melt or in the glass and then raising or lowering the theoretical C_{pliq} or C_{pc} curves respectively until the agreement between the curves both in the melt and in the glass is achieved (Method 2 and 3).

In order to estimate the uncertainty on the calculated thermodynamic heat of fusion, the crystallinity for several materials was determined by all three possible matching scenarios. In addition, the analysis in which the curves were matched only in the glass without any further data manipulation was added to the uncertainty calculations (Method 4). The results are demonstrated in Figure 5.3.3 and Table 5.3.1. The line in the Figure 5.3.3 corresponds to the linear fit through ΔH_f^0 values calculated from the crystallization data. These results suggest that the uncertainty is due to errors in both, instrumental limitations and theoretical C_{pliq} or C_{pc} curves. These conclusions will be important in Chapter 6, when the accuracy of the theoretical heat of fusion calculations will be discussed.

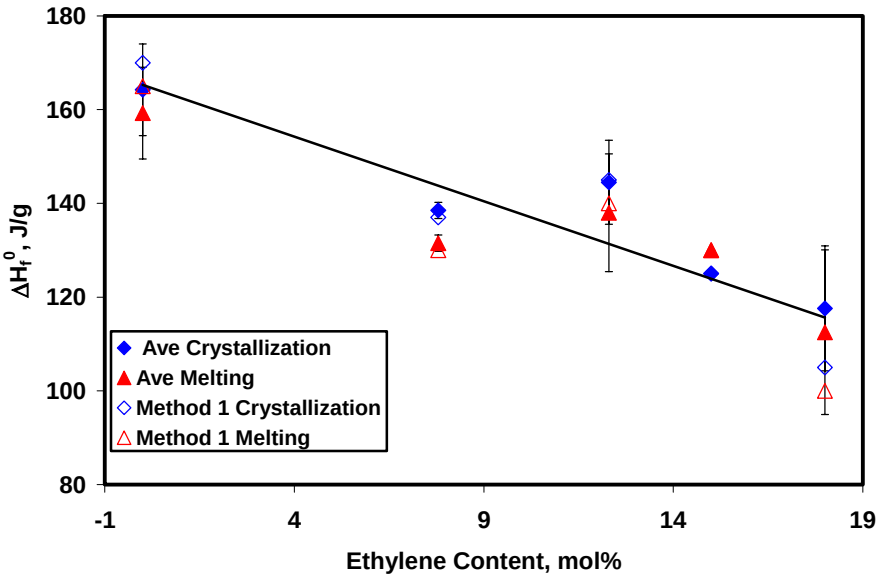

Figure 5.3.3 Heat of Fusion Uncertainty Analysis

Table 5.3.1 Heat of Fusion Uncertainty Analysis

Sample Name	Melting ΔH_f^0, J/g	Crystallization ΔH_f^0, J/g
PE-I (0.0, 320)	159.2 ± 9.8	163.0 ± 9.1
PE-III (7.8, 160)	139.5 ± 1.7	138.5 ± 1.7
PE-III (12.3, 310)	138.0 ± 12.6	144.5 ± 9.0
PE-III (15.0, 120)	130.0 ± 0.0*	125.0 ± 0.0*
PE-VI (18.0, 320)	112.5 ± 17.6	117.6 ± 13.3

* In this case the perfect match between the experimental and theoretical heat capacity curves was obtained without any data manipulation

5.4 T_g Determination

Thermodynamically, the glass transition is a pseudo-second order transition and, consequently, is marked by a step in the specific heat capacity curve. Five distinct temperature regions of the glass transition were described by Cheng et al.[92] and are demonstrated in Figure 5.4.1.

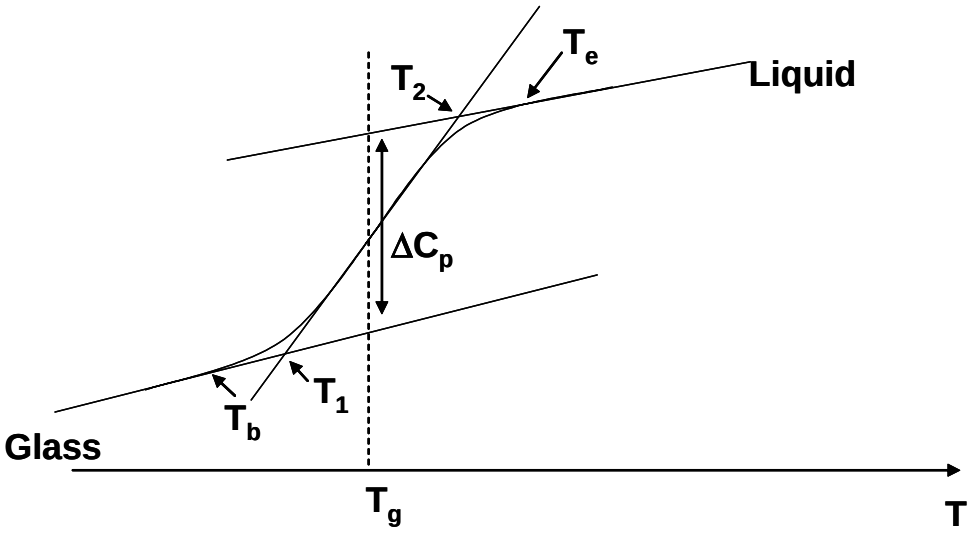

Figure 5.4.1 Schematic DSC Trace in the Glass Transition Region

T_b and T_e temperatures correspond to the first deviation from either the crystalline or the amorphous heat capacity curves on both sides of the transition. The temperatures T_1 and T_2 mark the beginning and the end of the major part of the transition and are used

in the calculations of the glass transition breadth. The glass transition temperature T_g corresponding to the half-devitrification, as judged by the heat capacity step increase.

In order to determine the ΔC_p change at T_g in this work, the glass and the liquid heat capacities adjacent to the glass transition onset were fitted by a linear fit. ΔC_p was then calculated by subtracting the values of the fit at the temperature corresponding to T_g.

5.5 Melting and Crystallization Temperatures

In this work, the concepts of the melting peak, onset and offset temperatures and crystallization peak, onset and offset temperatures will be used to describe the melting and the crystallization behavior of Dow copolymer system. Ordinarily, it is sufficient to define only the peak transition temperatures. However, as will be demonstrated in the next chapters, these propylene-ethylene copolymers have broad crystallization and melting transitions and the introduction of the onset and the offset concepts thus becomes necessary.

The typical melting curve is demonstrated in Figure 5.5.1. The melting temperature T_m is defined at the peak of the melting endotherm at point 2. The melting onset temperature is defined at point 1. Point 1 corresponds to the intersection of the extended baseline and the extended slope of the left side of the melting curve. Similarly, the melting offset temperature is defined at point 3. Point 3 corresponds to the intersection of the extended baseline and the extended slope of the right side of the melting curve. The crystallization temperature, T_x is defined at the peak of the crystallization curve. The onset and the offset crystallization temperatures are defined similarly to those for the melting temperatures, except that point 1 on the curve would correspond to the crystallization offset and point 3 would correspond to the crystallization onset.

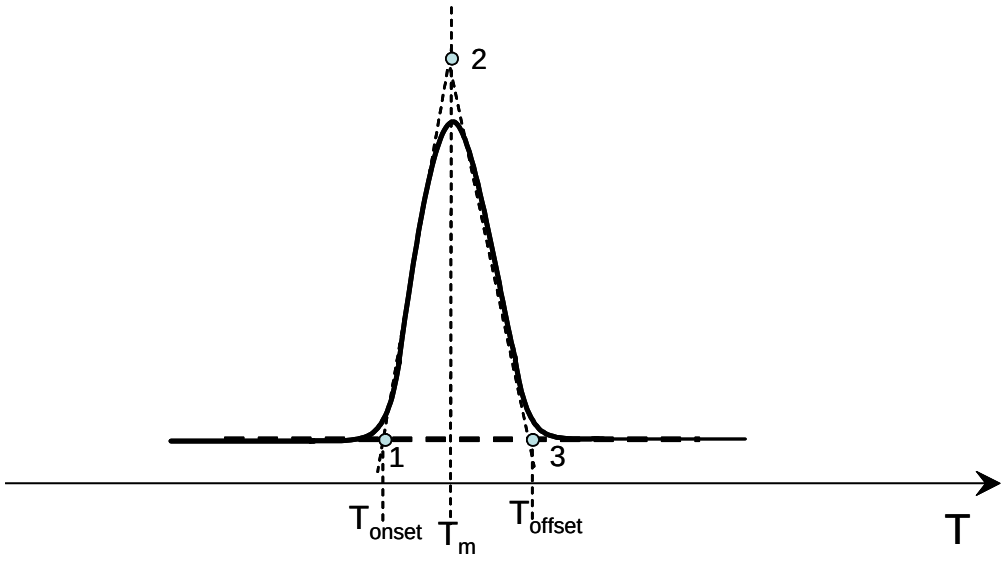

Figure 5.5.1 Schematic DSC Trace in the Melting Region

5.6 Kinetics of Isothermal Crystallization

The DSC data recorded during isothermal crystallization can provide information about the crystallization kinetics. In our case, as it will be discussed in Chapter 6, two melting peaks are observed during heating following the isothermal crystallization, which correspond to the two distinct crystal populations.

The rate of shift of the melting temperature $B(T_x)$ for low and high endotherms defined by Equation 5.6.1 can be calculated from the slope of the melting temperature T_m as a function of logarithm of time plot.

$$T_m = T_x + A(T_x) + B(T_x)\log(t_x) \qquad \textbf{Equation 5.6.1}$$

The deconvolution of the low and high endotherms was accomplished by drawing a vertical line at the lowest point of the valley between the corresponding peaks.

6 ANALYSIS OF DOW PROPYLENE-ETHYLENE COPOLYMERS

6.1 Results

In this section the results of the studies of bulk propylene-ethylene copolymers properties will be presented. First, the results of crystallization and melting behavior studies of Dow, Ziegler-Natta and Metallocene copolymers will be given. Then the results of the crystallinity and the thermodynamic heat of fusion calculations will be shown for both inclusion and RAF models. Finally, the results of the morphology studies of Dow materials will be presented.

6.1.1 Crystallization and Melting Studies

The apparent heat capacities during crystallization and melting for different series of copolymers were calculated from the DSC data by the method outlined in section 5.1 and are shown in Figure 6.1.1 and Figure 6.1.2. There is a steady decrease in the peak crystallization and melting temperatures with an increase in the ethylene content in all sets of data as demonstrated in Figure 6.1.3. The peak crystallization and melting temperatures of Dow Chemical copolymers follow the same linear trends throughout all series. The rate of decrease in the peak crystallization temperature is comparable with the rate of decrease in the peak melting temperature as judged by the slopes of the linear fits of two sets of data. The differences between samples from different series of Dow copolymers are evident when the materials of about the same composition are compared in Figure 6.1.5 and the results, demonstrated in Figure 6.1.6 and Figure 6.1.7, are examined. While the crystallization peak onsets follow the same linear decrease with increase in ethylene content for the copolymers of all series, the melting offsets do not. The change in the melting offsets with ethylene content for series I-III is similar to the change in the crystallization onsets. However, series VII and VIII demonstrate different trends. The change in the melting offsets is significantly lower than for series I-III,

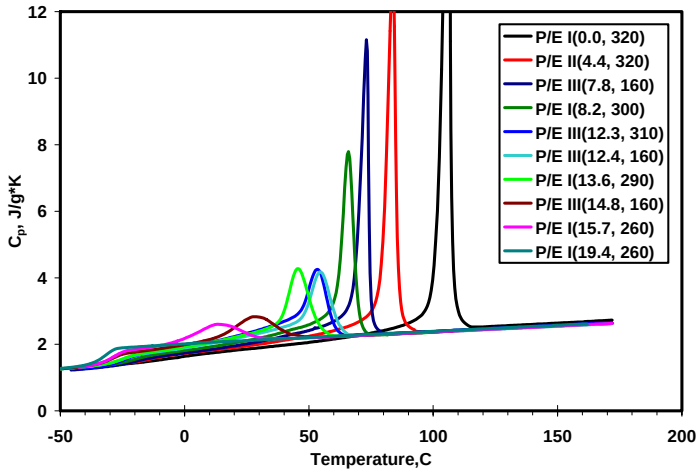

a)

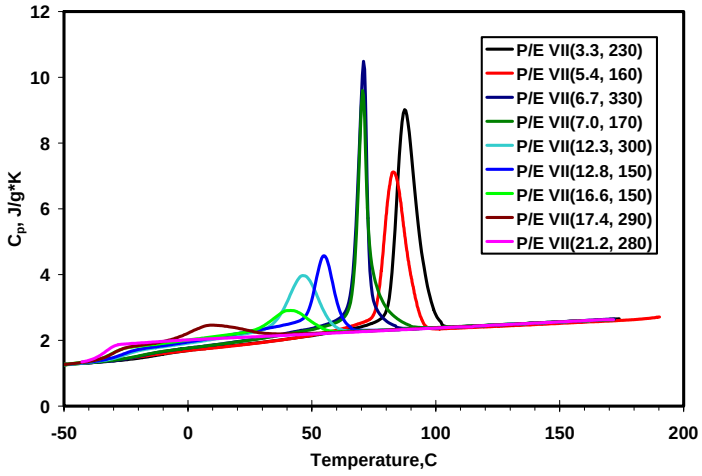

b)

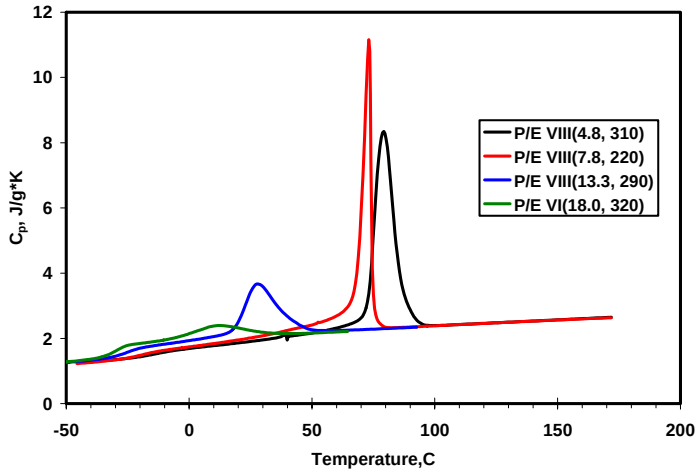

c)

Figure 6.1.1 DSC Crystallization Traces of Dow Copolymers: a) Series I-III, b) Series VII, c) Series VI and VIII

a)

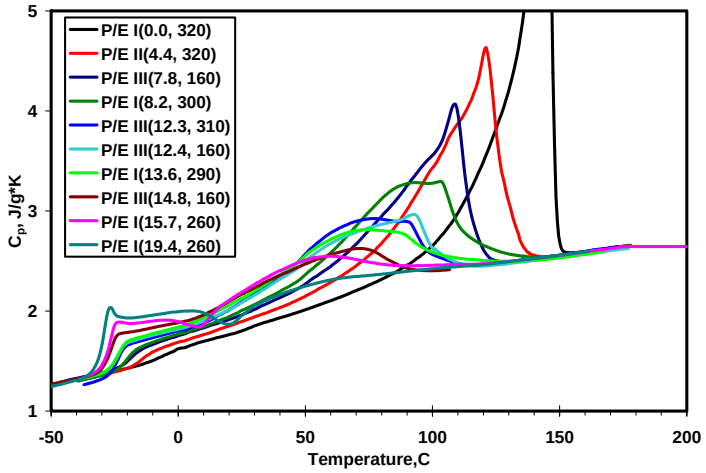

b)

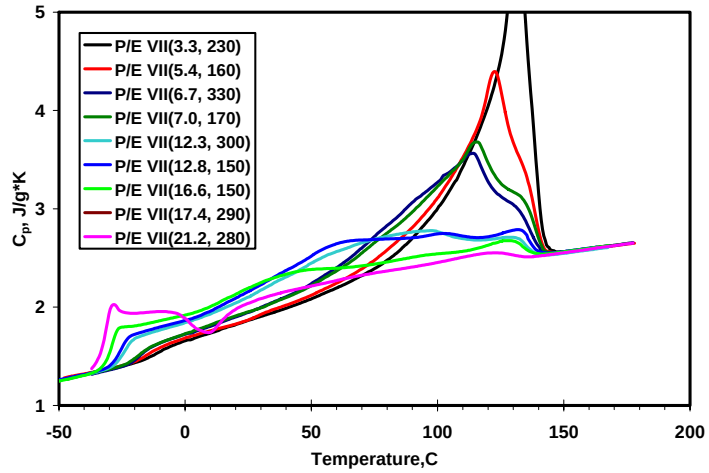

c)

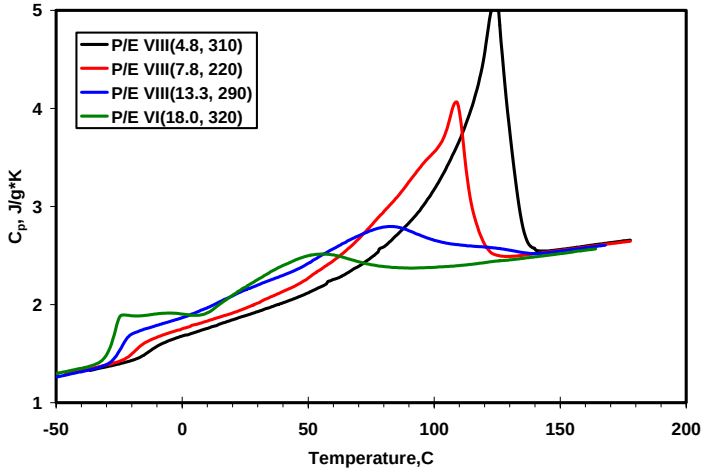

Figure 6.1.2 DSC Melting Traces of Dow Copolymers: a) Series I-III, b) Series VII, c) Series VI and VIIII

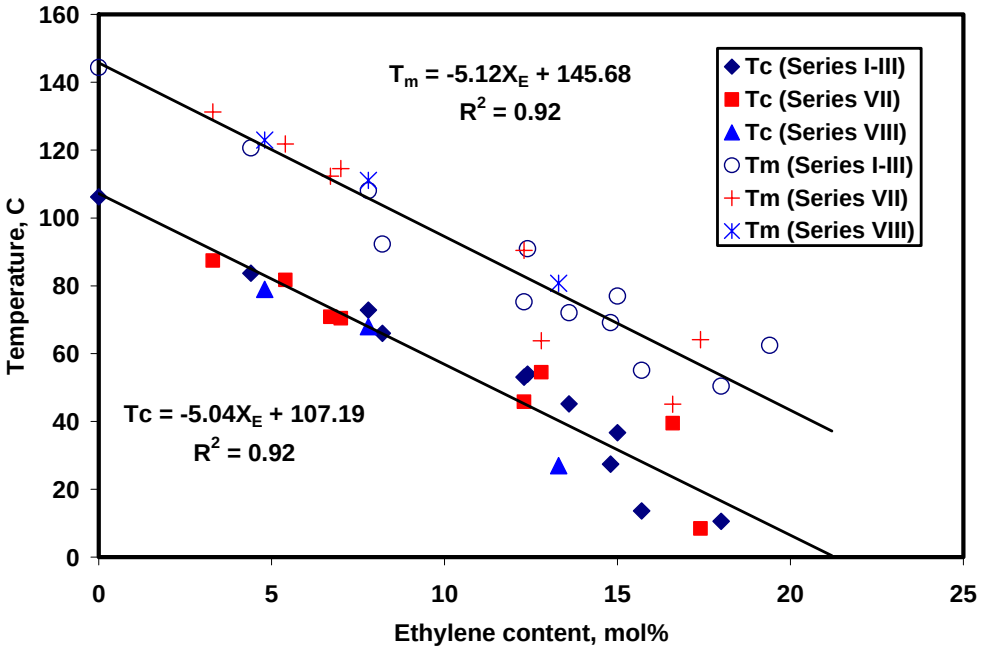

Figure 6.1.3 Crystallization and Melting Peak Temperatures of Dow Copolymers as a Function of Ethylene Content

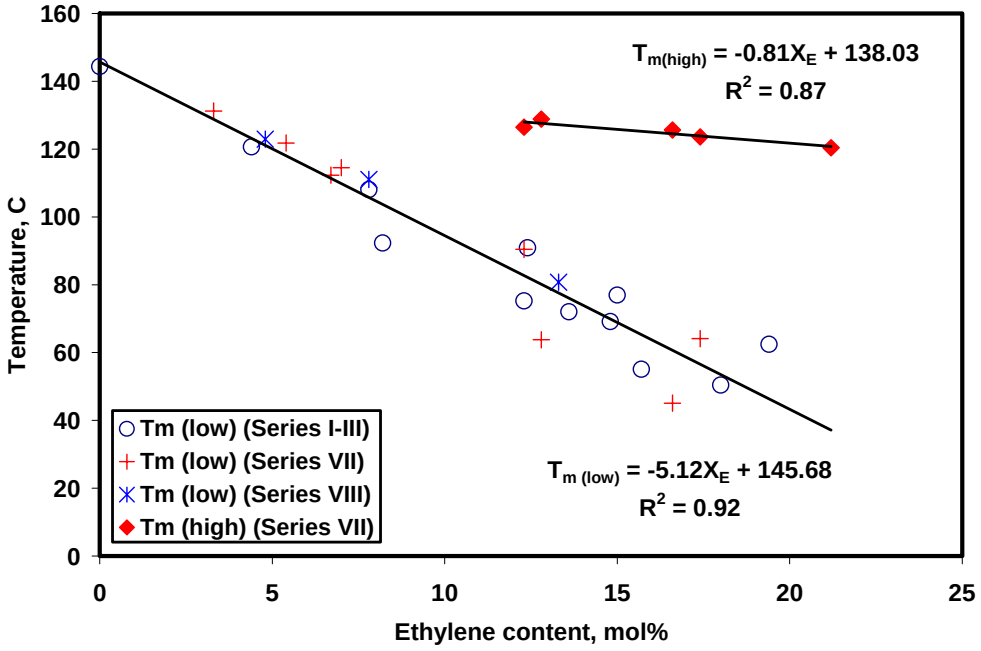

Figure 6.1.4 Low and High Melting Endotherms (Dow Copolymers) as a Function of Ethylene Content

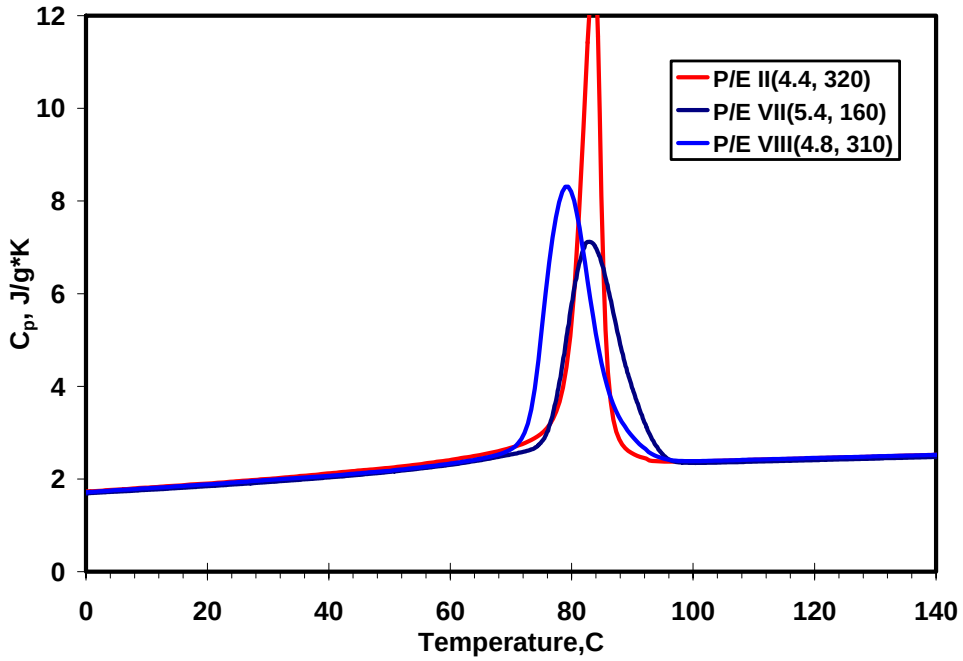

a)

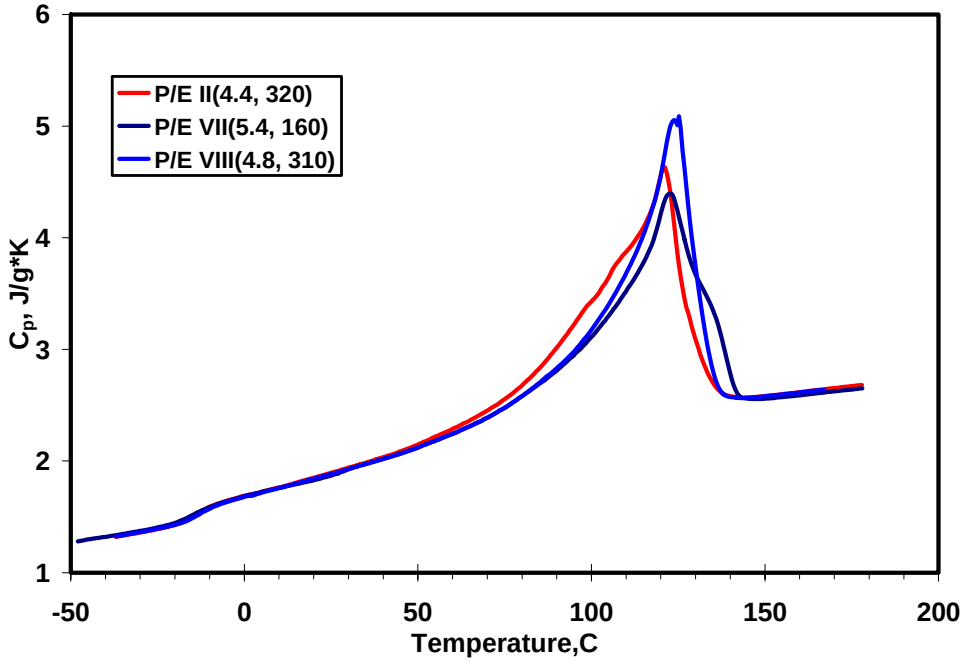

b)

Figure 6.1.5 Comparison of Dow Copolymers a) DSC Crystallization Traces, b) DSC Melting Traces

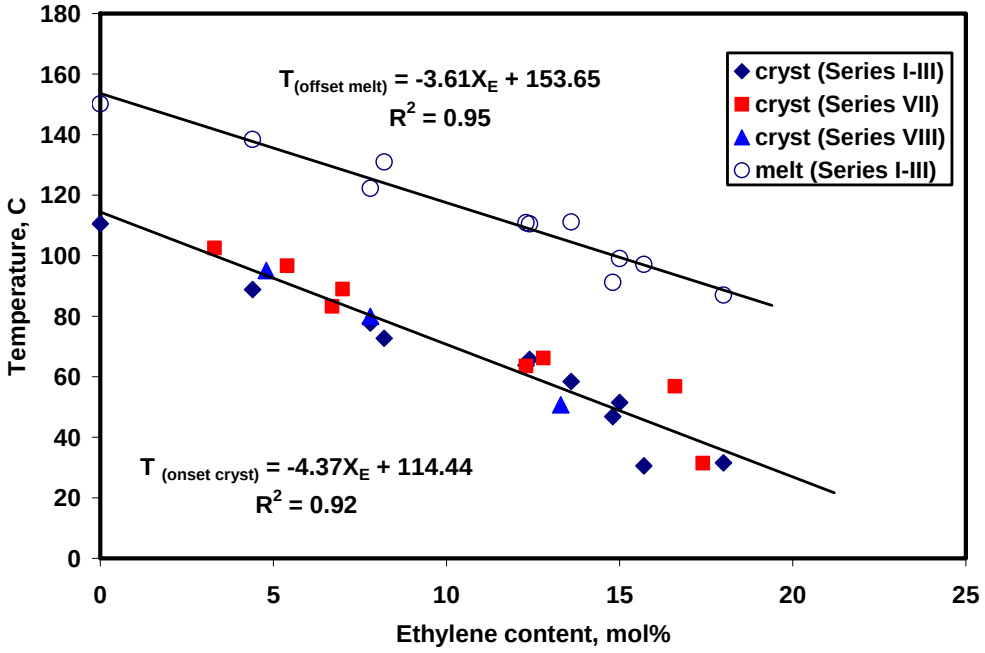

Figure 6.1.6 Crystallization Onset and Melt Offset Temperatures for Dow copolymers as a Function of Composition

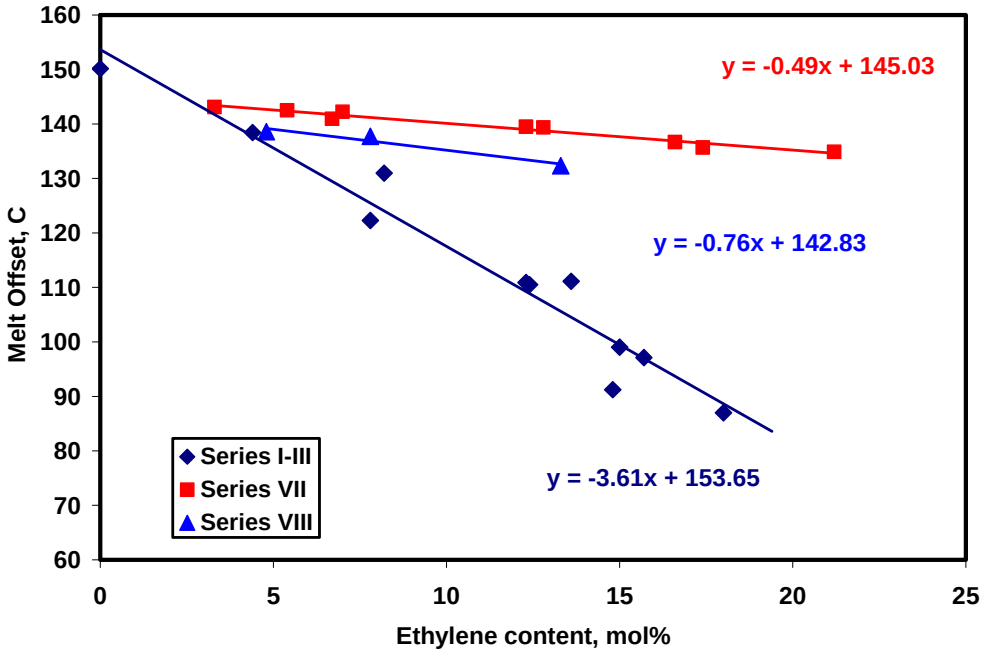

Figure 6.1.7 Melt Offset Temperatures for Dow copolymers as a Function of Composition

especially in the case of the series VII copolymers. There is also a high temperature endotherm present in the melting traces of series VII copolymers that is not found in other series (Figure 6.1.4). The high temperature endotherm melting peaks of series VII show a very weak dependence on the ethylene content.

The shapes of the crystallization and melting curves of series I-III, VII and VII are also quite different (Figure 6.1.5). While the crystallization exotherms for series I-III are sharp, the corresponding curves for series VII and VIII are much broader.

The glass transition temperatures and crystallinities of Dow Chemical copolymers are shown in Figure 6.1.8. The degrees of crystallinity were calculated just above the glass transition temperature using the inclusion model. Both, the glass transition temperature and crystallinity, decrease with increase in the ethylene concentration. The linear dependence of both the glass transition temperatures and crystallinities on the ethylene content is found for the copolymers of all series for up to 8.2 mol% of ethylene. The deviation from the linear behavior occurs for the copolymers of higher ethylene concentration.

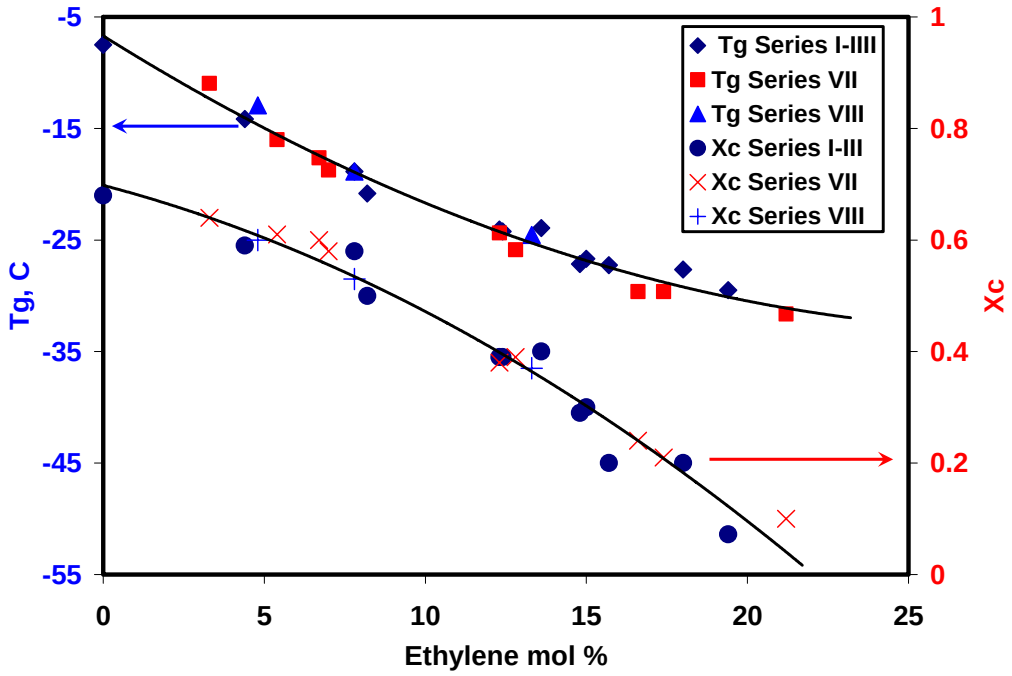

Figure 6.1.8 Glass Transition Temperatures and Crystallinity of Dow Copolymers as a Function of Composition

The apparent heat capacities during crystallization and melting of Ziegler-Natta and Metallocene copolymers are shown in Figure 6.1.9 and Figure 6.1.10. As demonstrated in Figure 6.1.12, Figure 6.1.13, Figure 6.1.14, the peak crystallization and melting temperatures, as well as the crystallization onsets for Metallocene copolymers follow exactly the same trends as the Dow copolymers. The corresponding temperatures for Ziegler-Natta materials are higher than those for Dow copolymers but they also decrease with an increase in the ethylene content. The change in the melting offset with ethylene content for Ziegler-Natta and Metallocene copolymers is shown in Figure 6.1.15. While it is almost the same for Metallocene and Dow series I-III copolymers, the change in the melt offset for Ziegler-Natta materials is lower and falls between the changes of Metallocenes and series I-III on one extreme and series VII and VIII on the other extreme.

The glass transition temperatures of both Ziegler-Natta and Metallocene copolymers fit exactly the same line of decrease as do the Dow copolymer T_gs (Figure 6.1.17). For the sake of comparing Dow copolymers with Metallocene and Ziegler-Natta materials, the degrees of crystallinity were calculated just above the glass transition temperature using the inclusion model. The crystallinities of Ziegler-Natta copolymers are slightly higher than those of the corresponding Dow materials (Figure 6.1.16); however the difference between the data sets might not be significant. The same can be said about the Metallocene crystallinities. While the crystallinities of lower ethylene content Metallocene copolymers lie precisely on the fit line for the Dow copolymers, the values for higher ethylene content Metallocenes are somewhat higher.

The shapes of the crystallization and melting heat capacity curves for Dow, Ziegler-Natta and Metallocene copolymers of about the same concentration are compared in Figure 6.1.11. Both crystallization curves of the Ziegler-Natta and Metallocene copolymers are narrow and tall and are similar to those of the series I-III Dow copolymers. The melting Ziegler-Natta peaks are significantly taller than the corresponding Dow materials peak. The melting peaks of the low ethylene concentration Metallocene samples are only slightly higher than those of the Dow copolymers; however as ethylene concentration increases, the difference between the peaks becomes

significant. At high ethylene concentration, the melting endotherms of Dow copolymers are broader than those for Metallocenes.

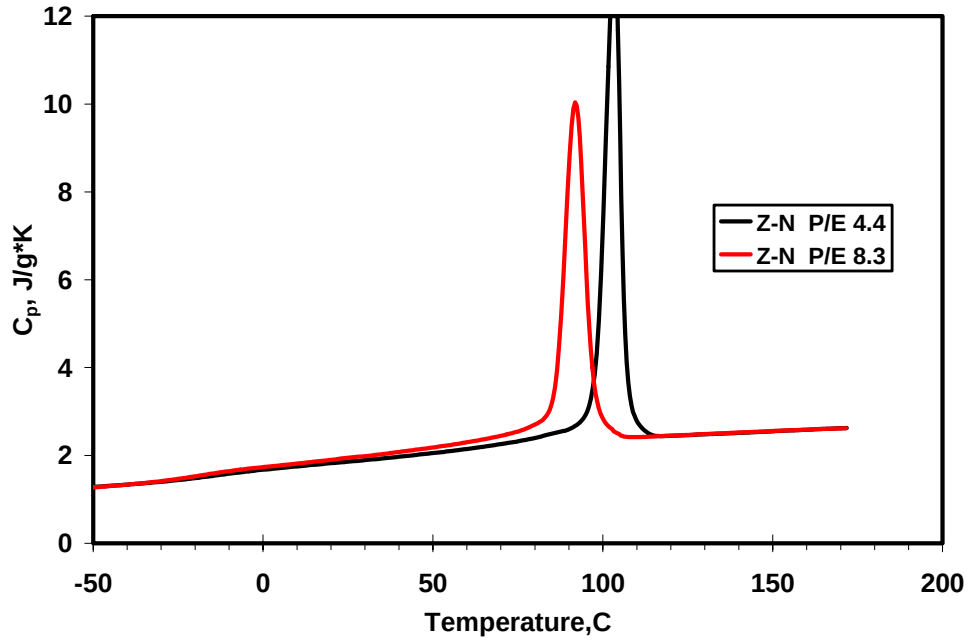

a)

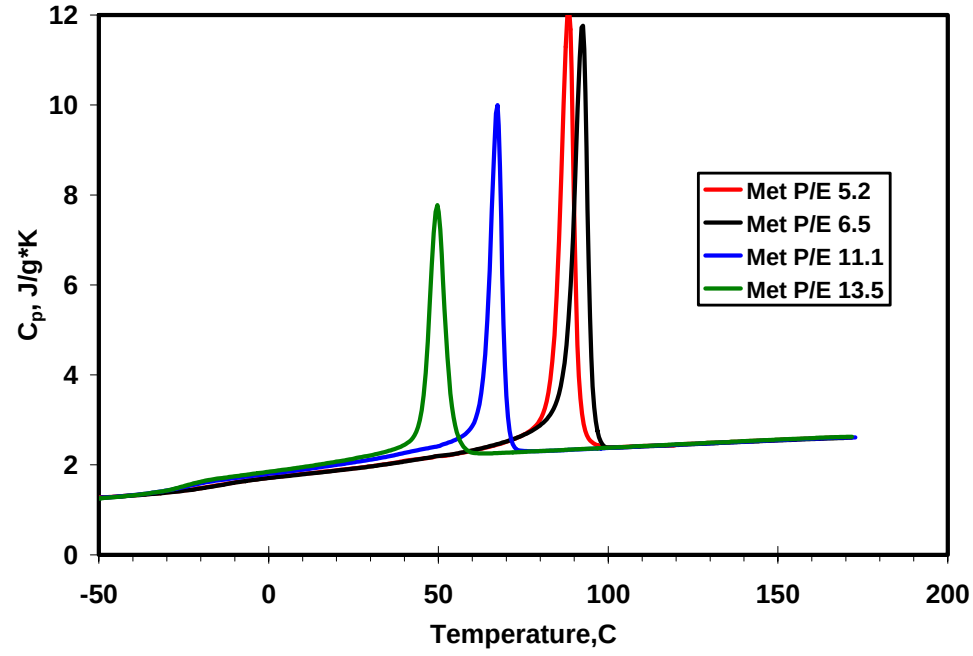

b)

Figure 6.1.9 DSC Crystallization Traces of P/E Copolymers: a) Ziegler-Natta, b) Metallocene

a)

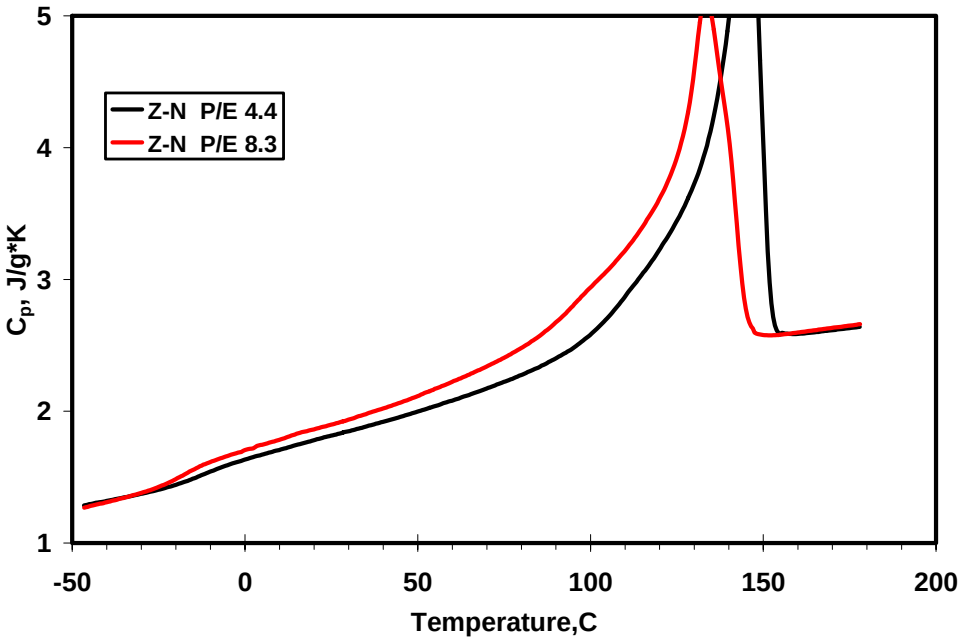

b)

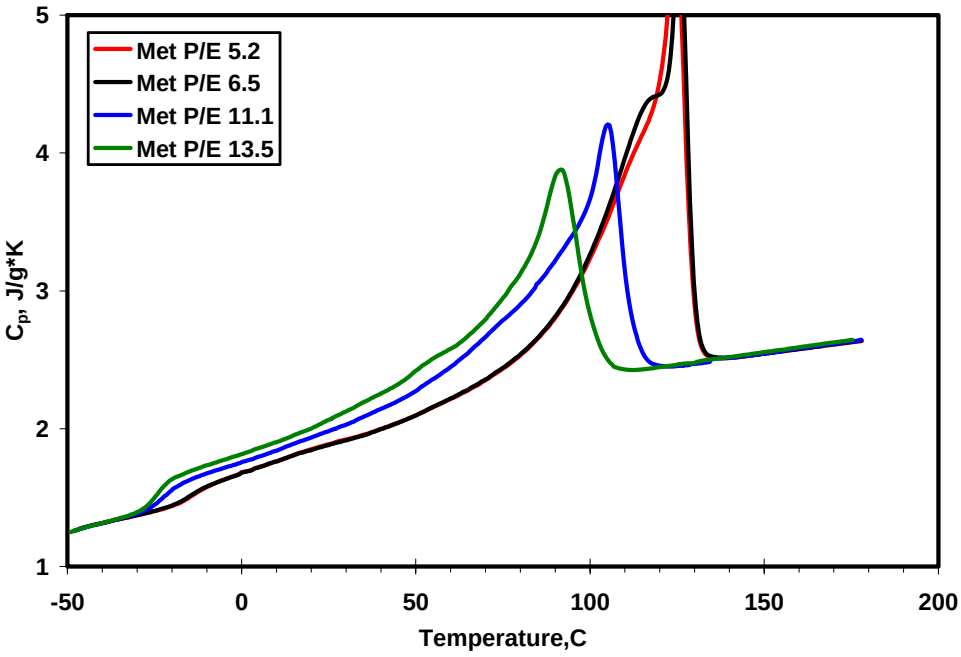

Figure 6.1.10 DSC Melting Traces of P/E Copolymers: a) Ziegler-Natta, b) Metallocene

a)

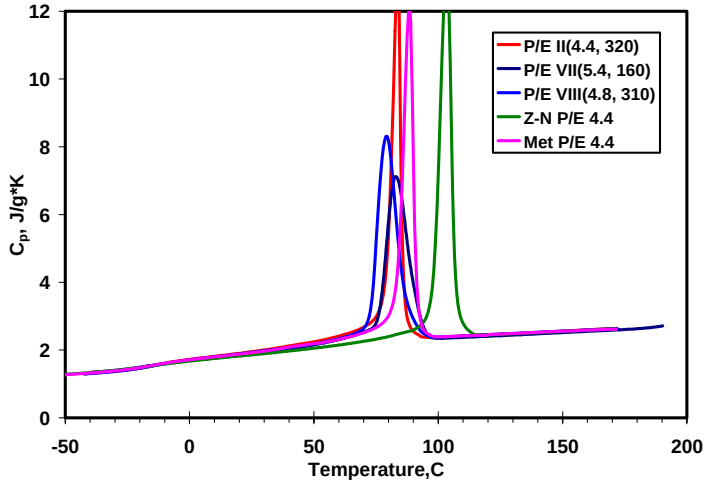

b)

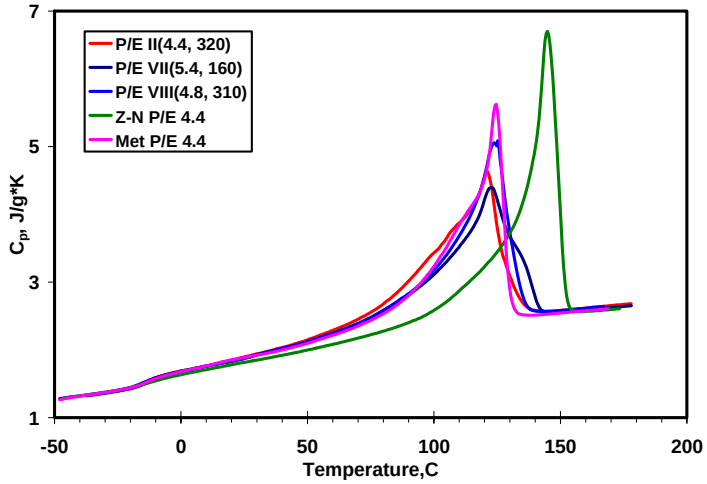

c)

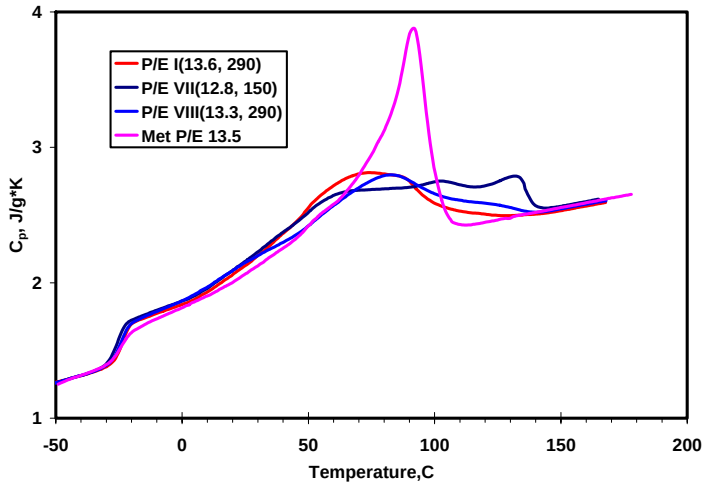

Figure 6.1.11 Comparison of Dow, Ziegler-Natta and Metallocene Copolymers: DSC Traces a) Crystallization, b) Melting (4.4-5.4mol% Ethylene), c) Melting (12.8-13.6mol% Ethylene)

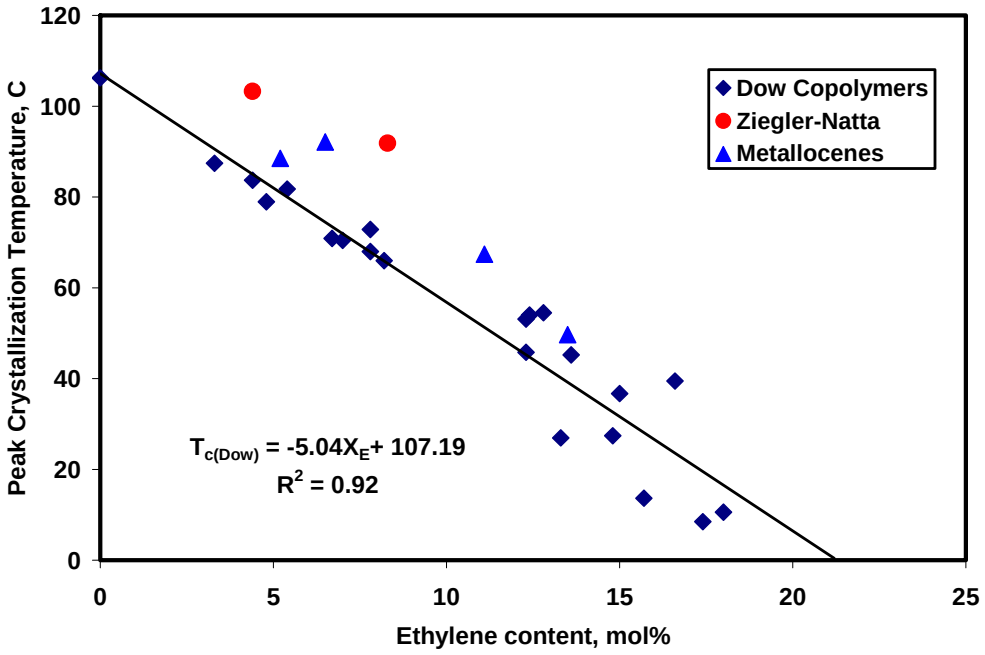

Figure 6.1.12 Crystallization Temperatures of Copolymers as a Function of Composition

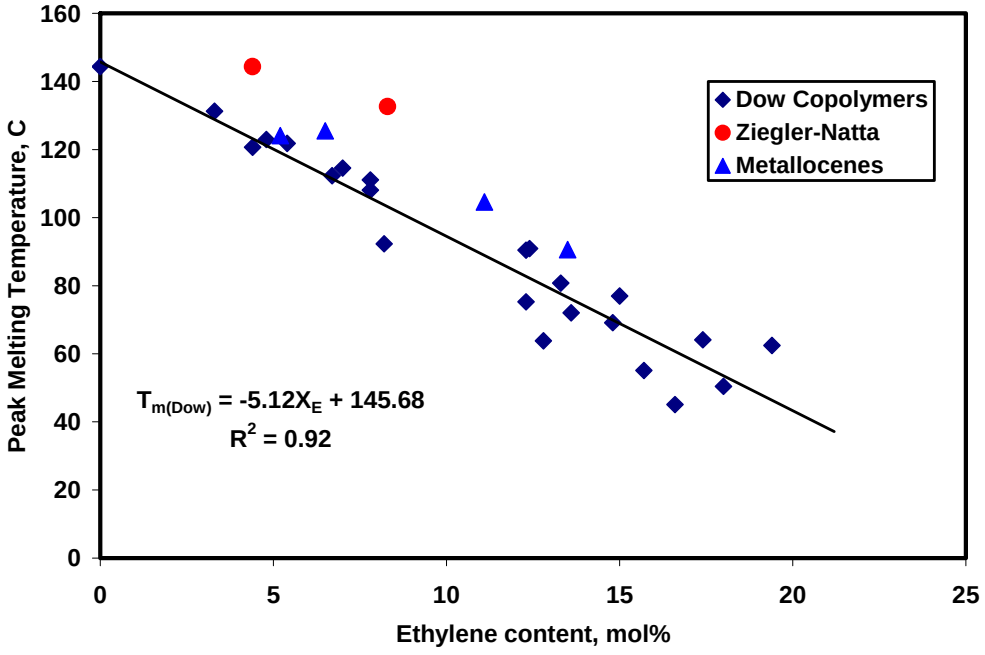

Figure 6.1.13 Melting Temperatures of Copolymers as a Function of Composition

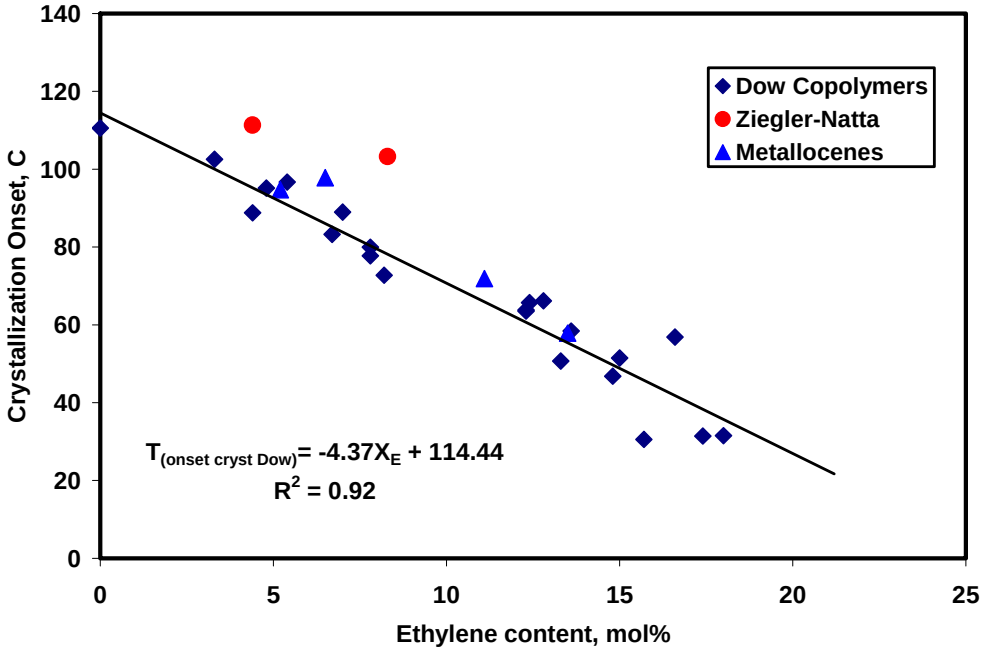

Figure 6.1.14 Crystallization Onset Temperatures of P/E Copolymers as a Function of Composition

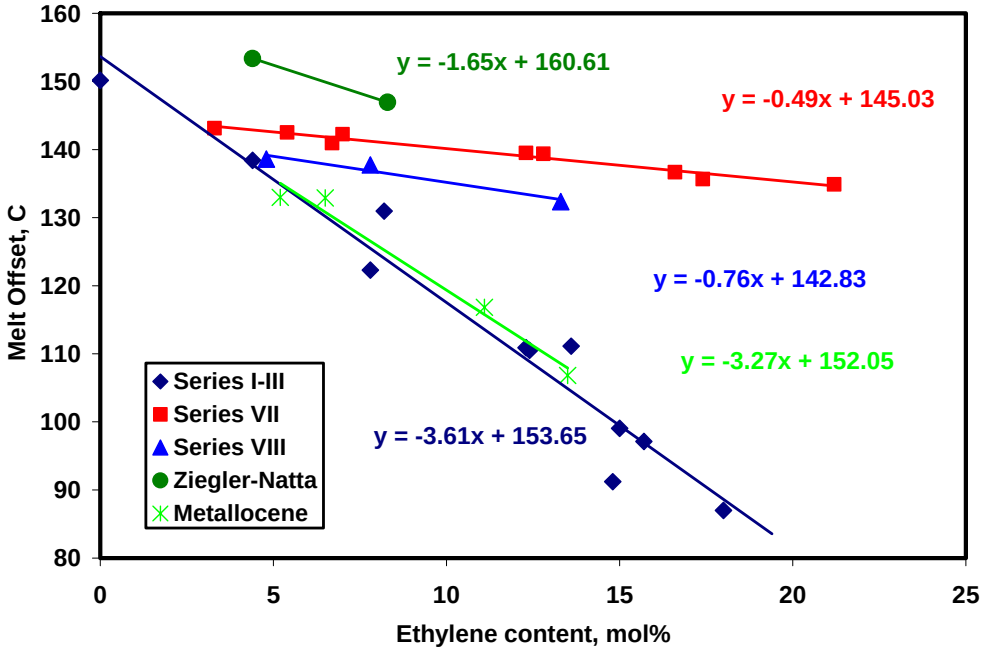

Figure 6.1.15 Melt Offset Temperatures of P/E Copolymers as a Function of Composition

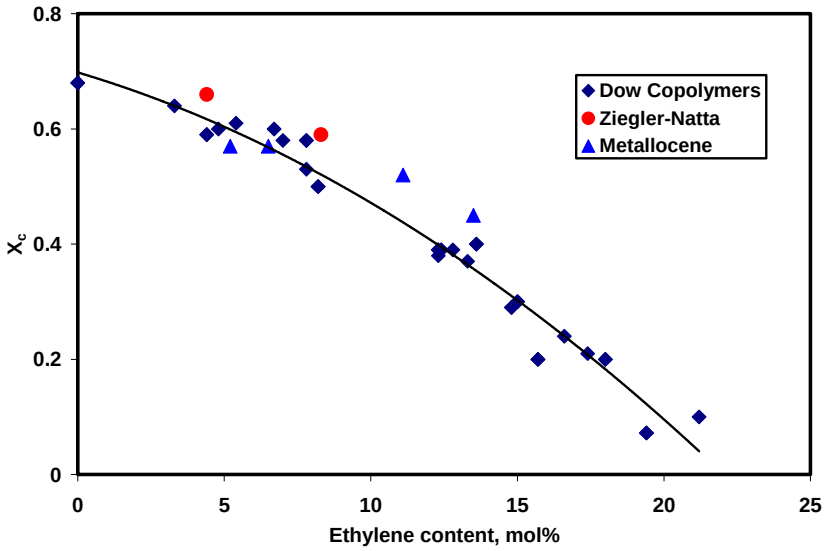

Figure 6.1.16 Crystallinity of P/E Copolymers as a Function of Composition

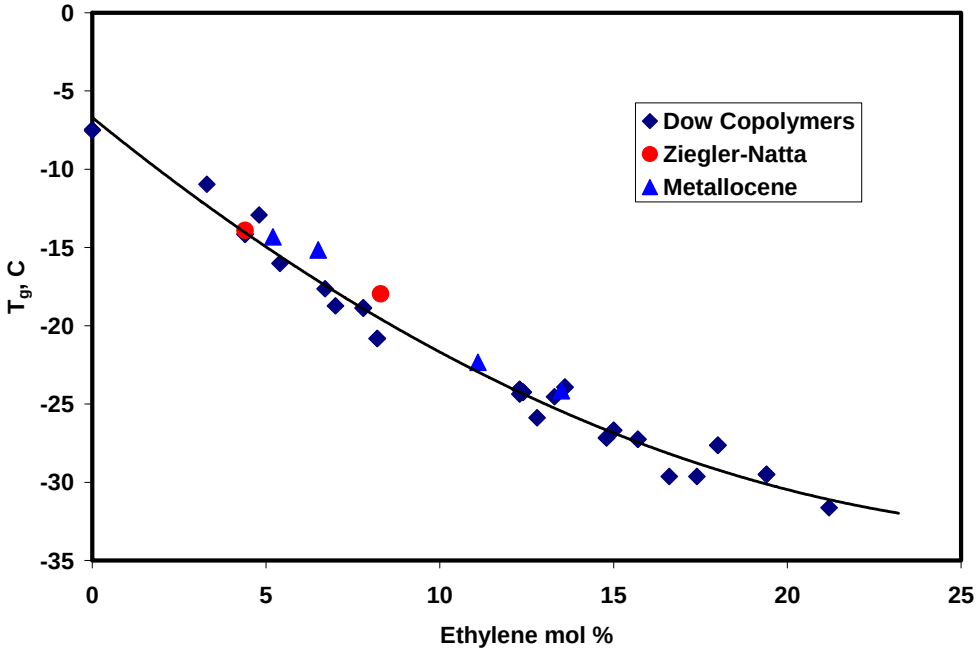

Figure 6.1.17 Glass Transition Temperatures of P/E Copolymers as a Function of Composition

6.1.2 Crystallinity and Thermodynamic Heat of Fusion

The dependence of the thermodynamic heat of fusion on the ethylene content was calculated from the cooling traces by the method outlined in Section 5.2.1 and is shown in Figure 6.1.18 for the crystallization data. Within the experimental error there is a steady linear decrease in the ΔH_f^0 values with an increase in the ethylene content. The thermodynamic heat of fusion values calculated from both crystallization and melting data are presented in Figure 6.1.19 together with a 10% deviation lines for the crystallization data set. The deviation boundary was chosen based on the results of the uncertainty analysis presented in Section 5.3. The figure of 10% was calculated by averaging the largest uncertainties in ΔH_f^0 values given in Table 5.3.1. Most of the calculated values for both melting and crystallization are within the boundaries of the deviation. The thermodynamic heat of fusion values calculated from the melting data are somewhat lower than those obtained from the crystallization data; however considering the possible 10% error in the thermodynamic heat of fusion values, the difference between two data sets is not significant. The scatter in the data becomes more substantial as the ethylene content increases.

Since the inclusion theory based on the Sanchez-Eby kinetic theory assumes that the ethylene is at least partially included in a propylene crystal, it is important to test this assumption. The evidence of the ethylene inclusion would be the dependence of the normalized thermodynamic heat of fusion on the ethylene content. The ΔH_f^0 values were normalized with respect to the mass of polypropylene units in the crystal. The dependence of the normalized thermodynamic heat of fusion at melting on the ethylene content, calculated from the data presented in Figure 6.1.18 is shown in Figure 6.1.20. There is a linear decrease in the normalized ΔH_f^0 values with an increase in the ethylene concentration.

Next several data sets will examine the inclusion and RAF models in the context of the heat of fusion, crystallinity and density calculations. The validity and implications of these results will be discussed in Section 6.2.2.

The normalized experimental enthalpy of fusion is shown for both the RAF and the inclusion model in Figure 6.1.21. The enthalpy of fusion for the inclusion model was

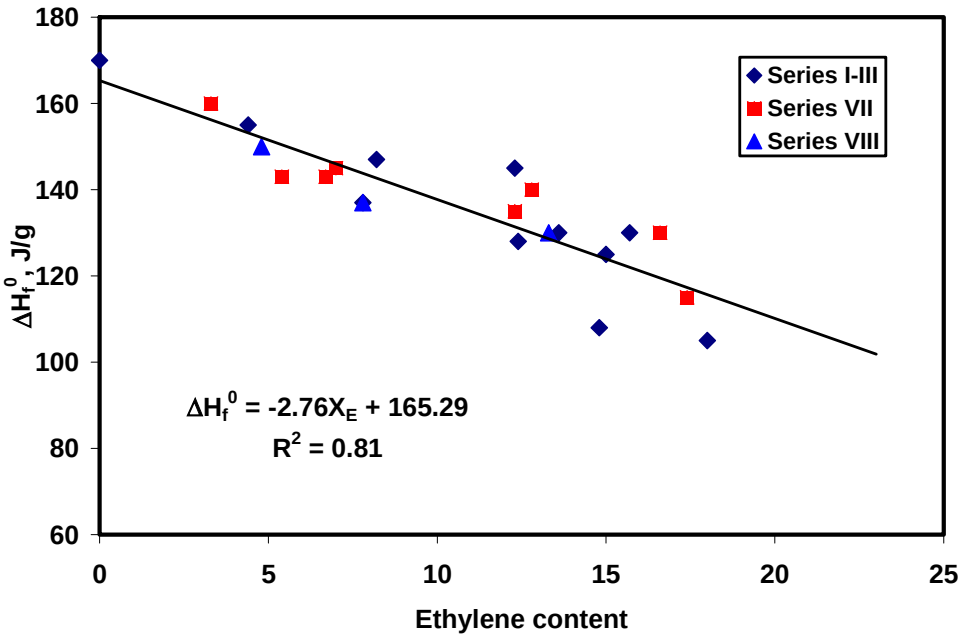

Figure 6.1.18 Dependence of the Thermodynamic Heat of Fusion on the Ethylene Content

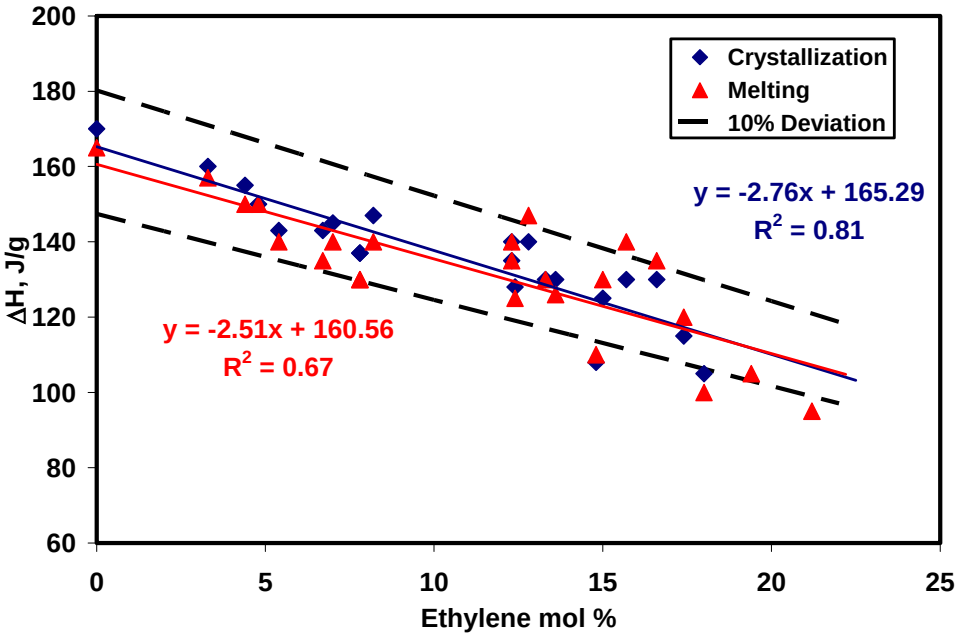

Figure 6.1.19 Dependence of the Thermodynamic Heat of Fusion on the Ethylene Content (Crystallization and Melting)

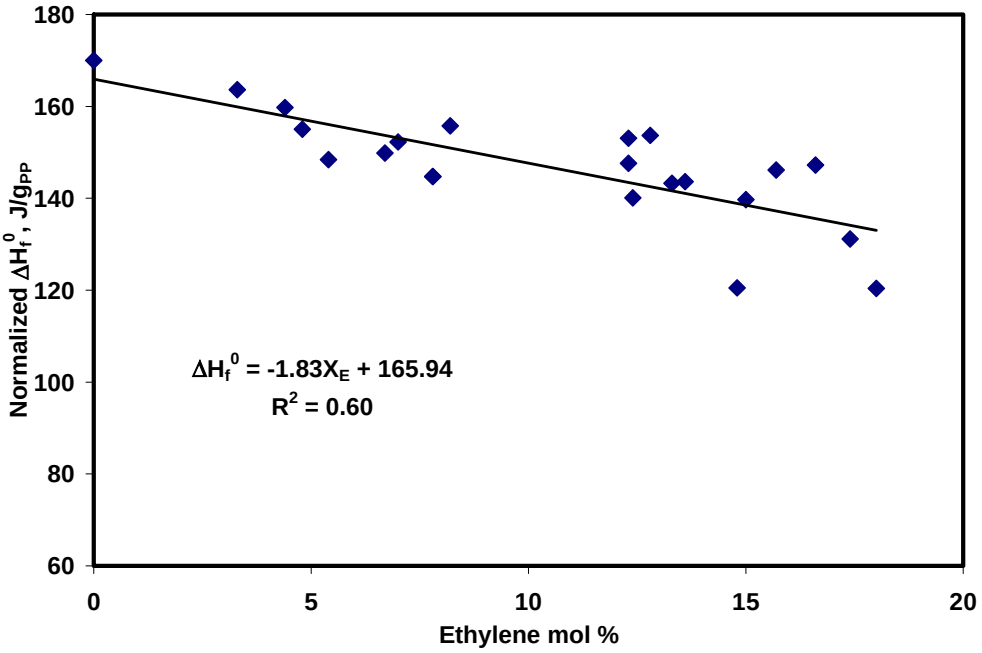

Figure 6.1.20 Normalized ΔH_f^0 as a Function of Composition

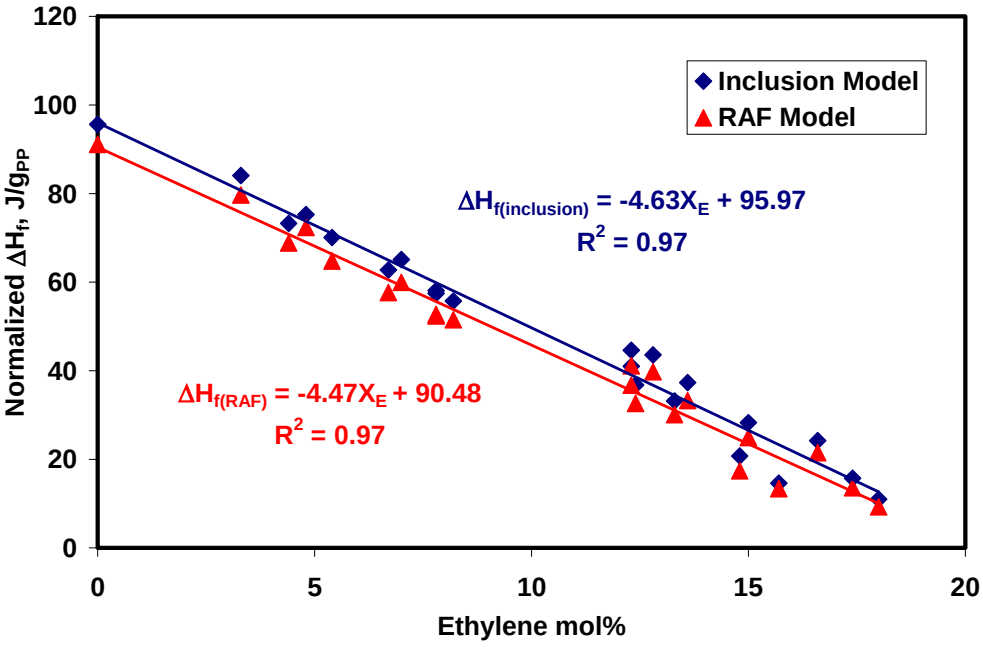

Figure 6.1.21 Normalized ΔH_f for Inclusion and RAF Models as a Function of Composition

calculated using the ΔH_f^0 values obtained from Figure 6.1.18. The enthalpy of fusion for the RAF model was calculated using the ΔH_f^0 values of 207 J/g from the ATHAS database. There is a linear decrease in the normalized enthalpy with an increase in the ethylene concentration for both inclusion and RAF models. However, the normalized ΔH_f values for RAF model are slightly lower than those for the inclusion model.

The crystallinities calculated from the DSC data for inclusion and RAF models are compared in Figure 6.1.22. There is a steady decrease in the crystallinity with an increase in the ethylene concentration for both sets of data. However, the RAF crystallinity values are significantly lower, especially in the low ethylene content region.

The amorphous and semicrystalline ΔC_ps as a function of ethylene content are plotted in Figure 6.1.23. The amorphous ΔC_p was calculated using the theoretical amorphous and crystalline heat capacities at T_g. The semicrystalline ΔC_p was calculated from the experimental data by the method outlined in Section 5.4. As expected, at high ethylene content, corresponding to negligible crystallinity values, the semicrystalline ΔC_p overlaps with the amorphous ΔC_p.

In order to evaluate the validity of the RAF model, the X_{RAF} and X_{MAF}, calculated using the amorphous and semicrystalline ΔC_ps from Figure 6.1.23 by the method outlined in Section 2.5.2 and 5.2.2, are plotted as a function of crystallinity (Figure 6.1.24). The crystallinity in this case was calculated using ΔH_f^0=207 J/g. The content of rigid amorphous fraction increases with an increase in the crystallinity, while the content of the mobile amorphous fraction decreases.

In order to obtain an estimation of the degree of crystallinity independent from the DSC measurements, the densities of these copolymers were measured and analyzed using Equation 2.5.4. The amorphous density, ρ_a, used in the computations was 0.8530 g/cm^3;[122] however, the choice of crystal density, ρ_c, was not as clear. Two sets of density base crystallinities were calculated using the unit cell volumes reported by Isasi et al.[123] (for polypropylene with regio- and stereo- defects, V=0.9125nm^3), and by Laihonen et al.[42] (for polypropylene, V=0.896nm^3, and propylene-ethylene copolymer, V=0.912 nm^3).

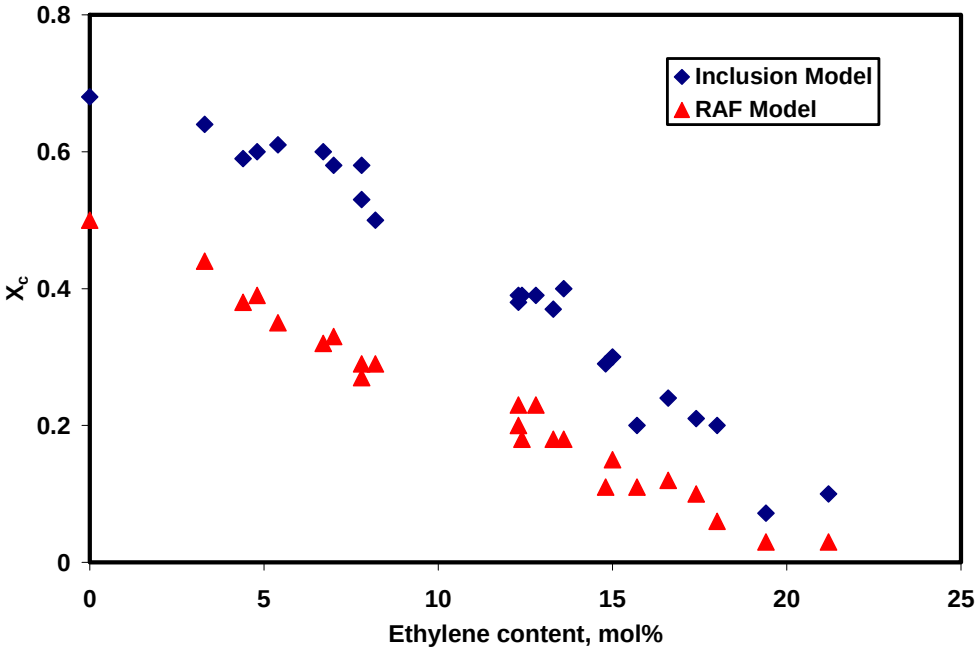

Figure 6.1.22 Crystallinity from Inclusion and RAF Models as a Function of Composition

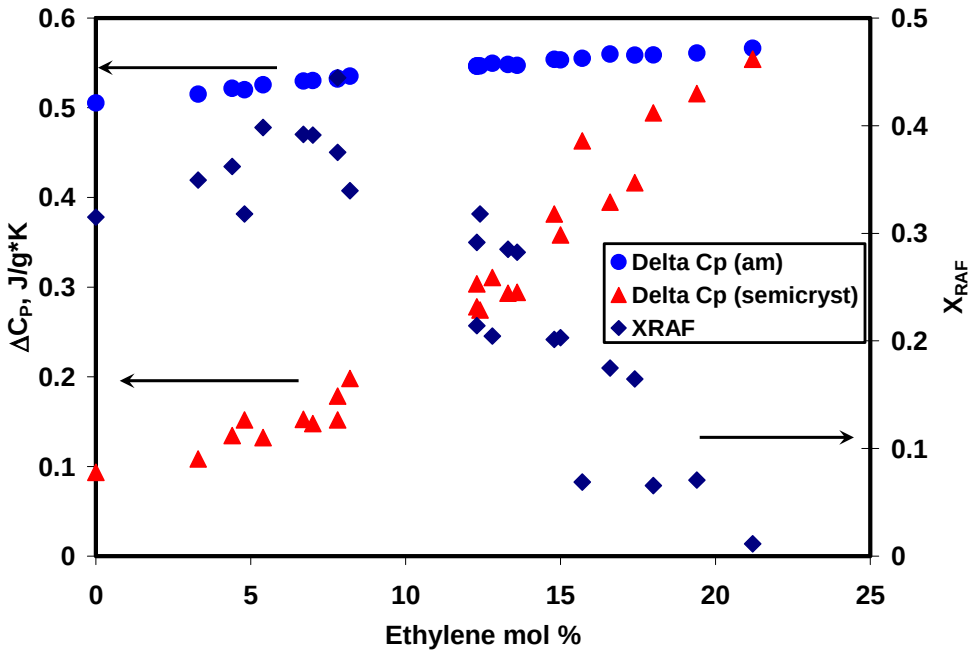

Figure 6.1.23 Heat Capacity Change at T_g and Rigid Amorphous Fraction as a Function of Ethylene Content

a)

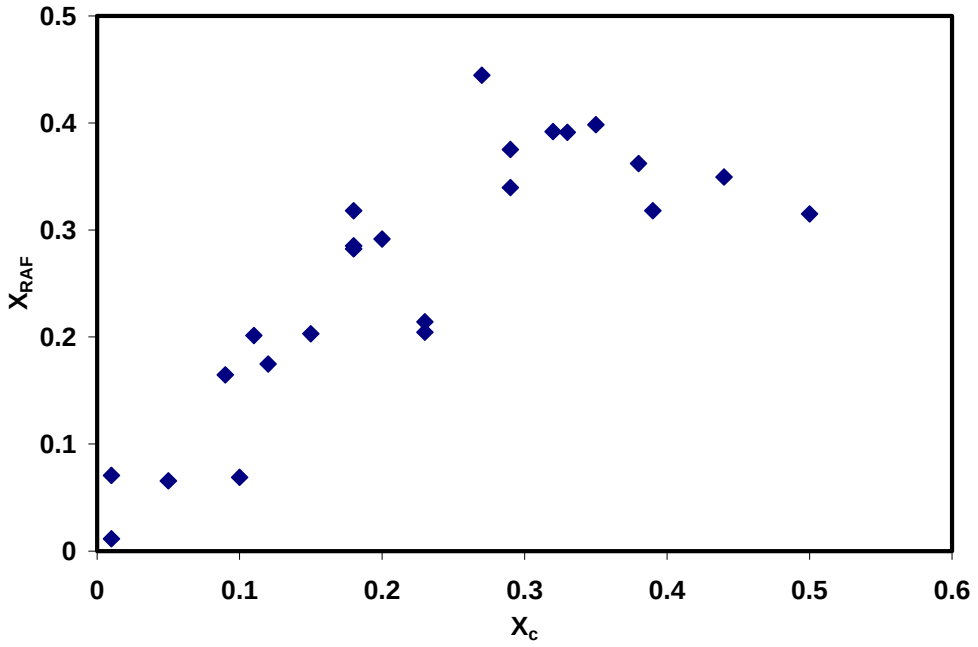

b)

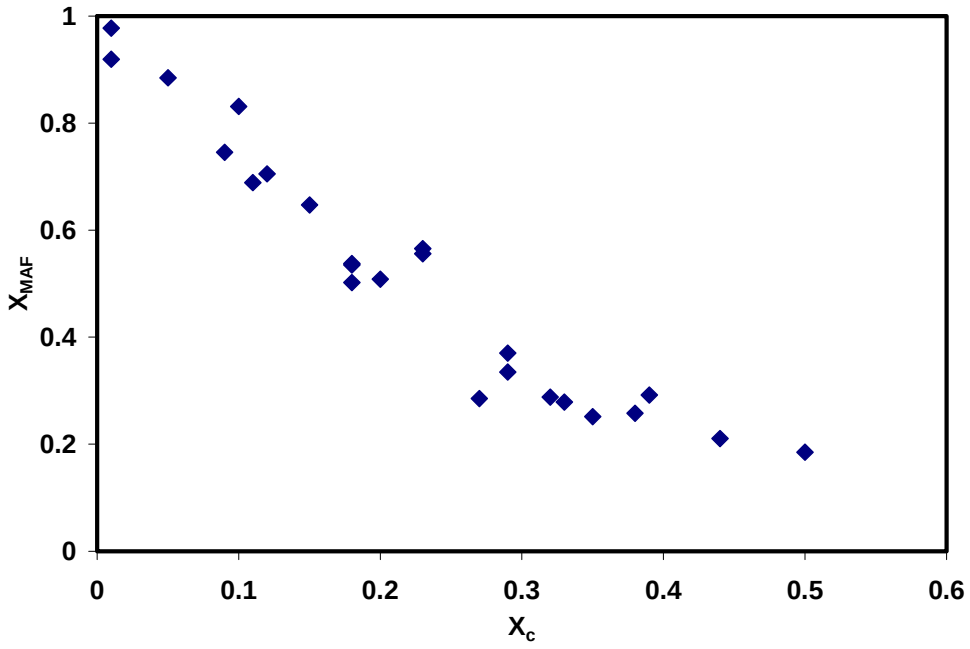

Figure 6.1.24 X_{RAF} and X_{MAF} as a Function of Crystallinity

The crystal densities corresponding to these unit cells are ρ_c=0.919 g/cm^3 (Alamo unit cell), $\rho_{c(PP)}$=0.934 g/cm^3 and $\rho_{c(PE)}$=0.9194 g/cm^3 (Laihonen unit cell). The crystal densities of the propylene-ethylene copolymers were further reduced by considering the effect of morphological partitioning of ethylene defects. Based on the study by Alamo et al.[50], it was assumed that 42% of ethylene units are included in the polypropylene crystal, independent of the overall copolymer composition. Hence, the unit cell masses must be accordingly corrected.

The results of the crystallinity calculations based on both Alamo and Laihonen unit cells together with the DSC crystallinity values for the RAF and inclusion models are presented in Figure 6.1.25 and Figure 6.1.26, respectively. The density crystallinities from Alamo and Laihonen unit cells are extremely close, except for pure polypropylene. The density crystallinities are slightly higher than those from the DSC inclusion model for low ethylene content copolymers. The disparity between these data sets becomes more pronounced as the ethylene concentration increases. The RAF crystallinity values are significantly lower than the density crystallinity through the whole ethylene concentration range.

As the inclusion model crystallinities, calculated from ΔC_p (T_g) and from C_{pb}(just above T_g) were compared, it was discovered that the materials evaluated by the inclusion model might have ΔC_p deficiency that can be, at first, attributed to RAF. As demonstrated in Figure 6.1.27a), the amount of this "rigid amorphous fraction" is significantly lower than predicted by the RAF model. It ranges between 8% and 15% for the copolymers with the 0-8 ethylene mol% and then decreases to 0% RAF. When evaluated as a function of crystallinity (Figure 6.1.27b), the copolymers with the X_c values of under 0.3 have the "RAF" below 0.05. However, as will be discussed in section 6.2.2, this supposed ΔC_p deficiency is not in fact an indication of the RAF presence.

Finally, the rigid amorphous fraction for the RAF models was included in the density calculations. Since the RAF density is unknown, the two extremes were considered. In the first case, it was assumed that the rigid amorphous fraction density is equal to the mobile amorphous fraction density of 0.853 g/cm^3. In the second case, it was

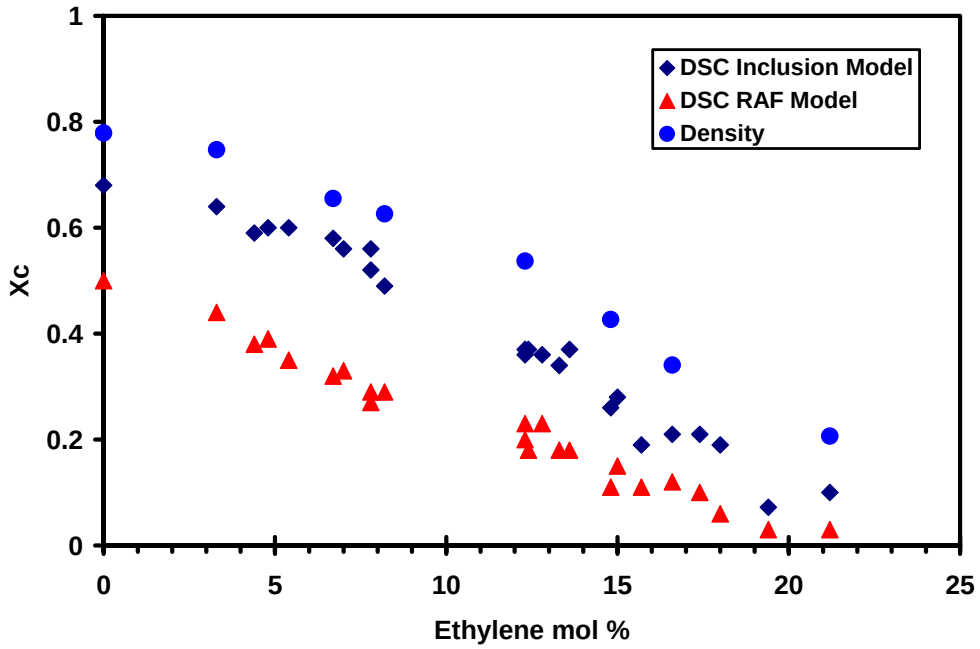

Figure 6.1.25 Xc by Density (Alamo Unit Cell) and DSC (RAF and Inclusion Model) as a Function of Composition

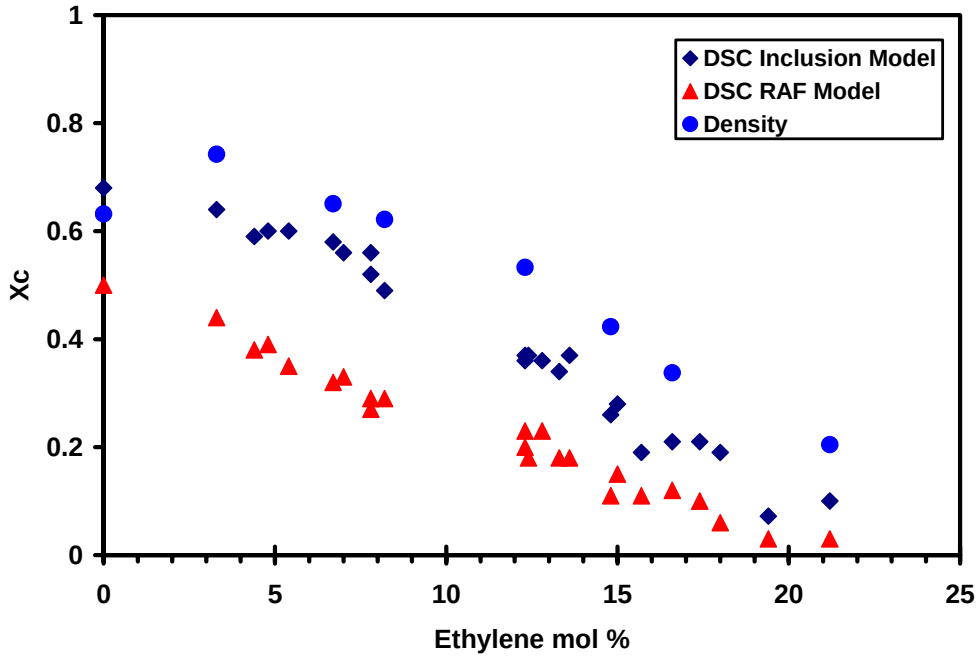

Figure 6.1.26 Xc by Density (Laihonen Unit Cell) and DSC (RAF and Inclusion Model) as a Function of Composition

a)

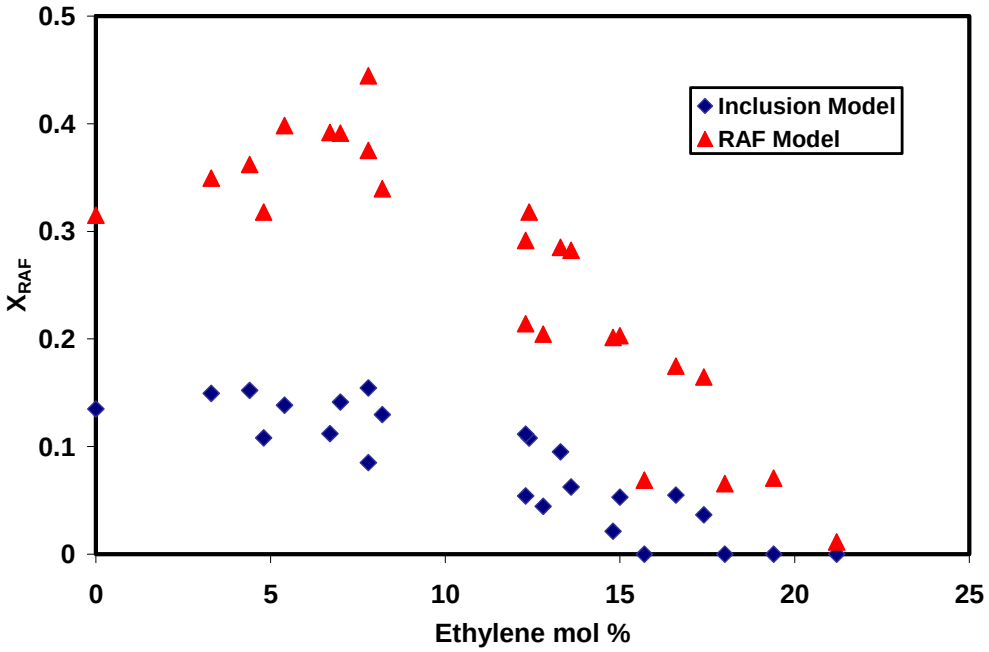

b)

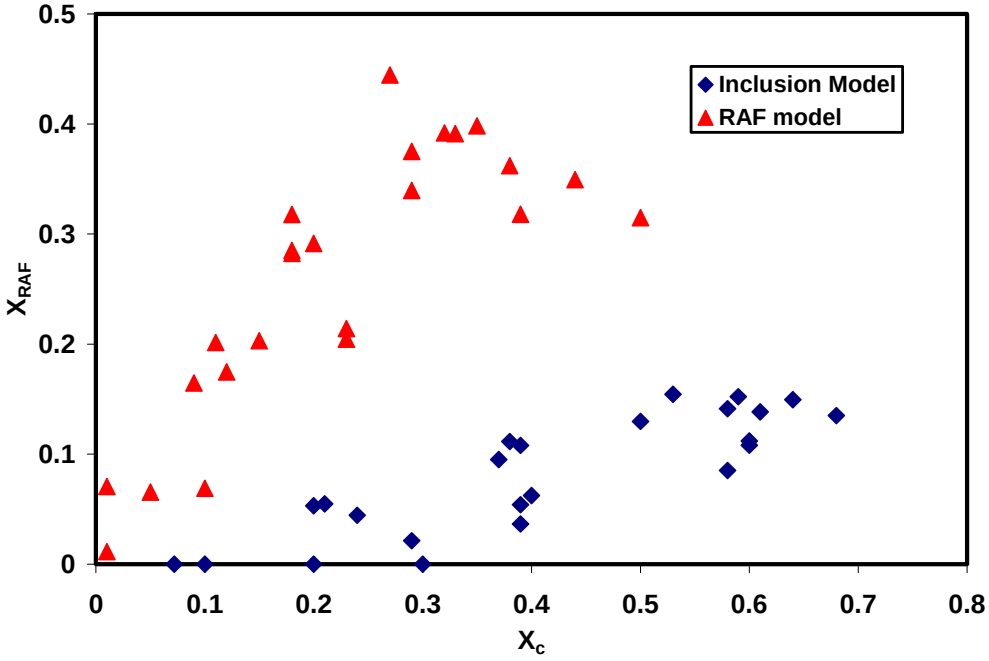

Figure 6.1.27 RAF from Inclusion and RAF Models: a) vs. Ethylene Content, b) vs. Crystallinity

a)

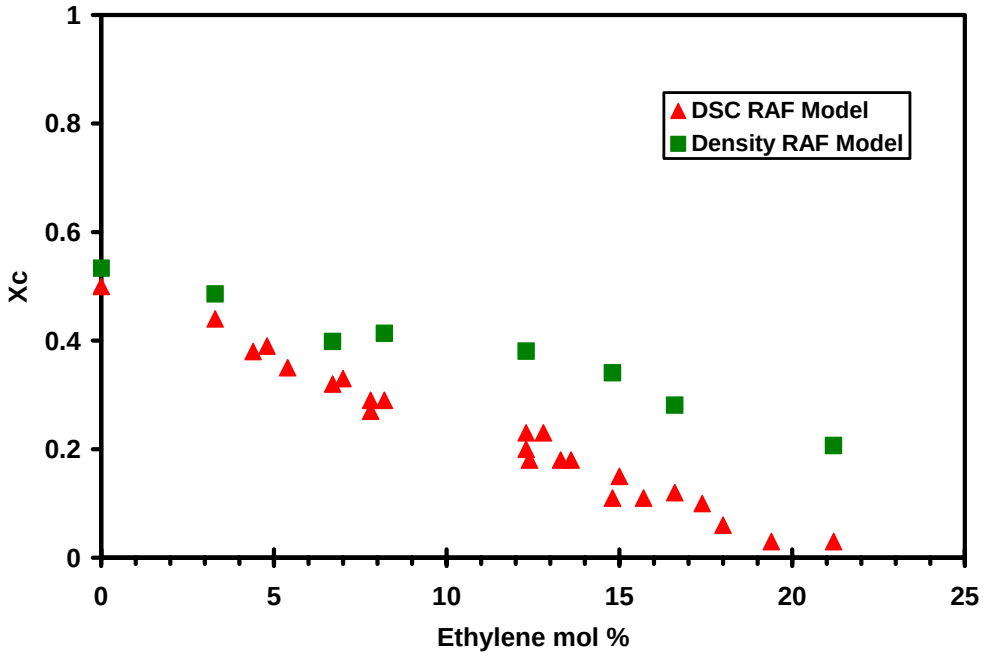

b)

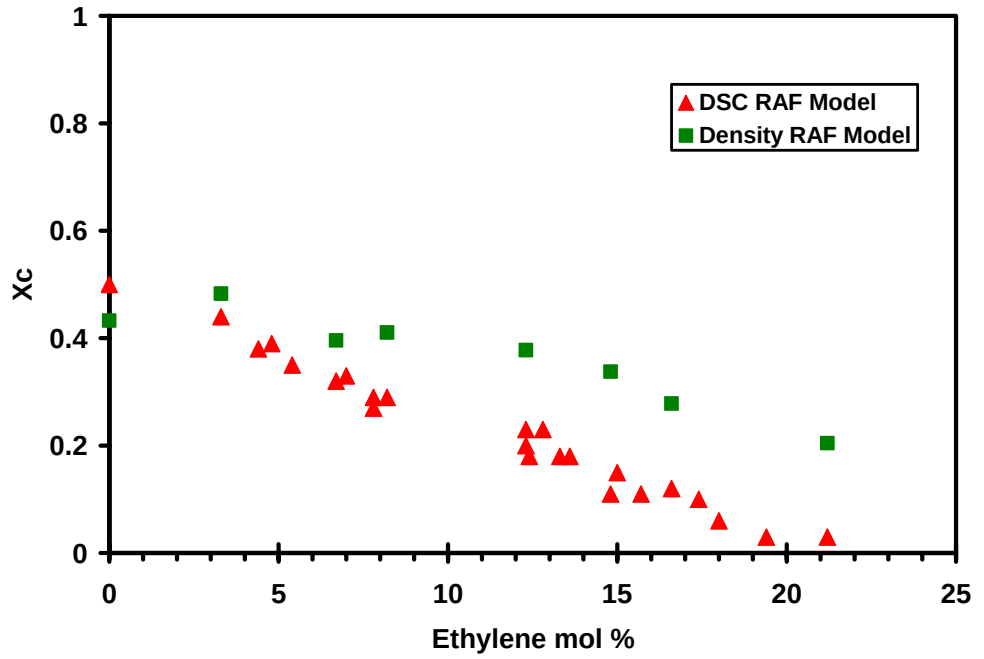

Figure 6.1.28 RAF Model Crystallinity from Density and DSC as a Function of Composition a) Alamo Unit Cell, b) Laihonen Unit Cell

assumed that the rigid amorphous fraction density is equal to the crystal density. The first case was already presented in Figure 6.1.25 and Figure 6.1.26. The second case is demonstrated in Figure 6.1.28a) for the Alamo unit cell and in Figure 6.1.28b) for the Laihonen unit cell. The results are similar for the Alamo and Laihonen unit cells with the exception of polypropylene homopolymer. For the most part, the RAF model density crystallinities are slightly higher than the crystallinities obtained from the DSC RAF model for the copolymers with low ethylene content. The discrepancy between the data sets increases with an increase in the ethylene content.

Overall, there is a relatively good agreement between the crystallinity values obtained from the density and the DSC inclusion model for the copolymers of low ethylene content. However, the dissimilarity increases with the increase in the ethylene content. The crystallinities calculated from the RAF model are generally significantly lower than the density crystallinities for all ethylene concentrations.

6.1.3 Morphology

The morphology of Dow copolymer materials was studied using DSC, Wide-angle X-ray analysis, AFM and SEM.

The effect of composition on the melting behavior following isothermal crystallization at the lowest practical temperature for each material is shown in Figure 6.1.29 for several copolymers. In all cases the development of the low temperature endotherm is preceded by the growth of the high temperature endotherm. In the case of isothermal crystallization of PE-I (0.0, 320), the relative height of the low endotherm peak is smaller than that of the high endotherm. However, as the concentration of the ethylene increases, the relative heights of the endotherms become reversed. In the PE-I (13.6, 290) and PE-I (15.7, 260), the low temperature endotherm is considerably larger than the high temperature endotherm after just 2min of isothermal crystallization. There is also a noticeable shift in the melting temperatures of both endotherms with an increase in the crystallization time.

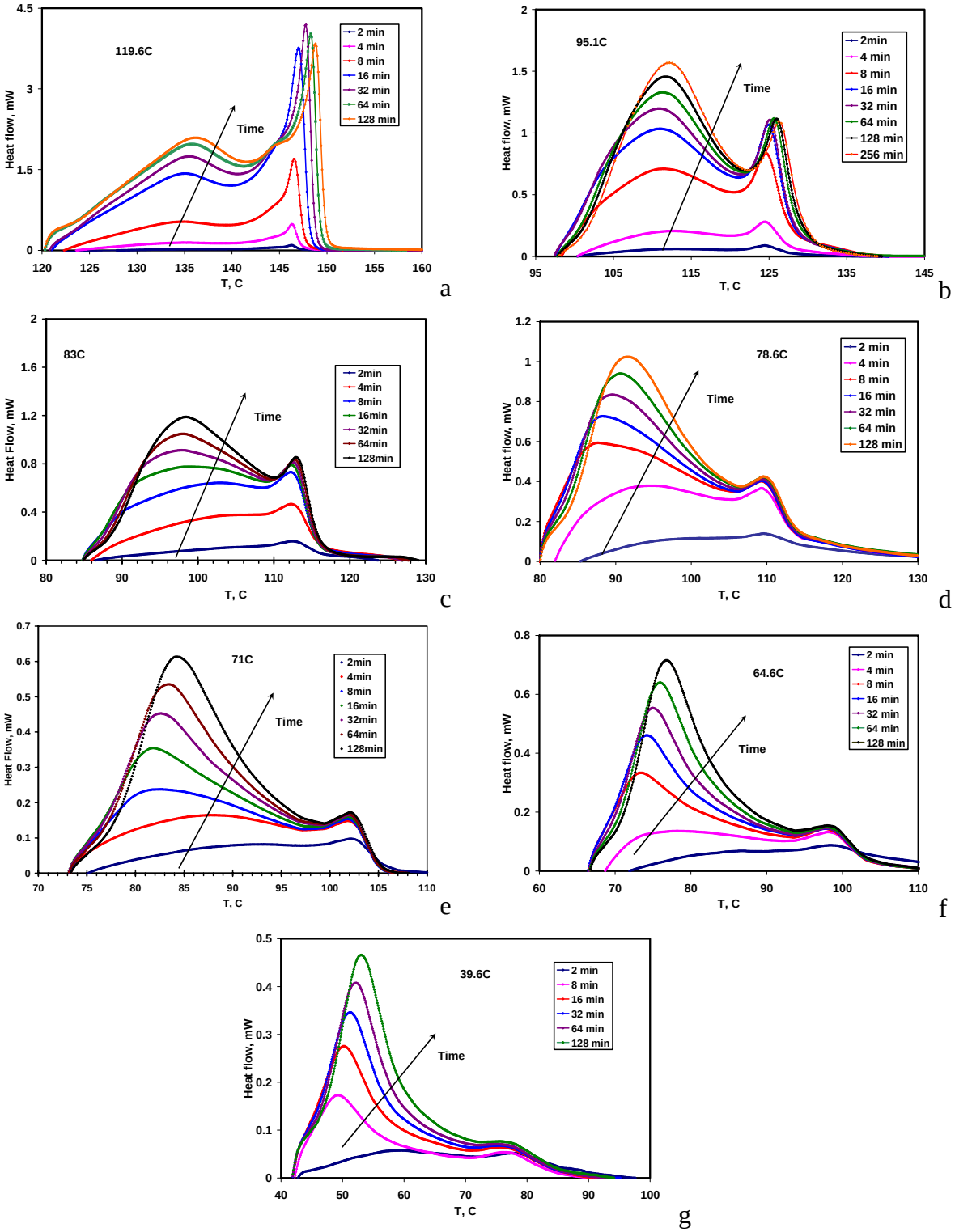

Figure 6.1.29Isothermal Crystallization: Effect of Composition a) PE-I (0.0, 320), b) PE-II (4.4, 320), c) PE-III (7.8, 160), d) PE-I (8.2, 300), e) PE-III (12.3, 310), f) PE-I (13.6, 290), g) PE-I (15.7, 260)

The effect of crystallization temperature on the behavior of PE-I (0.0, 320), PE-I (4.4, 320) and PE-I (15.7, 260) is shown in Figure 6.1.30, Figure 6.1.31 and Figure 6.1.32, respectively. With an increase in the crystallization temperature, the rate of crystallization decreases. The same effect is also apparent form the results given in Figure 6.1.33. For each copolymer the crystallization rate (as judged by the initial slopes of the crystallinity curves) and the overall crystallinity decrease with an increase in the crystallization temperature. There is also a significant decrease in the crystallinity with an increase in ethylene concentration.

The growth rates of the low and high endotherm are shown in Figure 6.1.34 for PE-I (0.0, 320) and PE-II (4.4, 320). At the shortest crystallization time of 2 min, the areas of these endotherms are the same. The effect of crystallization temperature rate of shift of the melting temperature $B(T_x)$ are shown in Figure 6.1.35. The $B(T_x)$ for PE-I (0.0, 320) values increase with the crystallization temperature. The dependence of $B(T_x)$ on the crystallization temperature for PE-II (4.4, 320) is not as strong as for PE-I (0.0, 320).

The WAXD data for several copolymers crystallized on the bench top are shown in Figure 6.1.36. The peak at the scattering angle 2θ around 18.4° is characteristic of α-phase crystals and the peak at the scattering angle 2θ around 19.4° is characteristic of γ-phase crystal.[118] Similar results were obtained for the other copolymers crystallized by slow, fast and bench top cooling methods outlined in Section 4.2.3. From these results, the relative γ-phase content values were calculated. These WAXD results demonstrate the effect of ethylene content and cooling rate on the formation of γ-phase crystals (Figure 6.1.37). The lines in Figure 6.1.37 represent the trend lines and not the fit lines to the data sets shown. There is a steady increase in the γ-phase crystal content with increasing ethylene concentration. The increase in the γ-phase content with ethylene concentration is larger at lower cooling rate. The dependence of the amount of γ-phase crystals on the defect concentration for Dow copolymers is shown in Figure 6.1.38. The defect mol% includes the contribution from the ethylene units as well as regio-errors. There is an increase in the γ-phase content with the increase in the defect concentration. For comparison, the data from Alamo et al.[50] for propylene-ethylene copolymers and De

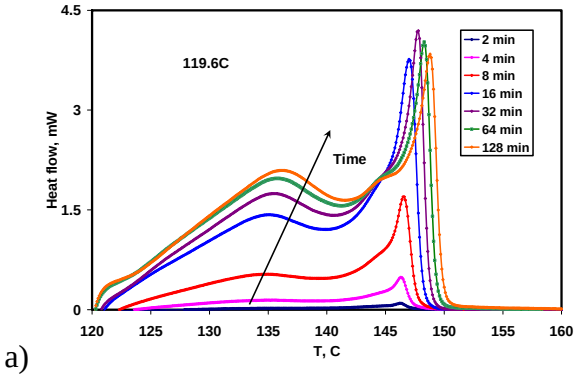

a)

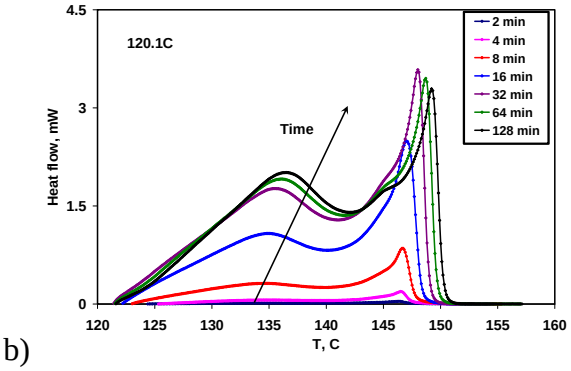

b)

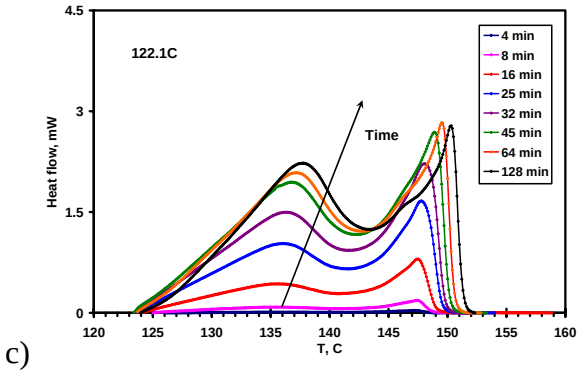

c)

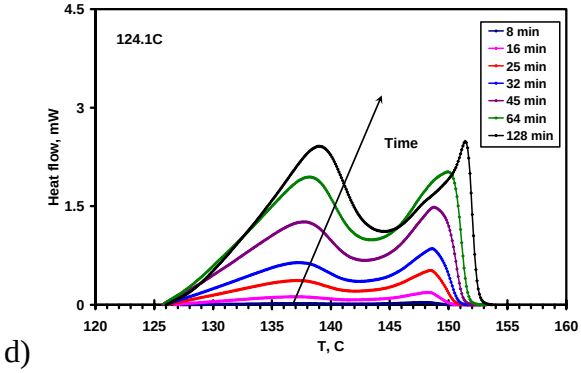

d)

Figure 6.1.30 Effect of the Crystallization Temperature on Isothermal Crystallization of PE-I (0.0, 320)

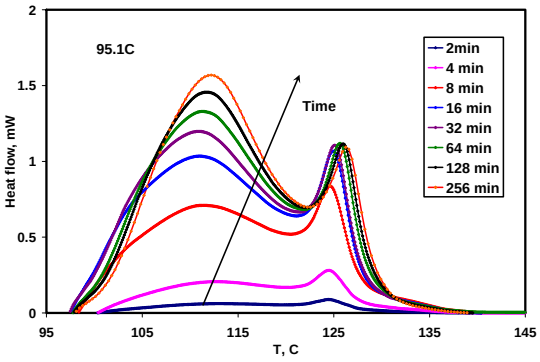

a)

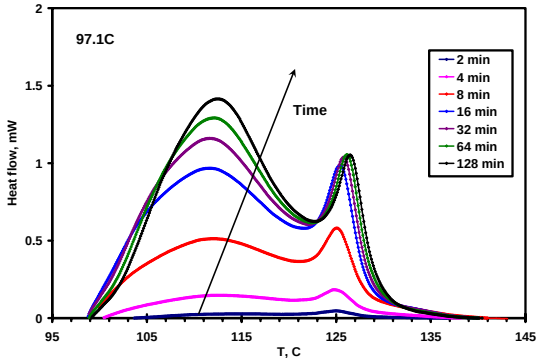

b)

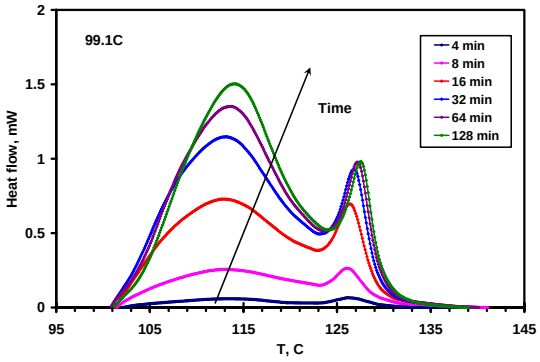

c)

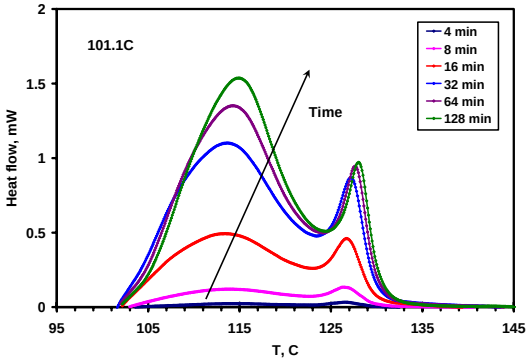

d)

Figure 6.1.31 Effect of the Crystallization Temperature on Isothermal Crystallization of PE-II (4.4, 320)

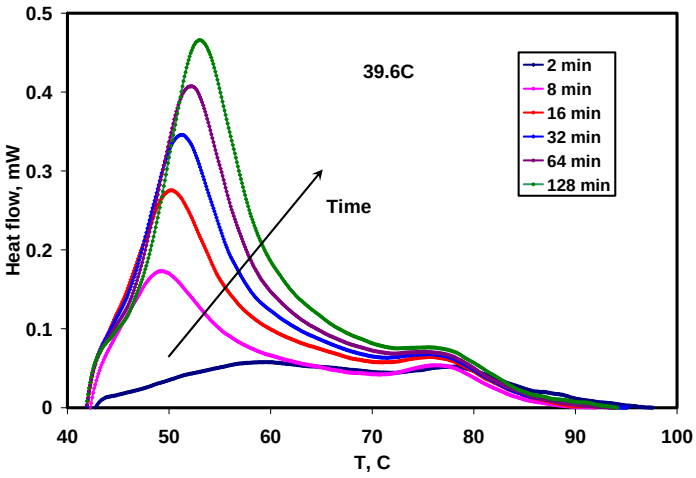

a)

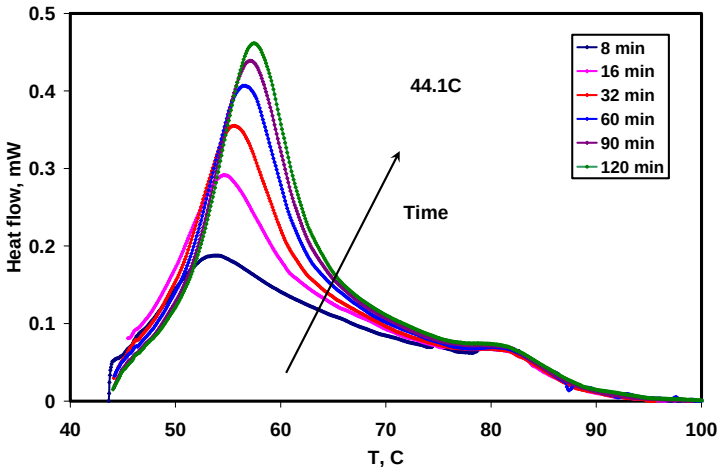

b)

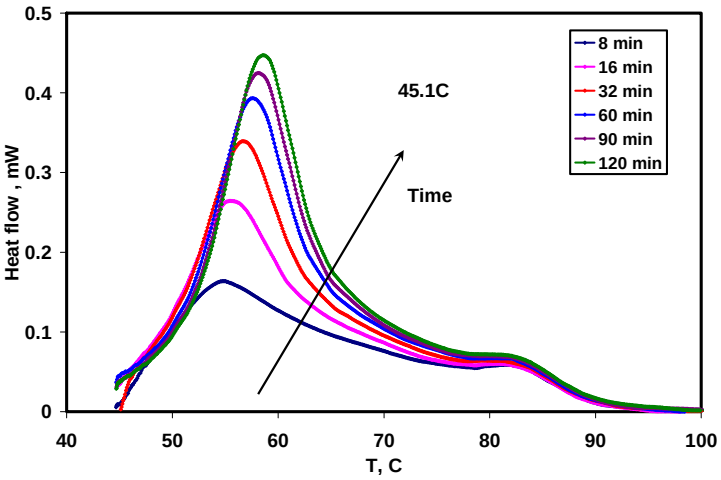

c)

Figure 6.1.32 Effect of the Crystallization Temperature on Isothermal Crystallization of PE-I (15.7, 260)

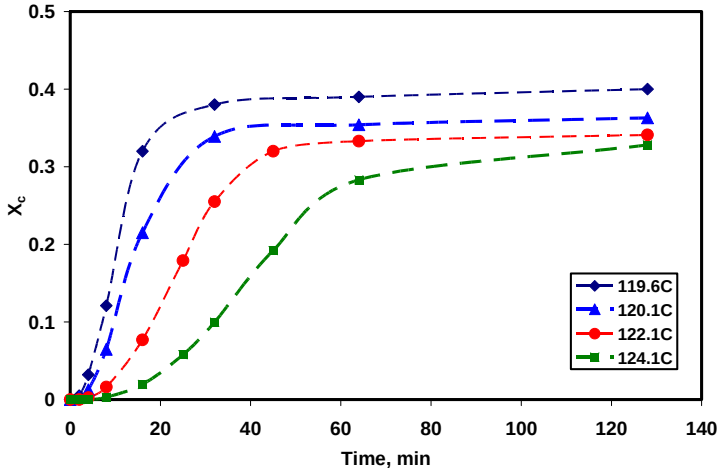
0.5
0.4
0.3
0.2
0.1
0
X_c
0
20
40
60
80
100
120
140
Time, min
119.6C
120.1C
122.1C
124.1C

a)

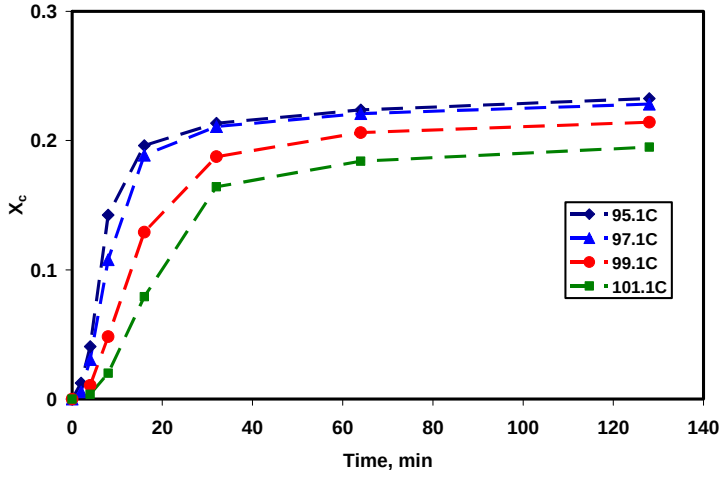
0.3
0.2
0.1
0
X_c
0
20
40
60
80
100
120
140
Time, min
95.1C
97.1C
99.1C
101.1C

b)

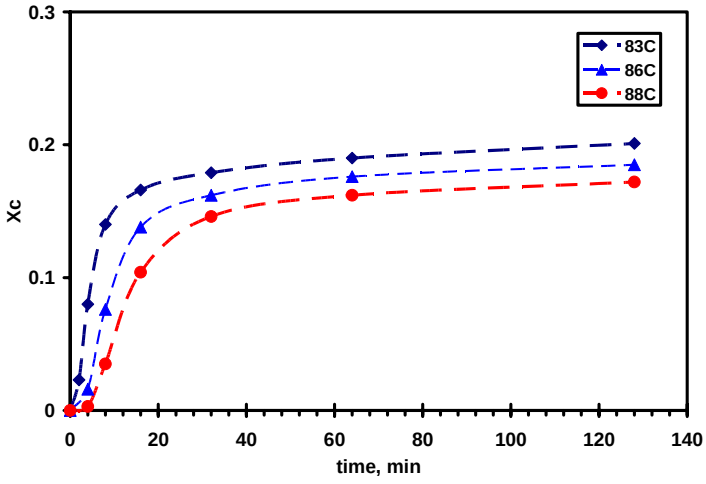
0.3
0.2
0.1
0
Xc
0
20
40
60
80
100
120
140
time, min
83C
86C
88C

c)

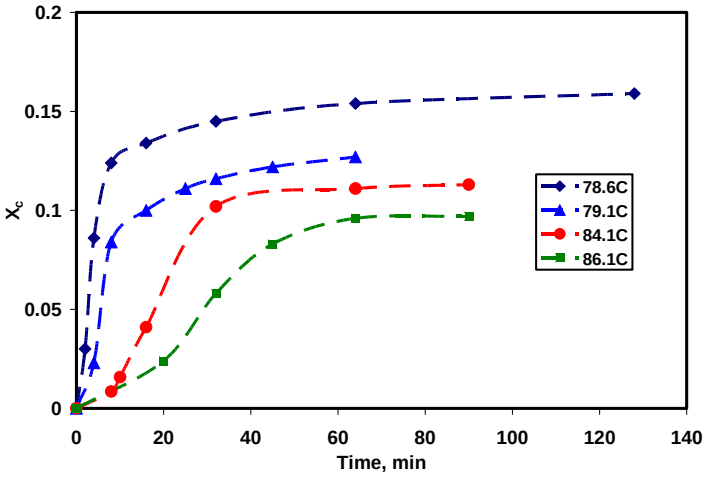

d)

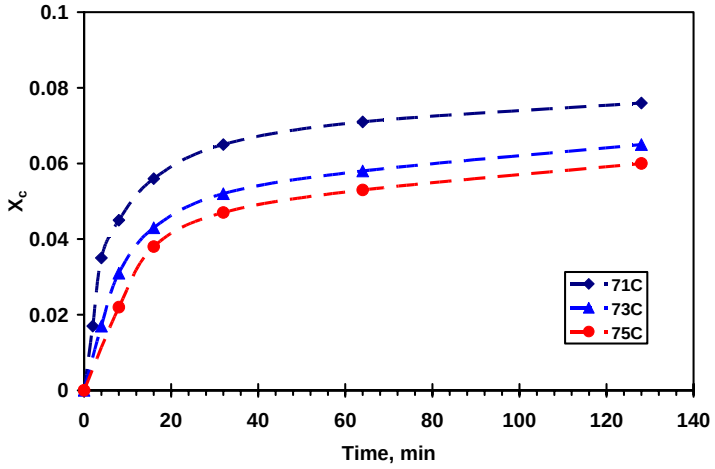

e)

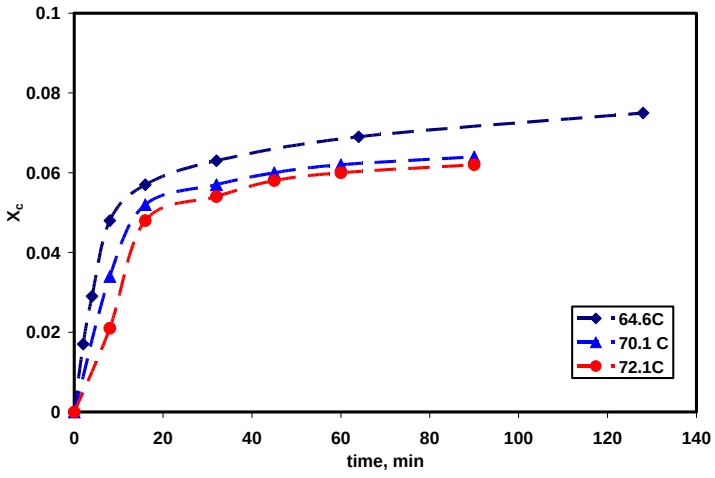

f)

Figure 6.1.33 Effect of the Ethylene Content and the Crystallization Temperature on Isothermal Crystallization: a) PE-I (0.0, 320), b) PE-II (4.4, 320), c) PE-III (7.8, 160), d) PE-I (8.2, 300), e) PE-III (12.3, 310), f) PE-I (13.6, 290)

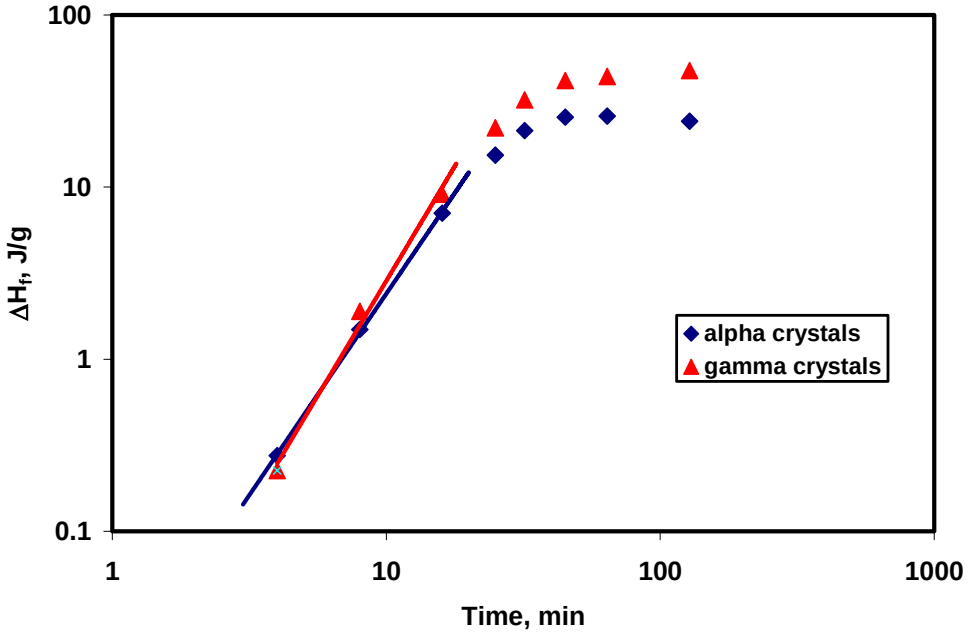

a)

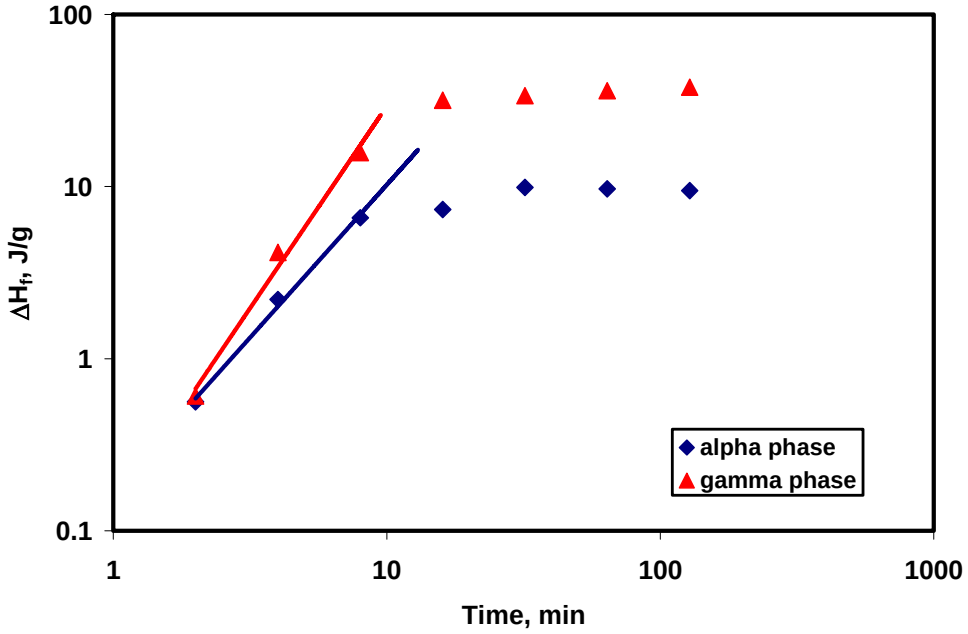

b)

Figure 6.1.34 Rate of the Crystal Phase Formation a) PE-I (0.0, 320) T_x = 122.1°C b) PE-II (4.4, 320), T_x = 96.1°C

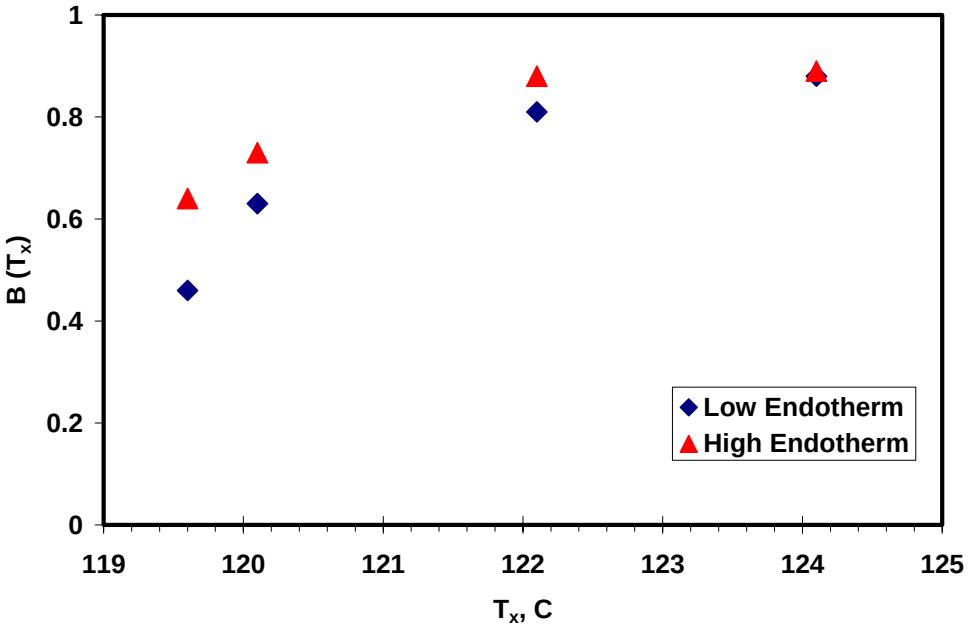

a)

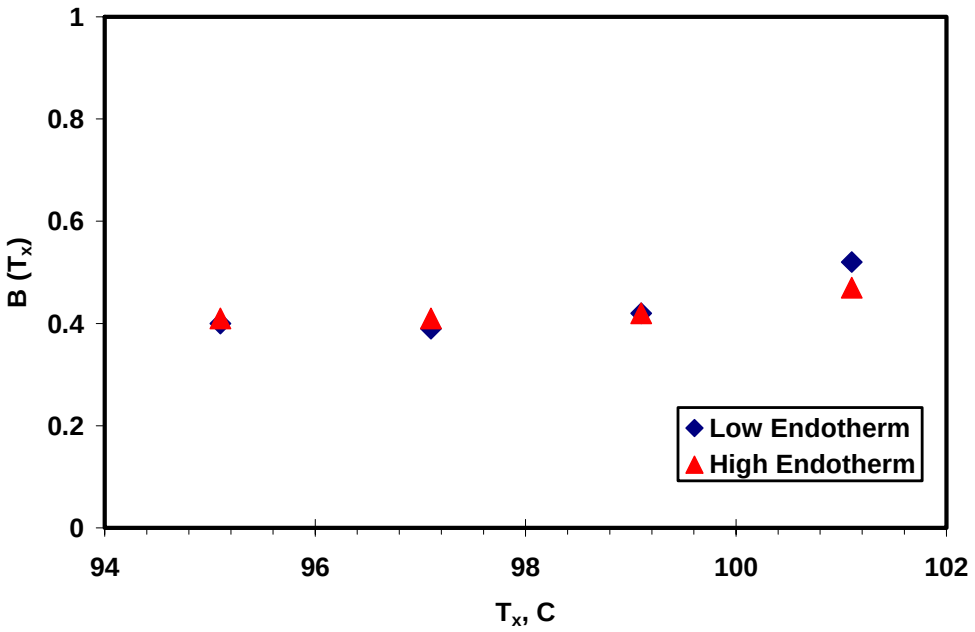

b)

Figure 6.1.35 Effect of the Crystallization Temperature on B(T_x) for a) PE-I (0.0,320), b) PE-II (4.4, 320)

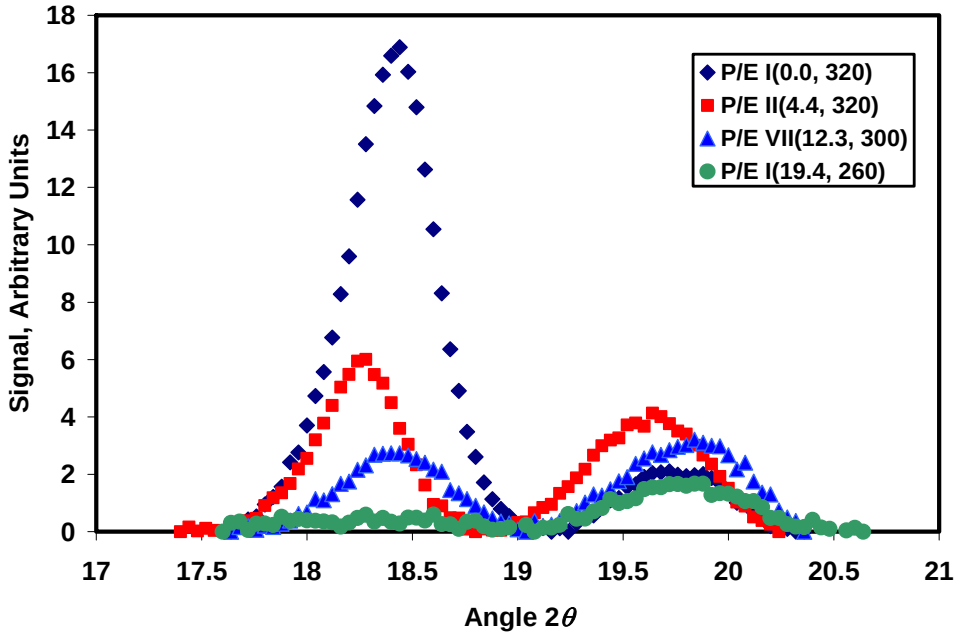

Figure 6.1.36 Effect of Composition on WAXD Signal for Selected Bench Top Cooled Dow Copolymers

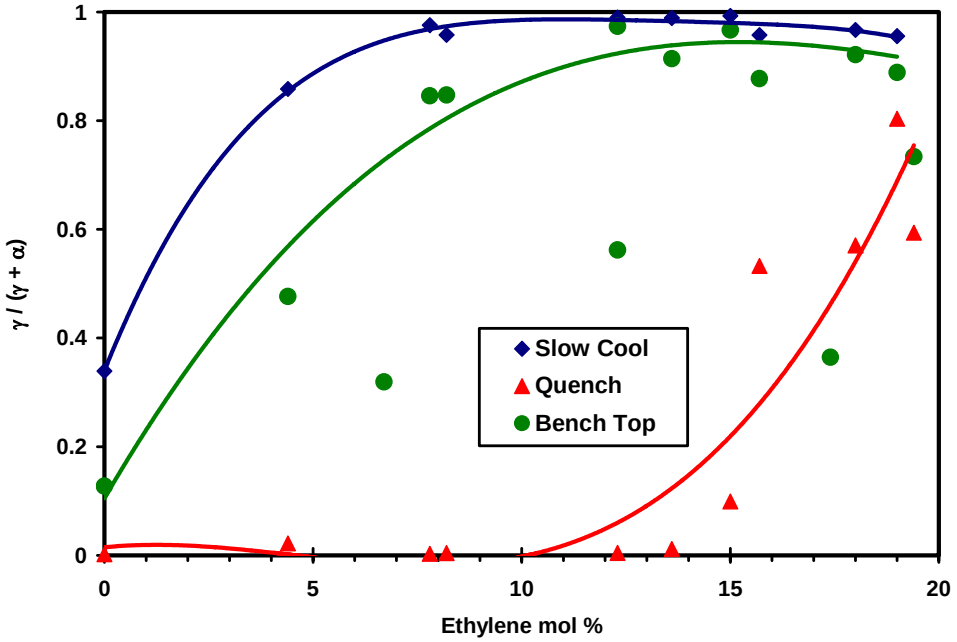

Figure 6.1.37 WAXD: Effect of the Ethylene Content and the Cooling Rate on the γ–Phase Content

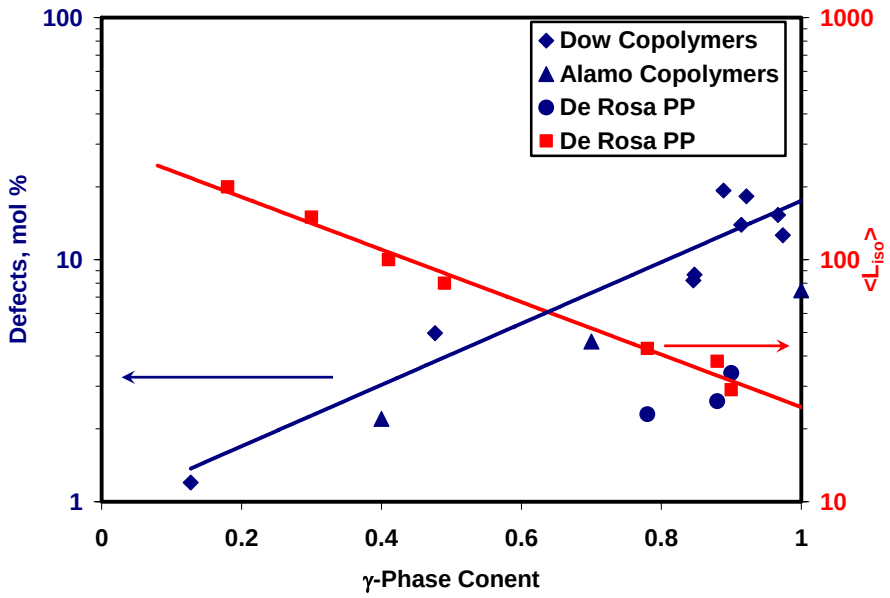

Figure 6.1.38 The Effect on the Defect Concentration and Isotactic Sequences Length <Liso> on γ-Phase Content for Dow Copolymers, Alamo et al.[50] P/E Copolymers, De Rosa et al.[124] PP (Blue Line Represents the Trendline only through Dow Copolymers Data Points)

Rosa et al.[124] for propylene homopolymer with regio- and stereo- defects are included in the same plot. For a given defect concentration, Dow copolymers exhibit slightly lower fraction of γ-phase crystals, especially when compared to the values reported by De Rosa et al. However, the rates of change of the γ-phase content with the defect concentration are similar for Dow copolymers for materials studied by Alamo et al. and De Rosa et al. The dependence of the isotactic sequences length, $<L_{iso}>$, on the amount of γ-phase crystals from De Rosa et al.[124] is also shown inFigure 6.1.38. $<L_{iso}>$ increase corresponds to the decrease in both, the defect concentration and γ-phase crystal content.

Figure 6.1.39 and Figure 6.1.40 contain the AFM and SEM micrographs of Dow copolymers of different ethylene content. The cross-hatching morphology is present in all images. As the ethylene content increases, the density of cross-hatching and the thickness and the length of lamellar crystals decrease. There is also an increase in the amount of amorphous phase as can be judged by the increase in the size and the number of dark regions on the AFM micrographs.

The morphologies of Dow, Ziegler-Natta and Metallocene copolymers of similar ethylene content are compared in Figure 6.1.41. All three structures are very similar and exhibit the signs of cross-hatching.

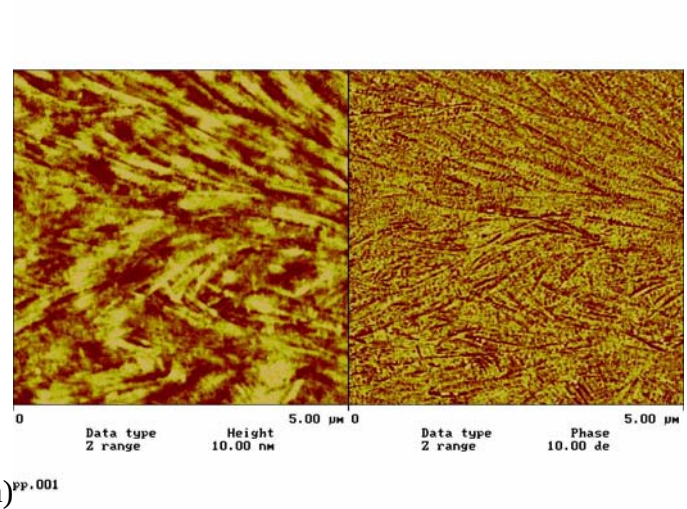
0
5.00 µm
Data type
Z range
Height
10.00 nm
0
5.00 µm
Data type
Z range
Phase
10.00 de
pp.001

a)

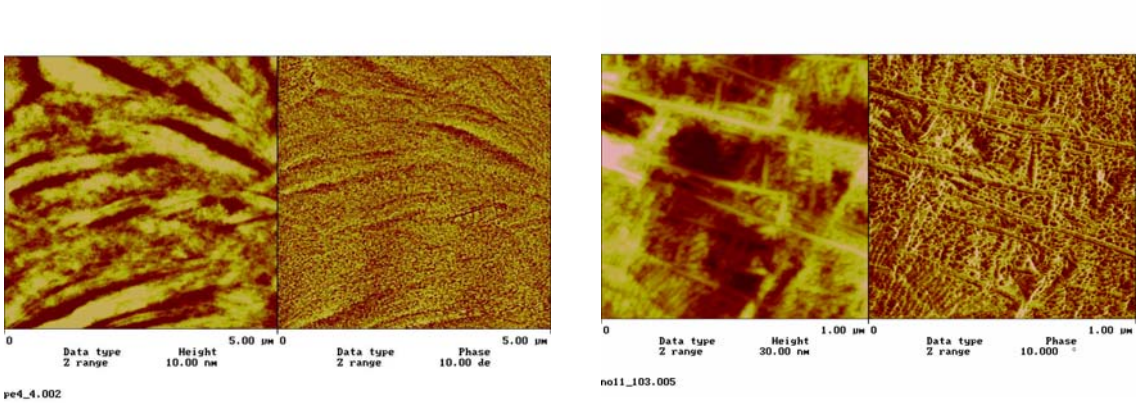
0
5.00 µm
Data type
Z range
Height
10.00 nm
0
5.00 µm
Data type
Z range
Phase
10.00 de
pe4_4.002
0
1.00 µm
Data type
Z range
Height
30.00 nm
0
1.00 µm
Data type
Z range
Phase
10.000
no11_103.005

b)

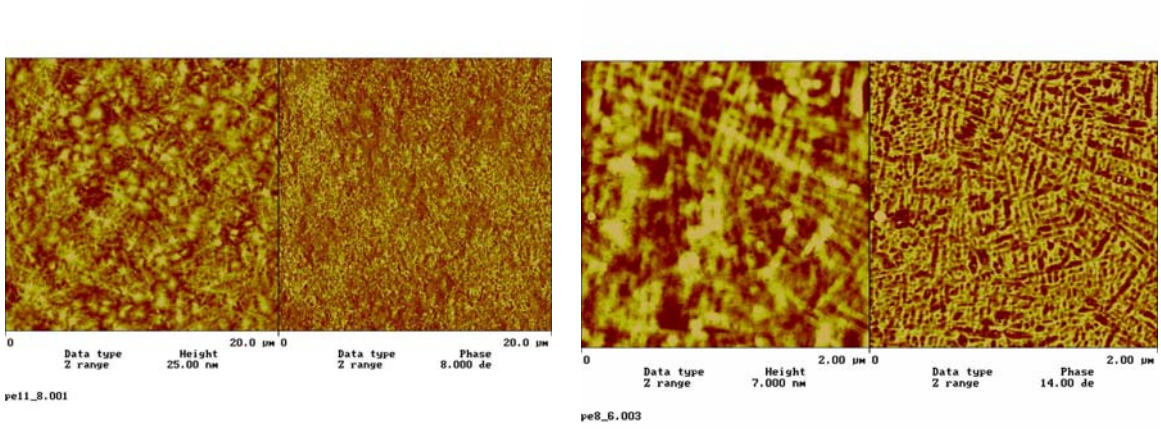
0
20.0 µm
Data type
Z range
Height
25.00 nm
0
20.0 µm
Data type
Z range
Phase
8.000 de
pe11_8.001
0
2.00 µm
Data type
Z range
Height
7.000 nm
0
2.00 µm
Data type
Z range
Phase
14.00 de
pe8_6.003

c)

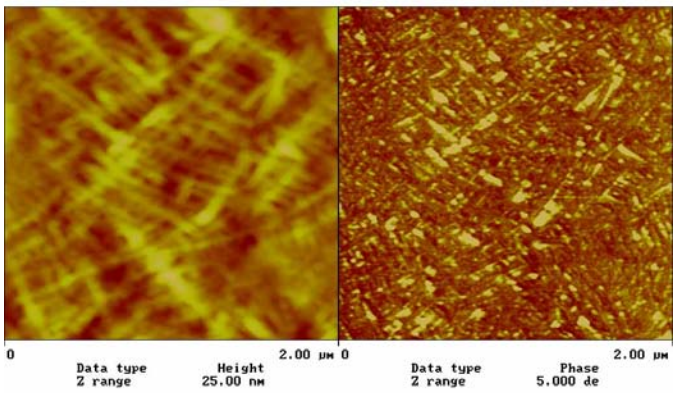

d) pe11_8.004

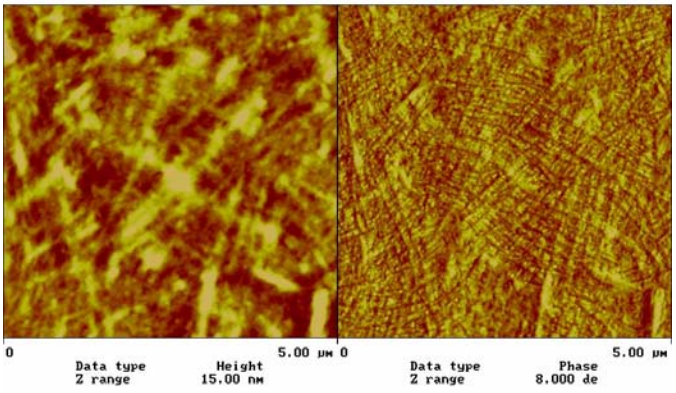

e) pe15_8.003

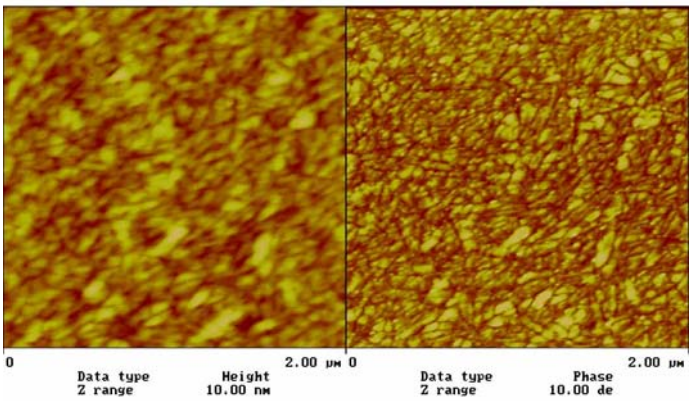

f) pe_18.004

Figure 6.1.39 AFM: Effect of Composition on the Morphology of Propylene-Ethylene Copolymers: a) PE-I (0.0, 320), b) PE-II (4.4, 320), c) PE-I (8.2, 300), d) PE-I (13.6, 290), e) PE-I (15.7, 260), f) PE-I (19.4, 260)

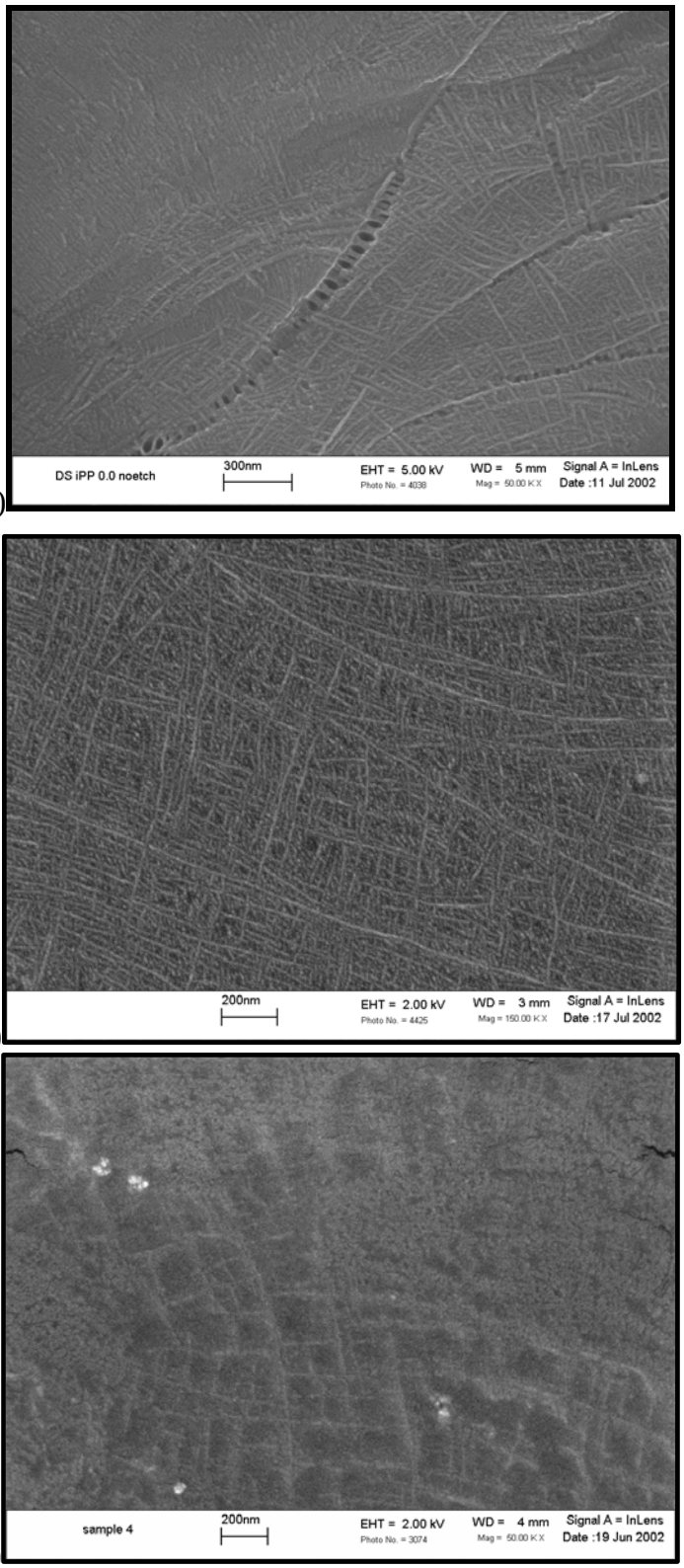

Figure 6.1.40 SEM: the Effect of Composition on Morphology of Propylene-Ethylene Copolymers: a) PE-I (0.0, 320), b) PE-I (8.2, 300) etched, c) PE-I (19.4, 260)

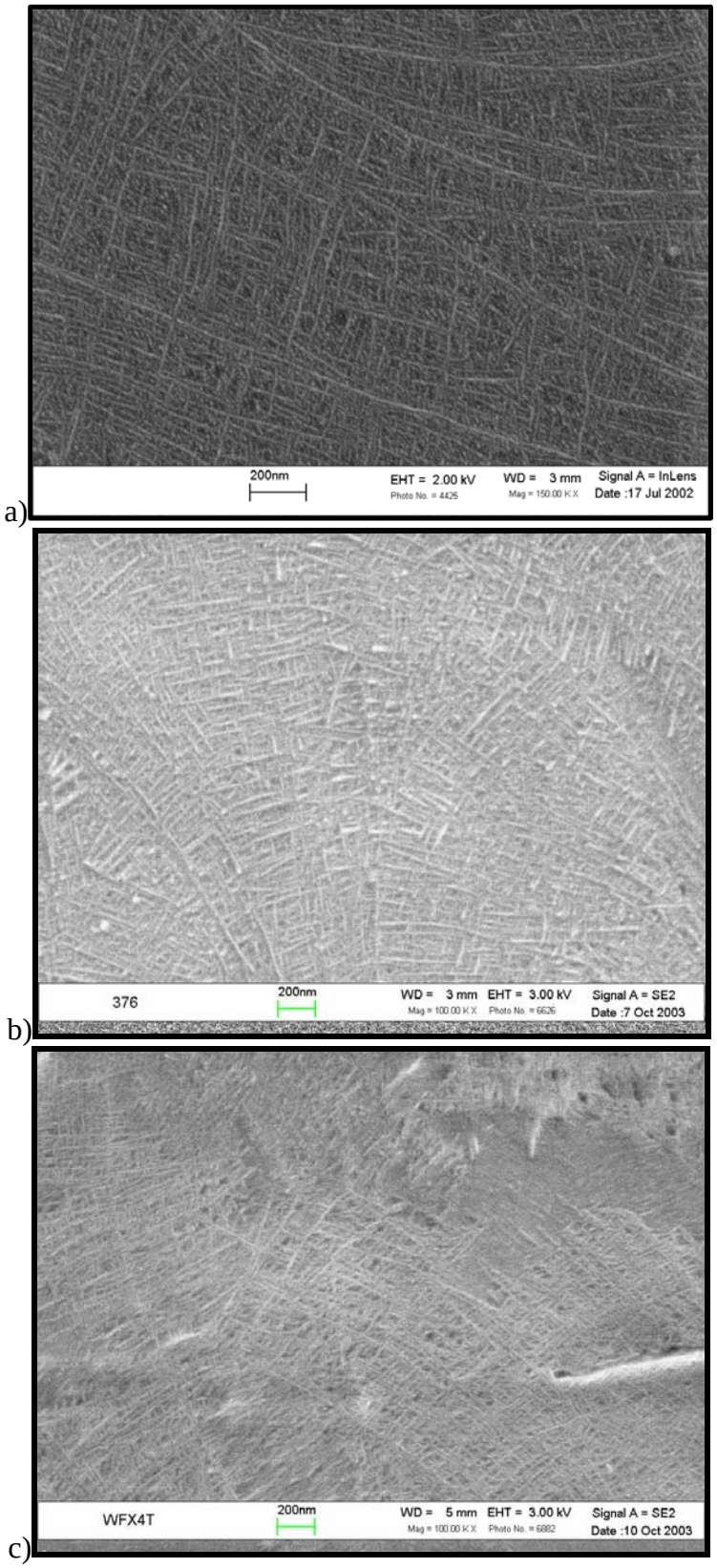

Figure 6.1.41 SEM: The Effect of the Catalyst System on Morphology of Propylene-Ethylene Copolymers: a) PE-I (8.2, 300) etched, b) ZN P/E 8.3 c) Met P/E 6.5

6.2 Discussion

6.2.1 Crystallization and Melting Studies

The crystallization and melting behavior of propylene-ethylene copolymers is to a large extent determined by the distribution polypropylene sequence lengths between defects and by the ability of these defects to enter the propylene crystal lattice. According to Flory's thermodynamic equilibrium theory[28,29,30], at any given temperature only the sequences of length larger than some critical value ξ are able to crystallize. As the crystallization temperature decreases, ξ decreases and shorter sequences can form crystals. Flory's treatment is applicable for copolymers where the "minor" comonomer is totally excluded from the lattice of the "major" comonomer. In the case of propylene-ethylene copolymers, defects along the polymer chain are either regio- or stereo-defects or ethylene units. A number of previous studies have suggested that a regio, stereo and small single co-unit defects can be included in the polypropylene crystal[42-49,85,86] One should expect that these different types of defects will disrupt the crystallization process of propylene sequences to various extents. In general, the larger the number of defects along the polymer chain, the lower the concentration of long chain sections able to crystallize at high temperatures and the larger the fraction of shorter sections able to crystallize at lower temperatures. It had been shown by Keller et al.[12] that the lamellar thickness is inversely proportional to the supercooling. The crystals formed at the lower crystallization temperatures then are composed of thinner lamella that melts at lower temperature. Hence, the inclusion of defects in the propylene chain leads to crystallization at lower temperature and formation of thinner crystals that melt at lower temperature. .

Dow copolymers contain region, stereo and ethylene defects. As PP-I (0.0, 320) is considered, peak crystallization and melting temperatures of 106°C and 144°C, respectively, are reported in this work for cooling and heating rates of 10^{o}C/min. These values are lower than these usually reported for PP homopolymer (e.g T_c of about 116°C and T_m of about 162°C were reported by Ojeda et al.[125] and T_c of 115°C and T_m of 170°C were reported by Feng et al.[40]). The reduction in melting and crystallization temperatures

is accounted for by the large defect content of this material. The content of regio defects in PP-I (0.0, 320) is 1.18 mol% and the content of stereo defects is 6.7 mol%.

As ethylene co-units are added to the polypropylene chain, they further disrupt the ability of these chains to crystallize. With an increase in ethylene concentration, one of two scenarios can occur. Each scenario is determined by the nature of the particular catalytic system and depends on the co-unit distribution.

If the ethylene units are distributed relatively randomly through the polymer chain (catalyst A), an increase in ethylene concentration leads to an increase in the amount of single E units. As a result of such incorporation, the copolymer chain has a substantial amount of short PP sequences surrounded by single ethylene units. As the number of E units increases, the energetic penalties become too large for this number of ethylene units to be included into the propylene crystal. Hence, the closely-spaced ethylene units and the short neighboring propylene sequences are rejected during crystallization, resulting in a lower degree of crystallinity.

On the other hand, if the distribution of ethylene units is fairly blocky (catalyst B), then, with an increase in ethylene concentration, the probability of formation of EE and longer sequences increases. Since these longer ethylene sequences can not be included in the crystal, the overall system crystallinity will decrease.

In both cases, a steady decrease in the degree of crystallinity, peak melting and crystallization temperatures is observed with increasing ethylene content (Figure 6.1.3 and Figure 6.1.8). However, the change in crystallinity observed with for the propylene-ethylene copolymers is much less severe than that observed for copolymers of propylene with 1-hexene or 1-octene.[126] In this latter investigation, it was shown that the depression in melting temperature, crystallization temperature and degree of crystallinity was the same for these two copolymer series, consistent with Flory's model for copolymers exhibiting exclusion effects. These results are in accordance with the present argument that ethylene units in the case of propylene-ethylene copolymers are at least partially included in the polypropylene crystals.

The increase in ethylene content must lead to a decrease in the thickness of crystal lamellae and consequently, to a decrease in the crystallization peak and onset temperatures, melting peak and offset temperatures and the overall system crystallinity

(Figure 6.1.3, Figure 6.1.6, Figure 6.1.7 and Figure 6.1.8). The plots of the crystallization onsets and melting offsets for the series I-III of Dow copolymers fit this theory well. However, series VII and VIII exhibit different behavior. Series VII copolymers with ethylene content in the range 12-21 mol% exhibit a high melting temperature shoulder that almost develops into a separate high temperature endotherm as the ethylene concentration is increased (Figure 6.1.4 and Figure 6.1.7). The peak associated with this endotherm has a very weak temperature dependence and corresponds to that expected for the copolymer with about 4 mol% of ethylene. The melting offsets for both series VII and VIII show almost no dependence on the ethylene content. These features are accompanied by a decrease in the crystallinity with increase in ethylene content for both Series of the same magnitude as was shown for series I-III Dow copolymers. These results suggest that copolymers in each of the series VII and VIII must have approximately the same long polypropylene sequences that allow crystallization at relatively high temperatures. This appears to be the case even for copolymers with an ethylene content as high as 21.2 mol%. These long polypropylene sequences form thicker lamellae that melt at temperatures corresponding to the melting of a copolymer with about 4 ethylene mol % for Series VII materials and about 6 mol % for series VIII materials.

The exact nature of the catalyst system used in the polymerization of Dow copolymers is unknown to us. However, it is known that the catalyst used for series I-III (catalyst A) is different form that used in series VII and VIII (catalyst B). While catalyst A is reported by Dow Chemical to yield a comonomer distribution that exhibits slight tendency toward alternation,[127] catalyst B results in materials that display significant blockiness in the ethylene unit distribution. Samples in series VII and VIII only differ in the polymerization conditions (pilot plant versus miniplant). Both series were polymerized by the same catalyst B. It can be speculated that the polymerization conditions of series VII and VIII copolymers led to the processing variability and that resulted in series VII copolymers having high crystalline fraction and series VIII copolymers having lower crystalline fraction present. Whatever maybe the source of the differences between series VII and VIII, it is clear that unit distribution plays a crucial role in shaping not only the crystallization and melting behavior of these materials but the

overall copolymer properties as well. For example, the presence of high crystalline fraction in series VII and VIII copolymers (responsible of the high melting temperature offset and the high temperature shoulder observed in DSC traces (Figure 6.1.2, Figure 6.1.4 and Figure 6.1.7) can become beneficial from the material processing standpoint. Since the melting window of theses copolymers is over 100°C, they should possess good processing flexibility that includes fiber spinning and film blowing.[5]

As the crystallinity of these copolymers decreases with an increase in the ethylene content, as was demonstrated for copolymers of all series, the amount of amorphous phase present between crystal lamellae increases. The behavior of a copolymer in amorphous regions is governed by the total amount of crystals and the intrinsic mobility of the parent homopolymers. Polypropylene exhibits a higher glass transition temperature than polyethylene due to restrictions in conformational changes associated with the presence of a pendant methyl group on every second carbon. An increase in ethylene concentration along the copolymer chain should, therefore, lead to a lower glass transition temperature. An increase in ethylene content also leads to a decrease in crystallinity, hence in the constraints exerted on the amorphous fraction. The net result of this decrease in crystallinity is therefore a further reduction of the glass transition temperature. This reduction in T_g is due to the decrease in the energy required to set off long range molecular motions in the less confined system. The glass transition depression for the Dow copolymers exhibit the same behavior for all series (Figure 6.1.8) and is consistent with the reduction from about -6°C for 0 mol% ethylene to about -35°C for 20 mol % previously reported for Ziegler-Natta propylene-ethylene copolymers by Gan et al.[128]

One of the goals of this work was to compare the properties of Dow copolymers to these of typical metallocene and Ziegler-Natta copolymers.

In general, metallocene and Ziegler-Natta catalysts differ in their nature and in the polymerization mechanism. While typical metallocene catalyst systems are homogeneous, the Ziegler-Natta catalysts are heterogeneous. Polymers prepared using Ziegler-Natta catalysts are characterized by much wider molecular weight distributions compared to the relatively narrow distribution achieved with metallocene systems (Mw/Mn ~ 2.0). Since the chain lengths vary greatly in Ziegler-Natta materials, their

crystallization and melting transitions tend to be wider than those for metallocene polymers.

Ziegler-Natta polypropylene generally crystallize in the α form even if the defect concentration is substantial. [57] α-phase crystals form thicker lamellae that melt at high temperature.[129,130] In contrast, metallocene polymers routinely crystallize into a mixture of α-phase and γ-phase crystals[50,82,124]. Since γ-phase crystals form thinner lamellae, these polymers usually have lower crystallization and melting temperatures than Ziegler-Natta polymers. These differences in crystal characteristics are due to the defect distribution along the polymer chain and relates to differences in the polymerization mechanism with metallocene and Ziegler-Natta catalyst systems.[131] Polymerization with metallocene catalysts leads to a polymer with more randomly distributed defects than does polymerization with Ziegler-Natta catalysts. In the latter case, the defects are concentrated in clusters of poorly crystallizable material.[85,131] As a result, the defects in metallocene catalyzed polymer disrupt the long polypropylene sequences leading to a large amount of poorly crystallizable sequences with high defect concentration. At the same time, the segregation of defects in the Ziegler-Natta catalyzed polymer into clusters leaves very long polypropylene sequences free of defects. The fact that shorter sequences tend to crystallize into γ-phase crystals[82] explains the preferable formation of the γ-phase in metallocene polymers as opposed to the Ziegler-Natta materials.

In our case, Dow copolymers have relatively narrow molecular weight distributions (Mw/Mn ~ 2.2-2.7) and crystallization and melting temperatures comparable to those of metallocene copolymers (Figure 6.1.12 and Figure 6.1.13). They also exhibit a substantial fraction of γ-phase crystals, even for the lowest ethylene content materials, as demonstrated by both, the isothermal crystallization and the WAXD data (Figure 6.1.29 and Figure 6.1.37). The crystallization and melting temperatures of the Ziegler-Natta copolymers of about the same concentration are substantially higher than those of metallocene and Dow copolymers. Judging by the lower crystallization and melting temperatures, which correspond to the crystallization and melting of thinner lamellae, the defect distribution in Dow copolymers is closer to that of metallocene catalyzed materials. On the other hand, the melting traces of Dow copolymers with 13 mol% ethylene and the crystallization traces of series VII and VIII have peaks that are

significantly broader than those for metallocene copolymers (Figure 6.1.11). These copolymers also have higher melting temperature offsets than do metallocene copolymers (Figure 6.1.15). These calorimetric studies confirm that while the Dow copolymers are in many respects similar to their metallocene-catalyzed counterparts, their propylene sequence distribution is less random and in the case of series VII and VIII, contains a much larger fraction of long propylene sequences.

6.2.2 Crystallinity and Thermodynamic Heat of Fusion

When crystallinities are calculated either from DSC or density data, a set of underlying assumptions has to be considered. Both approaches require the knowledge of some physical properties for the fully crystalline and fully amorphous materials. In the case of density calculations, these are the amorphous and the crystal densities. In the case of DSC analysis, these are the crystal and the amorphous heat capacities and the thermodynamic heat of fusion at melting.

In either of these approaches, the property of a semicrystalline polymer is principally governed by the amount of crystalline and amorphous phases, as well as by the properties of these phases. It has been proposed that the transition between the amorphous and the crystal phases is not sharp and can be described as an interphase composed of non-crystallizable units, defects that might be excluded from the crystal, and chain folds of varying lengths. The contribution of the interfacial region varies from polymer to polymer depending on the polymer molar mass, the stiffness of the polymer backbone, the bulkiness of the side-groups, the amount of defects, the distribution of crystallizable sequence lengths, etc… The properties of the interfacial region in propylene-ethylene copolymers are not well established. One approach followed by some researchers is to describe a semicrystalline polymer using a three-phase model with crystalline, mobile amorphous and constrained amorphous fractions.[87-99] While some studies claim that the density of the constrained amorphous phase is about the same as that of the mobile amorphous phase,[101] others report it to be higher.[102,103]

When the crystallinity of polypropylene is determined by the method outlined by Mathot,[117] the amorphous and crystalline heat capacities that are necessary for the calculations, are obtained from the ATHAS database. These database heat capacities were calculated using Tarasov functions. The experimental data was based on the average of a number of measurements performed on isotactic, syndiotactic and atactic polypropylenes.[132] Heat capacity values for a propylene-ethylene copolymer melt are obtained using the rule of mixture.

The polypropylene crystallinity calculations using the database values of Cp_{liq}, Cp_c and ΔH_f^0 = 207 J/g result in an underestimation of ΔC_p at the glass transition temperature, in agreement with results of Grebowicz et al.[91] Since the materials studied here contain stereo, regio and ethylene defects, their Cp_{liq}, Cp_c and ΔH_f^0 values may differ from those reported in the ATHAS database for pure polypropylene. Consequently, two approaches must be considered. In the first case, the Cp_{liq}, Cp_c and ΔH_f^0 values quoted for polypropylene are assumed to be applicable and the ΔC_p deficiency is then attributed to the presence of a third phase (i.e. the rigid amorphous fraction). In the second approach, the two-phase model is assumed to hold and the ΔC_p deficiency is a calculation artifact associated with the use of inappropriate values of Cp_{liq}, Cp_c and ΔH_f^0.

The possible disparity in amorphous and crystalline heat capacity values have been discussed in section 5.3 as a part of the uncertainty analysis. It was demonstrated that in the worse case, the heat capacity variability results in a 15% standard deviation and in most cases in less than 10% deviation from the calculated values. This uncertainty can not account for the ΔC_p deficiency.

The possible disparity in the values of the thermodynamic heat of fusion deserves a closer attention. It has been proposed by Sanchez and Eby[34,35] and demonstrated in a number of studies[41-50] that certain defects (stereo and single ethylene units) can be included in the propylene crystal. A dilation of the crystal unit cell as a result of defect incorporation in the polypropylene chain was shown by Laihonen et al.[41,42] in the case of ethylene defects and by Isasi et al.[123] for stereo and regio defects. As defects are included in a polypropylene crystal, the degree of crystal perfection decreases.

The thermodynamic heat of fusion at melting measures the amount of energy that is required to melt a perfect crystal. It is directly related to the crystal degree of

perfection. As a crystal with defects is considered, its equilibrium ΔH_f^0 value should reflect the amount of energy required to melt this particular defective crystal. This means that the thermodynamic heat of fusion at melting that is used in the crystallinity calculations should depend on the amount of stereo and structural defects that are included in the crystal. A linear decrease in ΔH_f^0 with increasing ethylene defect concentration is demonstrated for Dow propylene-ethylene copolymers in Figure 6.1.18.

Using solid-state NMR spectroscopy, Alamo et al.[50] showed that 42% of the ethylene units along a copolymer chain are included in the crystal phase. The partial inclusion of ethylene units in the crystal phase of Dow propylene-ethylene copolymers is demonstrated by the dependence of both the normalized calculated thermodynamic heat of fusion at melting and the normalized experimental enthalpy of fusion (Figure 6.1.20 and Figure 6.1.21). Normalization consisted in dividing the heat of fusion by the total mass of propylene units in the copolymer. Since both of these quantities are still a function of the ethylene content after normalization, then, ethylene units have to be included in the propylene crystal. The decrease in the normalized heat of fusion is shown to be ca. 4.5 J/g_{PP}/mol% ethylene, a value which is consistent with 3-4 J/g/mol% ethylene reported by Laihonen et al.[42]

It has been demonstrated that the ethylene defects are included in γ-phase crystals and an increase in the defect concentration further favors the formation of γ phase.[51] It can be then argued that a calculated change in the thermodynamic heat of fusion may be due to a decrease in the content of α-phase crystals and an increase in the content of γ-phase crystals. However, it has been determined by Ferro et al.[133] that the packing energies of α-phase and γ-phase crystals are almost the same. This means that the thermodynamic heat of fusion of the two phases should be about the same and the calculated change in the ΔH_f^0 values is not due to differences in the fractions of α-phase and γ-phase crystals obtained after crystallization.

We now examine the applicability of the RAF and inclusion models to describe the morphology of these copolymers. The dependence of crystallinity on ethylene content calculated by both the RAF and the inclusion models is shown in Figure 6.1.22. Since the thermodynamic heat of fusion values used in the inclusion model calculations are lower than the value of 207 J/g used in the RAF model, the crystallinities calculated for

the inclusion model are significantly higher than those obtained with the RAF model. For comparison purpose, it would therefore be valuable to obtain an estimate of the degree of crystallinity through a non-calorimetric method.

A second estimate of crystallinity was obtained from density measurements. The issue related to the choice of crystal density for the crystallinity calculations has been presented in Section 6.1.2. Since the crystal density is closely related to the degree of crystal packing, it should be greatly affected by the inclusion of defects into the crystal phase. Two studies addressed the issue of density for defective polypropylene crystals. Isasi et al.[123] investigated the effect of regio and stereo defects on the crystal density, while Laihonen et al.[42] studied the effect of ethylene inclusion on the crystal density. The unit cell dimensions determined in both of these studies have been used for the density calculations. As was shown in Section 6.1.2, the crystallinities calculated using these unit cells are very similar except for the propylene homopolymer.

The crystallinities calculated by the inclusion model are slightly lower than the density crystallinities calculated using the unit cell dilation parameters from the Alamo and Laihonen studies for low ethylene content materials. The disparity between these crystallinities increases with ethylene content. There can be several reasons for the disparities between the two data sets. Alamo's study demonstrated that the presence of regio defects causes unit cell dilation. However, it did not describe the dependence of the crystal density on the defect concentration. Laihonen et al.[42] investigated the effect of ethylene inclusion on the propylene unit cell dilation in the range of 0-11 ethylene mol%. Finally, to calculate copolymer crystal densities from unit cell dimensions, one must account for the mass deficiency associated with the substitution of some propylene units by ethylene units. This was achieved by recalling the conclusion of a NMR study of 0.8 - 7.5 mol% ethylene copolymers that 42% of ethylene units are partitioned in the crystal phase.[50] It is reasonable to assume that with a further increase in ethylene content, a saturation of the crystal by ethylene units could be reached and the partitioning coefficient may decrease. The partitioning coefficients for the low ethylene content copolymers could also be lower than 42%. Dow copolymers have a large number of regio and stereo defects. The inclusion of these defects in the propylene crystal alongside the ethylene defects can effectively reduce the fraction of the included ethylene units.

Unfortunately, there is no reliable data in the literature that addresses both, the crystal density for copolymers with a large amount of ethylene defects and the partitioning coefficients for propylene-ethylene copolymers with a significant amount of regio- and stereo defects included in the chain. The disparity between DSC crystallinities calculated with the inclusion model and density crystallinities can then be attributed to uncertainties in the values of crystal densities for high ethylene content copolymers and the partition coefficients for these particular copolymers.

The crystallinities calculated with the RAF model are systematically lower than the density crystallinities. Let us assume for the sake of argument that a RAF is present in the material in the amount predicted by the RAF model and let us make the extreme assumption that the density of the rigid amorphous phase is the same as crystal density. While the RAF density should be somewhat higher than the amorphous density since the interphase is the region where the crystalline order is dissipated, it is a disordered phase and should be less dense than the crystal phase. Even with this extreme assumption, the density crystallinity values do not agree with the RAF DSC crystallinities.

In Figure 6.1.27, the presence of a rigid amorphous fraction was also considered within the scope of the inclusion model. In fact, the observed ΔC_p deficiency does not need to be a proof for the existence of rigid amorphous fraction. As demonstrated in Figure 6.2.1 for higher crystallinity copolymers, the region just above T_g exhibits contributions from both, the continuing relaxation of the glass transition and the onset of melting. As a result, the slope of the extrapolated C_{pb} line is overestimated, leading to the underestimation of $\Delta C_p(T_g)$. The ΔC_p deficiency artifact is shown in Equation 6.2.1 and Equation 6.2.2 and in Figure 6.2.1.

$$\frac{theoretical\Delta Cp_{sc}}{theoretical\Delta Cp_{liq}} = 1 - X_c \qquad \textbf{Equation 6.2.1}$$

$$\frac{measured\Delta Cp_{sc}}{measured\Delta Cp_{liq}} = 1 - X_c - X_{RAF} \qquad \textbf{Equation 6.2.2}$$

Among the two approaches used to calculate the crystallinities of Dow copolymers, the RAF and inclusion model, the inclusion model agrees with the density crystallinities to a higher degree. The inclusion of ethylene units into the polypropylene crystal phase has been demonstrated and the application of the inclusion model to this copolymer system appears rational. At the same time, application of the rigid amorphous phase concept to copolymers with included defects was shown to be inadequate when attempting to account for a ΔC_p deficiency at T_g.

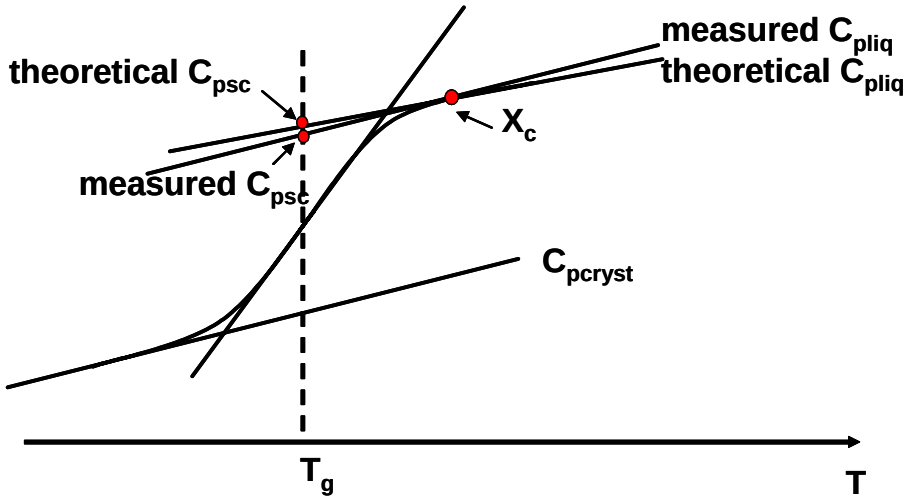

Figure 6.2.1 ΔC_p Deficiency Calculations

6.2.3 Morphology

Crystallization of polypropylenes with low defect concentrations leads primarily to α-phase crystals. It was demonstrated in a number of studies that if the chirality of two consecutive sheets (of R or L it-PP helices) is the same, then, epitaxial lamellar branching is observed.[56,65,64] This leads to the cross-hatched morphology, characteristic of propylene-based materials. In the case of epitaxial lamellar branching, a daughter lamella nucleates at angles of 80° or 100° from the parent lamella. As defects are added to a polypropylene chain, they become mostly included in γ-phase crystals which nucleate at 40° angles from the parent α-phase lamellae.[70]

Propylene-ethylene copolymers exhibit both α-phase and γ-phase crystals. Isothermal crystallization studies clearly reveal two distinct crystal populations as demonstrated by two distinct melting endotherms (Figure 6.1.29, Figure 6.1.30, Figure 6.1.31 and Figure 6.1.32) for all propylene-ethylene copolymers. These two endotherms correspond to the melting of α-phase and γ-phase crystals.

The relative ease of formation of α-phase and γ-phase crystals is governed by the local density of ethylene defects. It was already discussed in Section 6.2.1 that shorter sections of polypropylene chain or sections of polypropylene chain with a larger concentration of defects tend to crystallize into γ-phase crystals. These form thinner lamellae that melt at lower temperature. Since γ-phase crystals are expected to melt at lower temperature than do α-phase crystals, the lower melting endotherm in the isothermal crystallization studies corresponds to the melting of the γ-phase crystals and the high endotherm corresponds to the melting of the α-phase crystals. This assignment of the endotherms correlates well with the results in Figure 6.1.29. The PE-I (0.0, 320) polymer with no ethylene units, has a large number of long polypropylene sequences free of defects. Consequently, it crystallizes predominantly into α-phase crystals. The γ-phase crystals formed for this polymer are the result of the partial inclusion of some stereo and regio defects. The isothermal crystallization trace reflects this scenario: PE-I (0.0, 320) low temperature endotherm peak, which was assigned to the melting of γ-phase crystals, is lower than the high temperature endotherm peak which was assigned to the melting of α-phase crystals. As the ethylene content increases, the availability of long propylene sequences decreases. As a result, for higher ethylene content copolymers, the γ-phase content increases, leading to a more prominent low temperature endotherm.

An increase in crystallization temperature is typically associated with an increase in lamellar thickness. However, the number of propylene sequences of a given length decreases with the sequence length. Hence, a lesser number of sections of polypropylene chains will tend to crystallize at higher temperature. The predicted decrease in crystallinity with an increase in crystallization temperature is shown in Figure 6.1.33 for each copolymer. The larger the ethylene content, the shorter the average propylene sequence free of defects, the lower the crystallization temperature of that copolymer.

Consequently, high ethylene content copolymers crystallize at lower temperatures and achieve lower overall crystallinities.

One of the questions concerning the morphology of propylene-ethylene copolymers is which phase (α or γ) crystallizes first. As demonstrated in Figure 6.1.34, at short crystallization times (2 min) the α-phase peak is about the same height as the γ-phase peak. This suggests that the α-phase and γ phase crystals develop simultaneously. As the crystallization time increases, the peak associated with the growth of α-phase crystals reaches a maximum at an earlier time than that associated with the growth of γ -phase crystals. Similar results were obtained by Alamo et al.[82] in the study of polypropylene with regio-defects. These results agree with the assumption that γ -phase crystals form by epitaxial nucleation on α-phase crystals using the more defective chain sections. As the long propylene sequences are used up during the formation of α-phase crystals, the γ -phase continues growing as long as the shorter polypropylene sequences are available.

The rate of shift of the melting temperature $B(T_x)$ for PE-I (0.0, 320) and PE-II (4.4, 320) is shown in Figure 6.1.35. The shift of the melting temperature with crystallization time results from the lamellar thickening process and is associated with secondary crystallization. As the thickness of a lamella increases, its melting temperature increases as well. Since the lamellar thickening process is made possible by the existence of conformational motion within the crystal phase, an increase in temperature implies an increase in the rate of conformational changes, hence, an increase in the rate of lamellar thickening.[134] The values of $B(T_x)$ then should increase with an increase in the crystallization temperature, as demonstrated in Figure 6.1.35.

The results of the WAXD data analysis support the conclusions reached in the isothermal crystallization studies of propylene-ethylene copolymers. As the propylene sequence lengths decrease as a result of the increase in the ethylene concentration, the amount of the γ -phase crystals increases (Figure 6.1.37).

The ease of formation of γ-phase crystals is also dependent on the crystallization rate. The copolymers crystallized at slower rates have larger amount of γ-phase crystals as compared with copolymers crystallized at higher rates. At higher temperatures, corresponding to the crystallization at the slower rates, only the longer propylene

segments can crystallize. For propylene-ethylene copolymers, especially for those with high ethylene content, the sequences that can crystallize at high temperature necessarily include a number of ethylene defects. Since α-phase crystals can not accept these defects, predominantly γ-phase crystals will form. Of course, if the crystallization temperature is sufficiently high, then the necessary crystallizable sequence must be large. Consequently, the fraction of chains sections that can crystallize into γ-phase crystals eventually decreases. At high cooling rates, corresponding to the crystallization at lower temperature, the shorter sequences without defects can crystallize into α-phase crystals. Alamo et al.[82] demonstrated that with an increase in the crystallization temperature the content of the γ-phase goes through the maximum. These findings are consistent with the explanation of the cooling rate effect on the γ-phase crystal content.

The relationship between the defect content, isotactic sequence length and the γ-phase crystal content is demonstrated in Figure 6.1.38, where the data obtained in this study is combined with data from Alamo et al.[50] and De Rosa et al.[124] The increase in the γ-phase crystal content with isotactic propylene sequence length is clearly demonstrated by the data of De Rosa et al. These results fit well with the argument that the introduction of defects into a propylene chain leads to a decrease in the long sequences and, consequently, to a preferential nucleation of γ-phase crystals from shorter propylene sequences.

The evolution of the morphology with an increase in ethylene content is further demonstrated by the results of AFM and SEM studies.

The epitaxial lamellar branching, typical of the polypropylene morphology, is present in most AFM and SEM micrographs (Figure 6.1.39 and Figure 6.1.40), as evidenced by crystal orientations at 80° and 100° angles to each other. The 40° angle, corresponding to γ-phase branching is especially well observed in the AFM micrograph of PE-II (4.4, 320) material.

In PE-I (0.0, 320) and PE-II (4.4, 320) materials, the spherulitic behavior is observed, as evidenced by the radial orientation of lamellae. However, as the ethylene content is increased, the evidence of spherulitic behavior is no longer found. Similar results were reported by Hosier et al.[49] who observed the spherulitic behavior only in the

propylene-ethylene copolymers with ethylene concentration below 6 mol%. These results suggest that the spherulitic lamellar arrangement is disrupted by high concentration of defects and not by the branching of γ-phase crystals.[49]

With an increase in ethylene concentration, the amount of amorphous phase present in the copolymers is increased. This change can be monitored by considering the increase in the dark areas on the AFM micrographs, corresponding to a presence of a softer material, for copolymers of increased ethylene content. Also, as the concentration of ethylene defects increases, α-phase crystals become shorter and thinner (Figure 6.1.40).

These results correlate well with the discussion of the effect of defect concentration on the morphology of propylene-ethylene copolymers. The increase in ethylene content leads to a decrease in the length of the crystallizable isotactic polypropylene sequences. This effect is exemplified by a decrease in length, thickness and number density of the α-phase lamellae and an increase in length, thickness and number density of the γ-phase lamellae.

7 NUCLEATED COPOLYMERS

In this chapter, the results of studies of P/E-I(8.2, 320) Dow copolymer modified by four different nucleating agents (vanilla iPP-low MFR, vanilla iPP-high MFR, commercial HMS iPP and HDPE) will be presented. In the first section, the results of the crystallization and melting behavior studies of the nucleated copolymers will be given, followed by the results of morphological studies of these materials. The second section will contain the discussion of the presented results.

7.1 Results

The apparent heat capacities during crystallization and melting of the P/E-I(8.2, 320) nucleated by 3 wt% of vanilla iPP-low MFR, vanilla iPP-high MFR, commercial HMS iPP and HDPE additives that were calculated from the DSC data by the method outlined in Section 5.1, are shown in Figure 7.1.1. The addition of nucleating agent leads to an increase in the crystallization temperature of the copolymer. As evident from Figure 7.1.1, the non-nucleated sample has the lowest crystallization temperature. The order of increase in crystallization temperature as a result of adding 3 wt% of nucleator from the lowest T_x to the highest is the following: vanilla iPP-low MFR < HDPE < vanilla iPP-high MFR < HMS iPP. In the copolymer, nucleated by 3 wt% of HMS iPP, a second crystallization peak is visible at the temperature corresponding to T_x of the non-nucleated P/E-I(8.2, 320). The crystallization exotherms of nucleated copolymers are broader than for the virgin copolymer. The apparent melting heat capacities of the copolymers modified by 3 wt % nucleating agent exhibit three distinct melting peaks. The lowest temperature peak corresponds to the melting of the non-nucleated P/E-I(8.2, 320).

The effect of the level of nucleating agent on the crystallization heat capacities of the P/E-I(8.2, 320) copolymer for each additive is demonstrated in Figure 7.1.2. In each case there is an increase in the crystallization temperature of the materials with an increase in the concentration of the nucleating agent. In the case of nucleation by vanilla iPP- high MFR, the second exotherm appears at the T_x corresponding to the

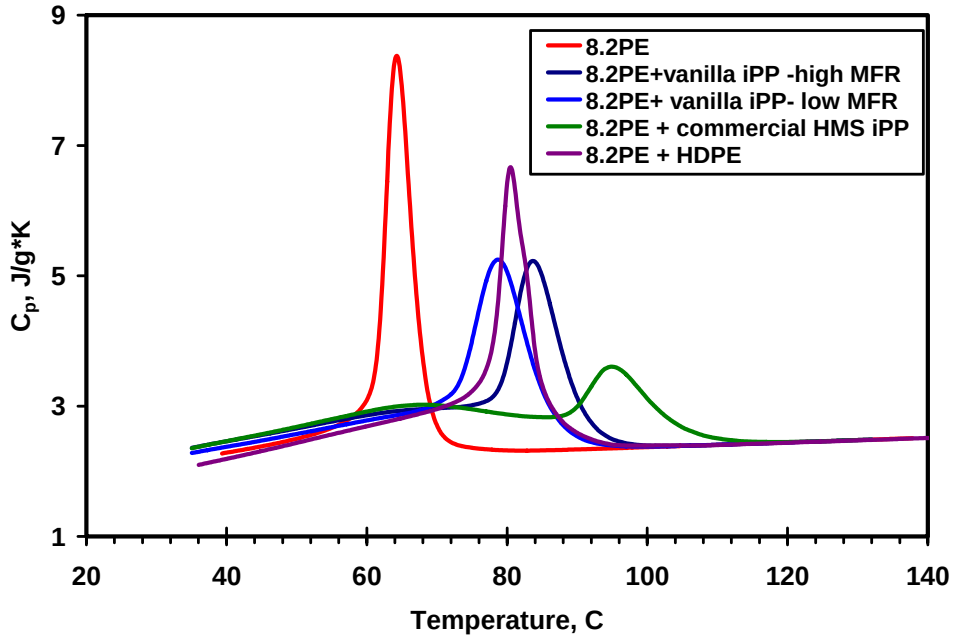

a)

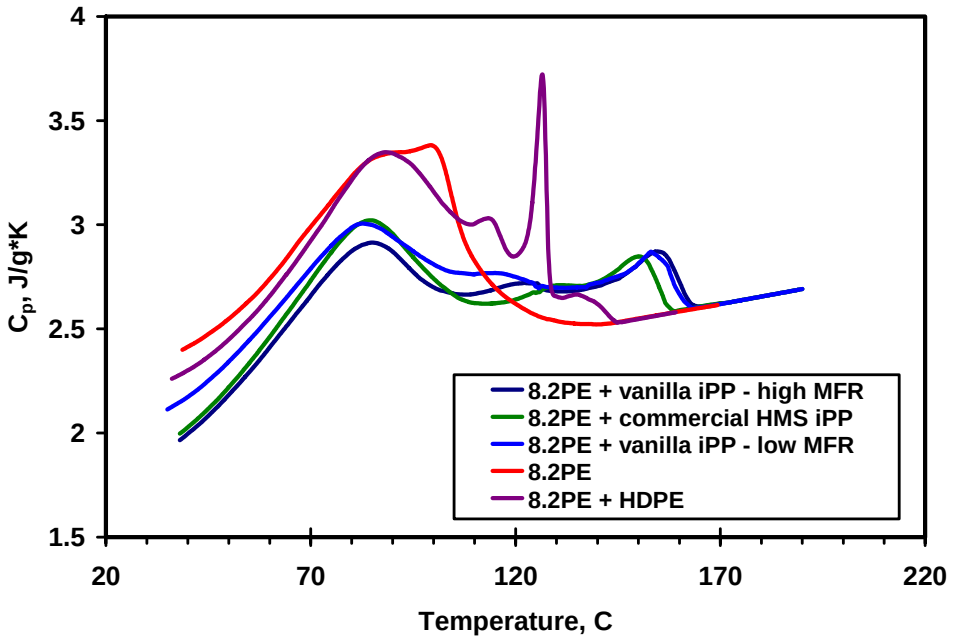

b)

Figure 7.1.1 Effect of the Type of Nucleating Agent at 3wt% on the a) Crystallization DSC Trace, b) Melting DSC Trace

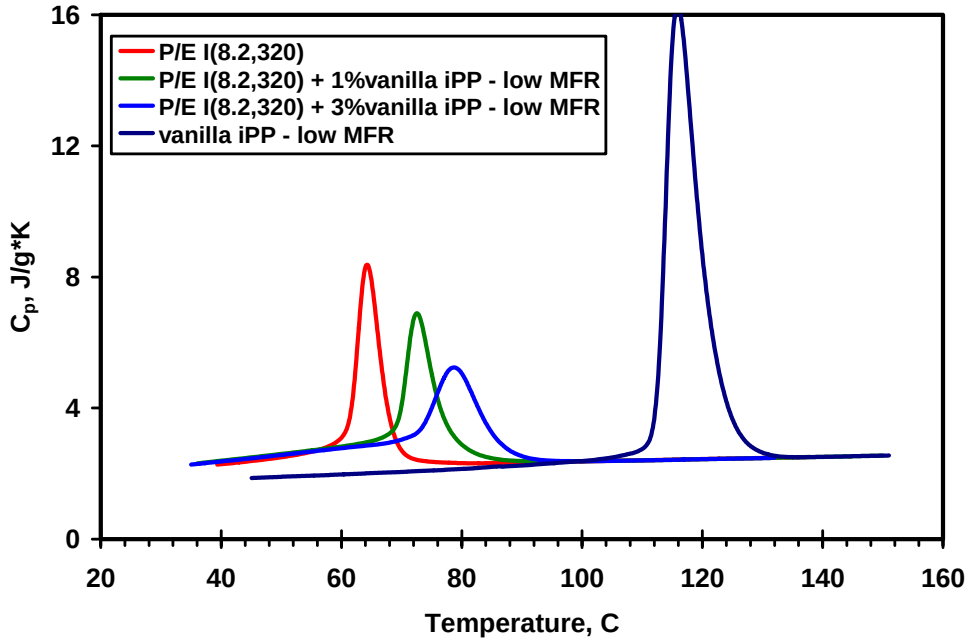
P/E I(8.2,320)
P/E I(8.2,320) + 1%vanilla iPP - low MFR
P/E I(8.2,320) + 3%vanilla iPP - low MFR
vanilla iPP - low MFR
Cp, J/g*K
Temperature, C
0
4
8
12
16
20
40
60
80
100
120
140
160

a)

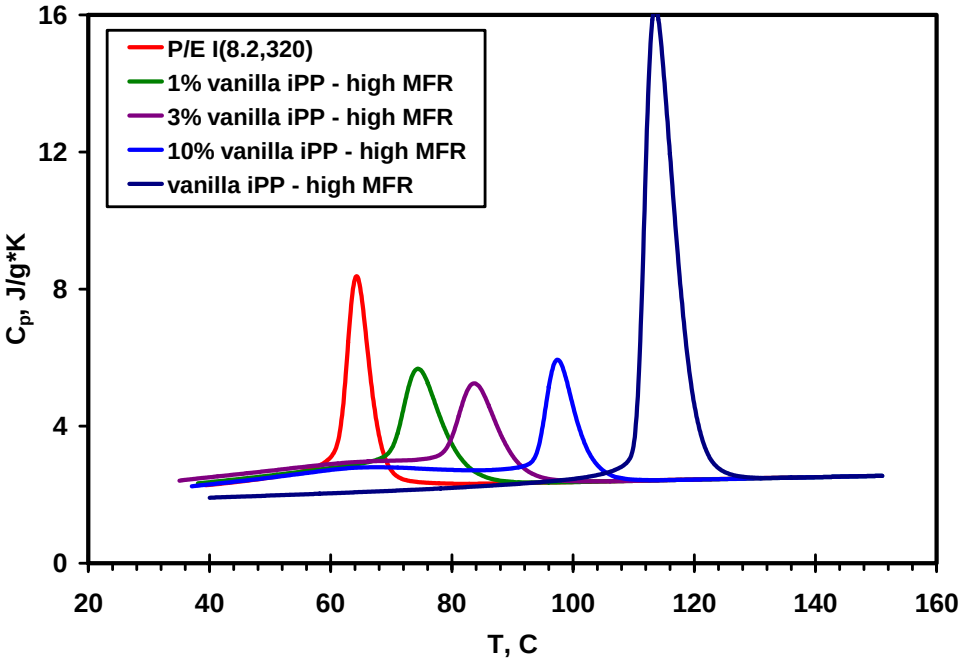
P/E I(8.2,320)
1% vanilla iPP - high MFR
3% vanilla iPP - high MFR
10% vanilla iPP - high MFR
vanilla iPP - high MFR
Cp, J/g*K
T, C
0
4
8
12
16
20
40
60
80
100
120
140
160

b)

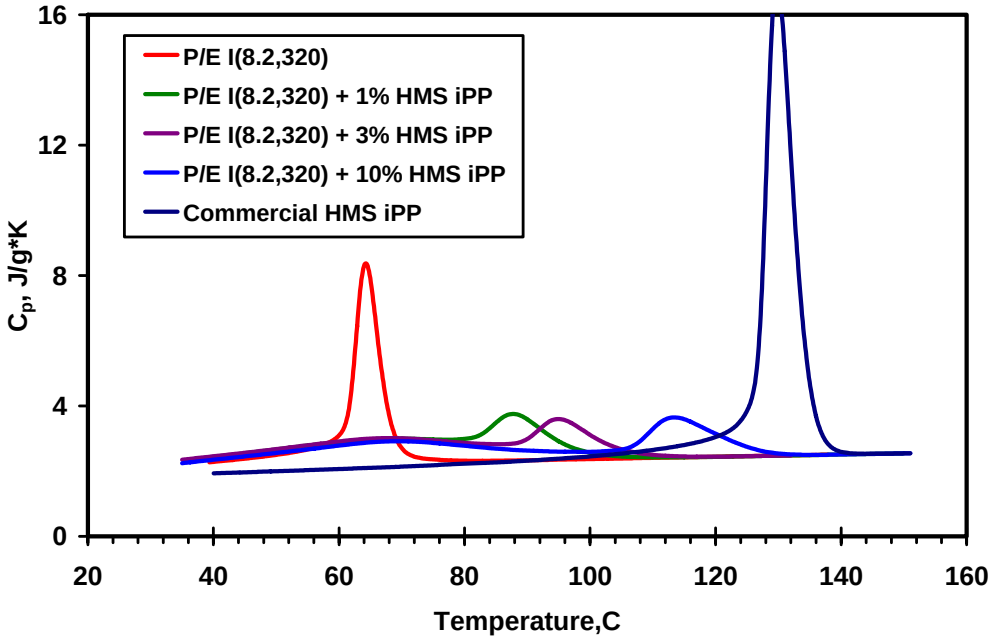

c)

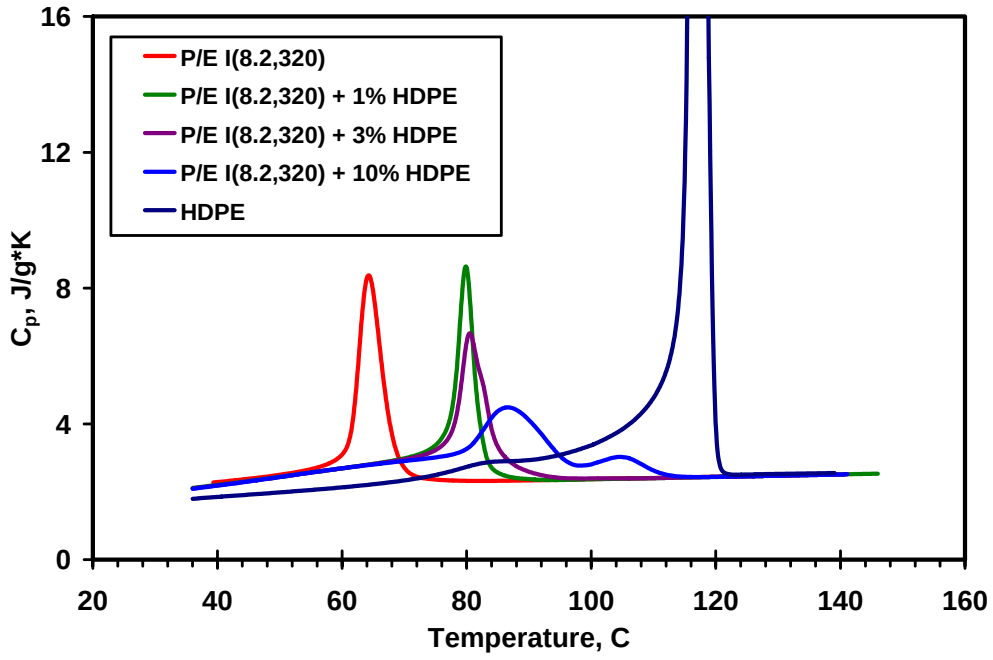

d)

Figure 7.1.2 Effect of Nucleating Agent Content on Crystallization DSC Trace of P/E I (8.2, 320): a) vanilla iPP-low MFR, b) vanilla iPP-high MFR, c) commercial HMS iPP, d) HDPE

crystallization temperature of virgin P/E-I(8.2, 320) copolymer, at the concentration of 10 wt% of the nucleator. In the case of nucleation by HMS iPP, the second peak at T_x of P/E-I(8.2, 320) is present for all nucleator concentrations. In the case of nucleation by HDPE, the high temperature shoulder appears at the T_x corresponding to the crystallization temperature of HDPE at the concentration of 3 wt% of the nucleator. The shoulder develops into a separate high temperature exotherm at the concentration of 10 wt% of the HDPE.

The effect of content in nucleating agent on the apparent melting heat capacities of the P/E-I(8.2, 320) copolymer is demonstrated in Figure 7.1.3 for each additive. For all materials, a melting endotherm is observed at the temperature corresponding to the melting of P/E-I(8.2, 320) copolymer. The second endotherm at the temperature corresponding to T_m of the nucleator is present in the copolymers modified by vanilla iPP-low MFR, vanilla iPP-high MFR and commercial HMS iPP. The copolymers modified by HDPE have two high temperature endotherms, one corresponding to T_m of HDPE and another, at the temperatures between the T_m of P/E-I(8.2, 320) and T_m of HDPE.

The effect of content in and type of nucleating agent on the copolymer crystallization onset is shown in Figure 7.1.4. The increase in crystallization onset temperature with nucleator concentration is observed for all types of modifiers. Out of the four nucleating agents, the commercial HMS iPP has the largest impact on the crystallization onset of P/E-I(8.2, 320) copolymer.

The changes in the morphology of the P/E-I(8.2, 320) copolymer as a result of the modification by the nucleating agents was studied by means of the WAXD analysis and SEM.

The results of the WAXD measurements for copolymers nucleated by vanilla iPP-high MFR, commercial HMS iPP and HDPE are shown in Figure 7.1.5 and Figure 7.1.6. With the addition of any modifier, the crystallinity of the P/E-I(8.2, 320) decreased. On the other hand, the amount of γ-phase in the nucleated copolymers increased, especially in the case of nucleation by HDPE.

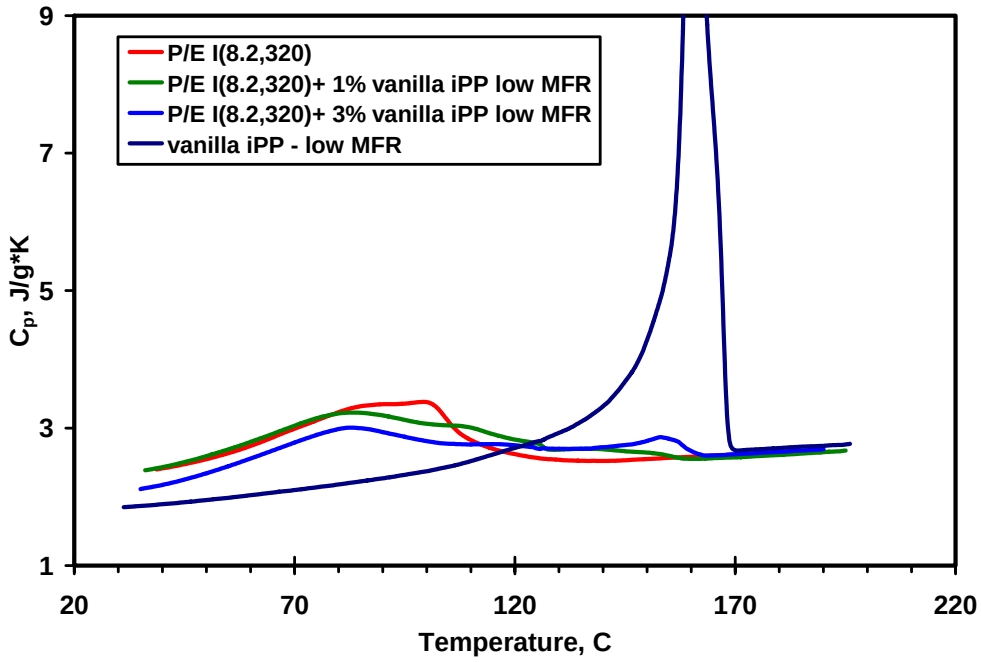
P/E I(8.2,320)
P/E I(8.2,320)+ 1% vanilla iPP low MFR
P/E I(8.2,320)+ 3% vanilla iPP low MFR
vanilla iPP - low MFR
Cp, J/g*K
Temperature, C
9
7
5
3
1
20
70
120
170
220

a)

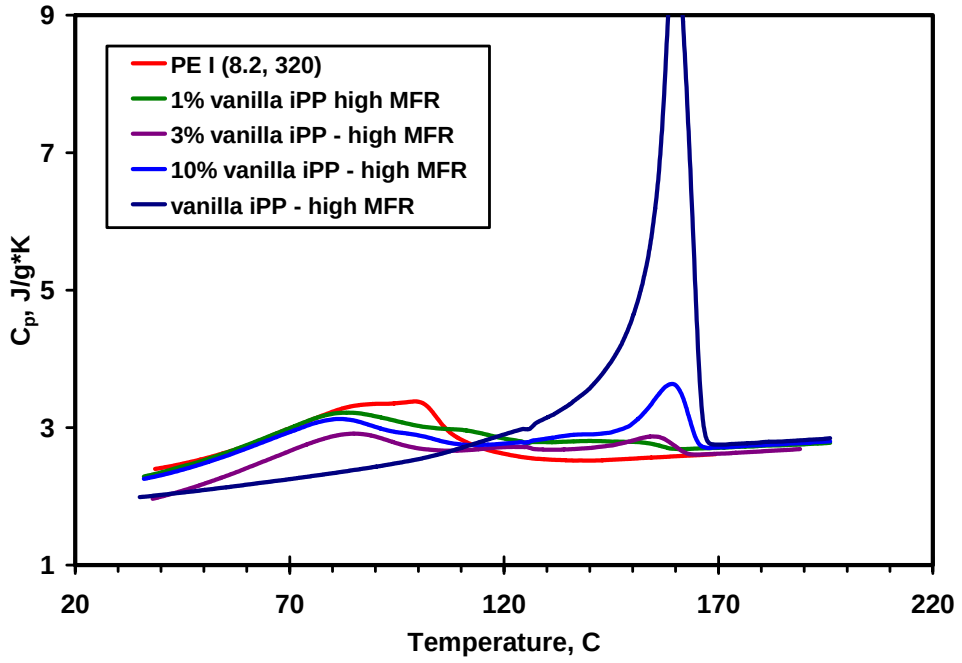
PE I (8.2, 320)
1% vanilla iPP high MFR
3% vanilla iPP - high MFR
10% vanilla iPP - high MFR
vanilla iPP - high MFR
Cp, J/g*K
Temperature, C
9
7
5
3
1
20
70
120
170
220

b)

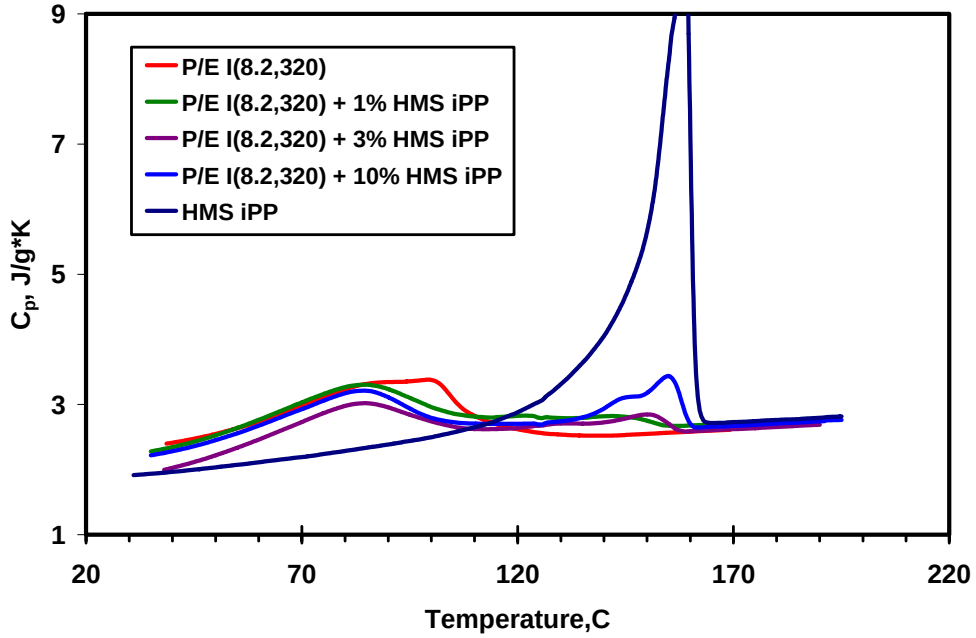

c)

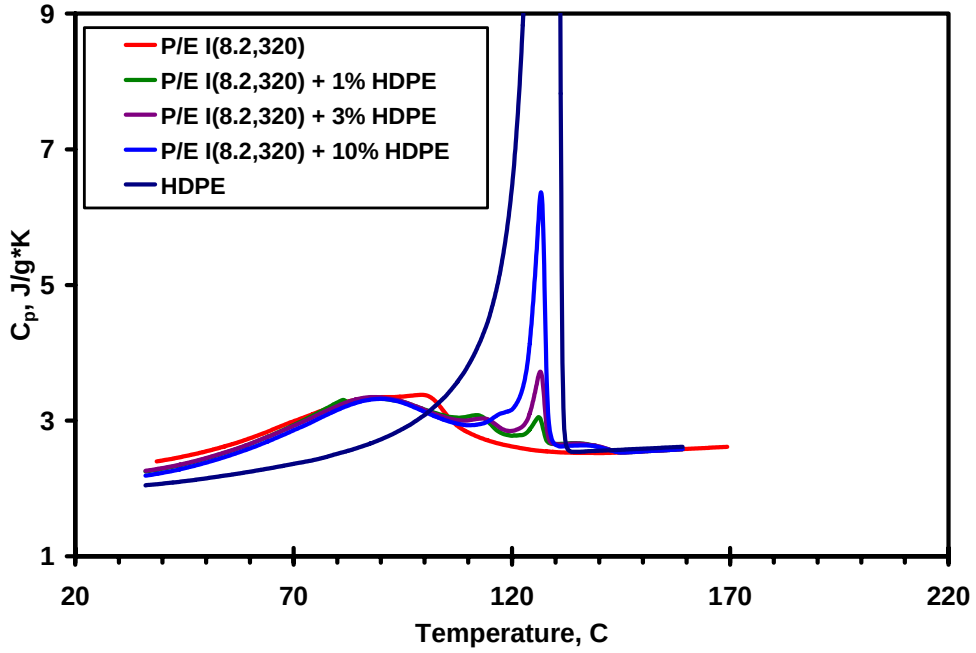

d)

Figure 7.1.3 Effect of the Nucleating Agent Content on Melting DSC Trace of P/E I (8.2, 320): a) vanilla iPP-low MFR, b) vanilla iPP-high MFR, c) commercial HMS iPP, d) HDPE

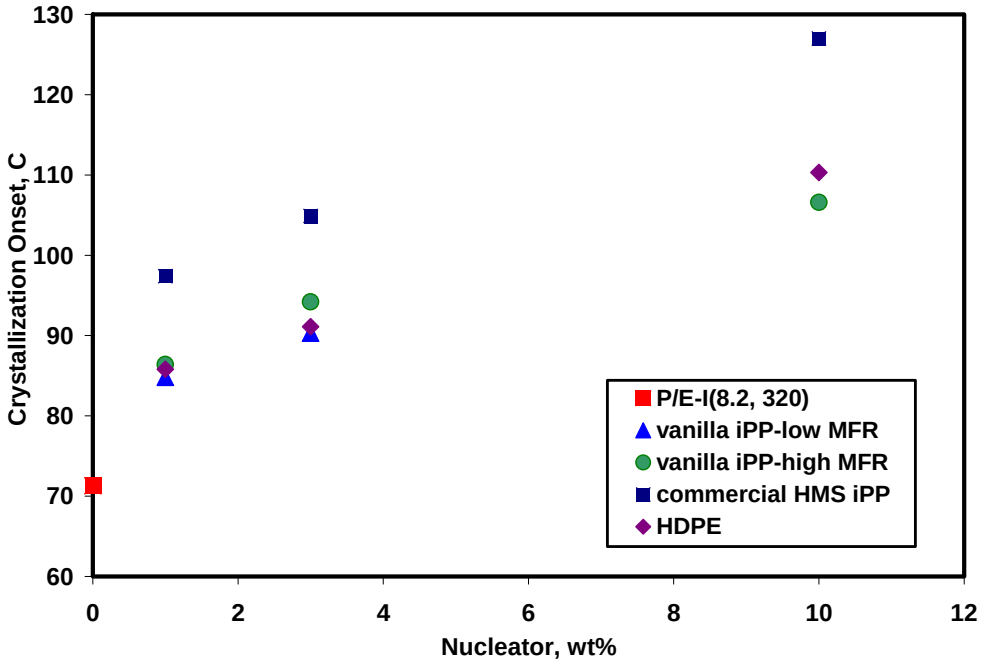

Figure 7.1.4 Effect of the Nucleator Type and Level on Crystallization Onset of P/E I (8.2, 320)

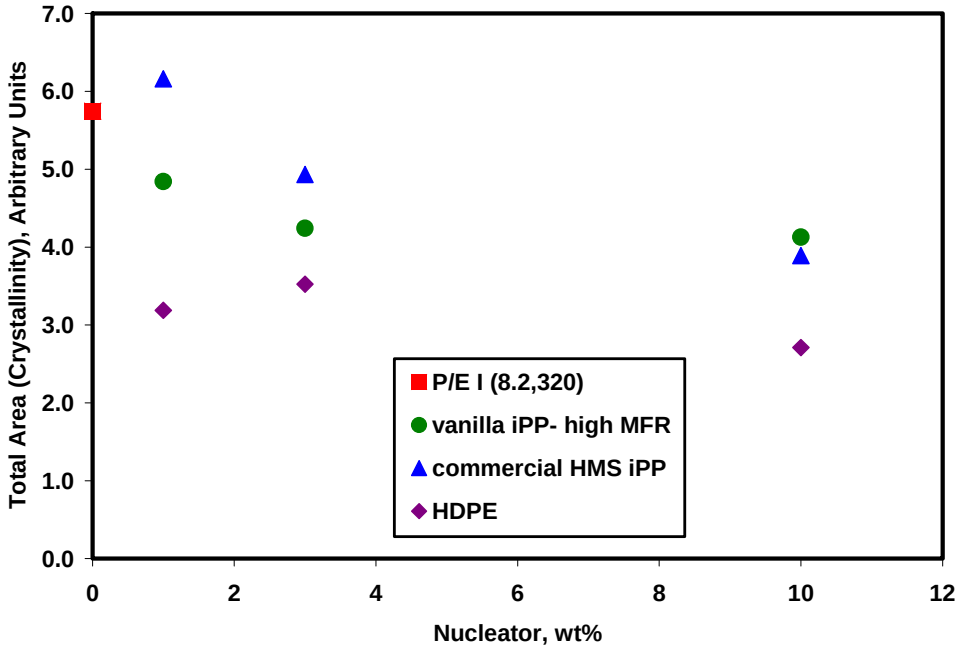

Figure 7.1.5 WAXD: Effect of the Nucleator Type and Level on Crystallinity of P/E I (8.2, 320)

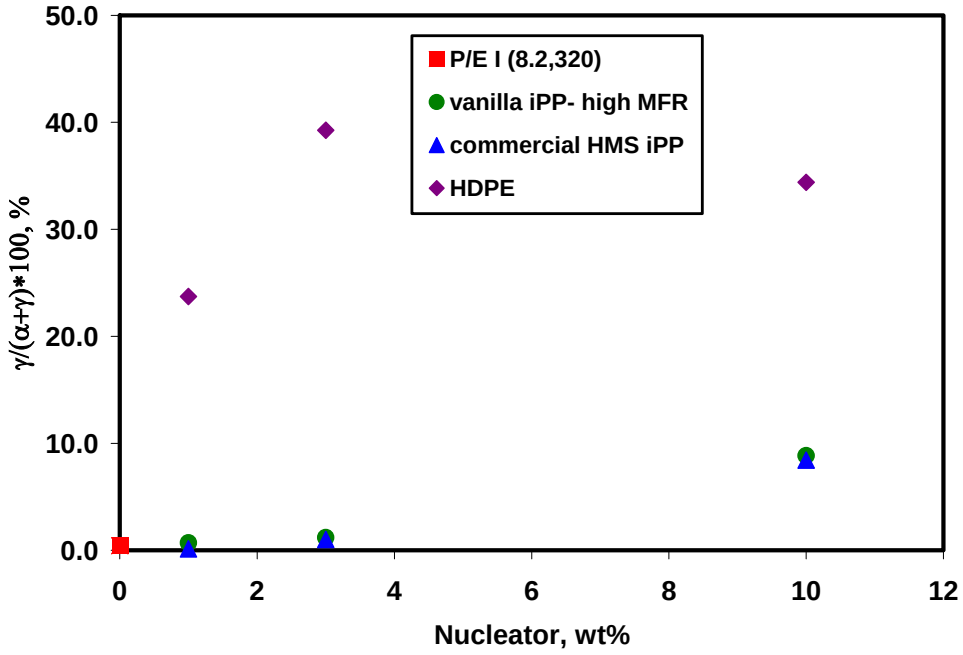

Figure 7.1.6 WAXD: Effect of the Nucleator Type and Level on γ-Phase content of P/E I (8.2, 320)

The addition of vanilla iPP-low MFR, vanilla iPP-high MFR and commercial HMS iPP to P/E-I(8.2, 320) leads to a decrease in the length and increase in the thickness of α-phase crystals, as demonstrated in Figure 7.1.7 and Figure 7.1.8. The addition of HDPE results in a two-phase morphology with HDPE and P/E-I(8.2, 320) present in different phases.

a)

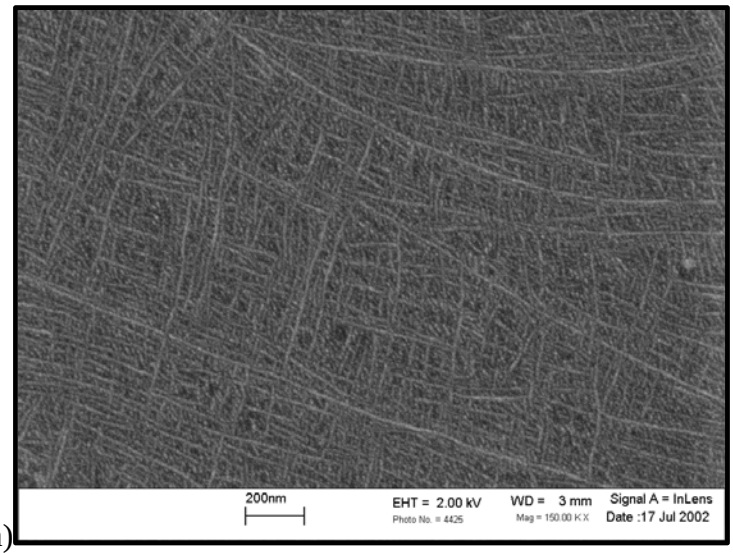

b)

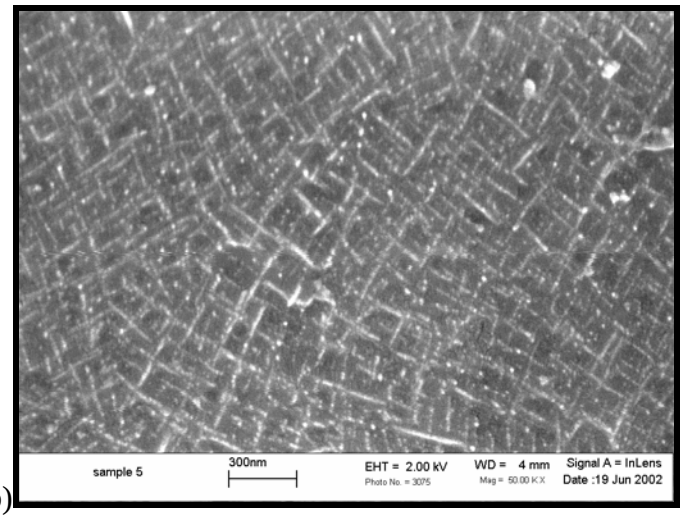

c)

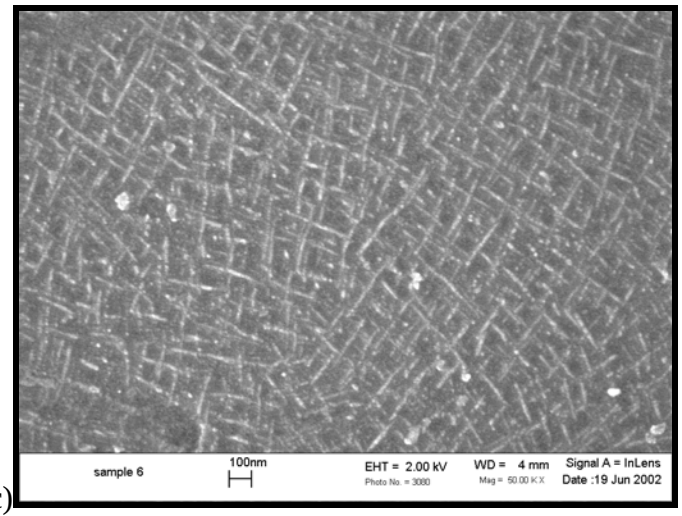

d)

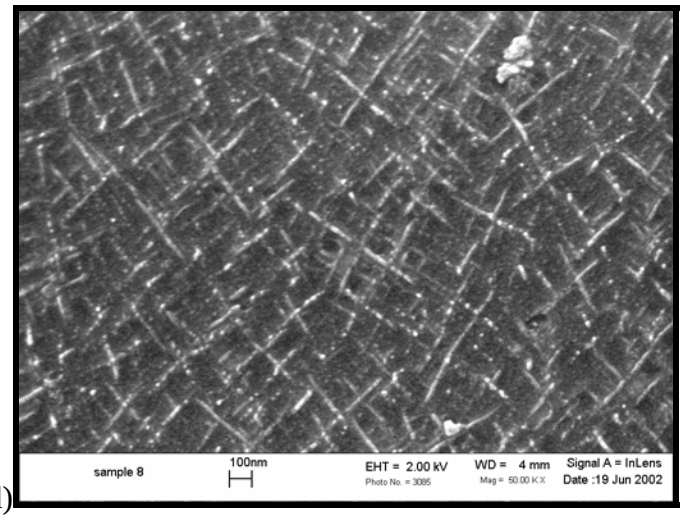

Figure 7.1.7 SEM: Effect of Nucleating Agent Type on Morphology of P/E-1(8.2,320) at 3wt% of Nucleator a) no nucleator, b) vanilla iPP-low MFR, c) vanilla iPP-high MFR, d) commercial HMS iPP

a)

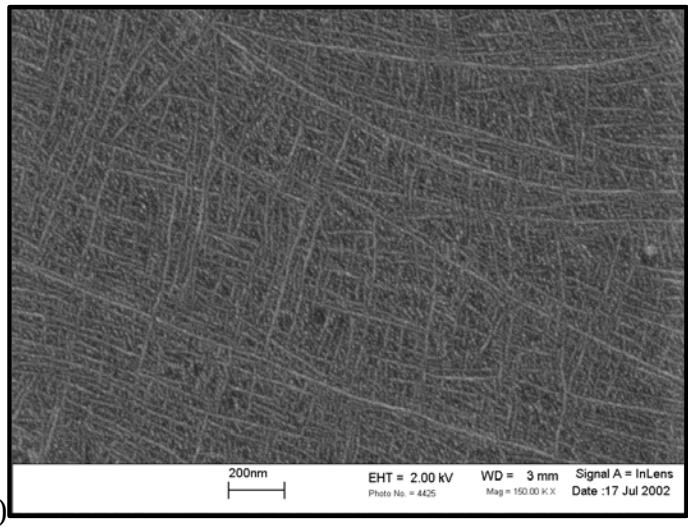

b)

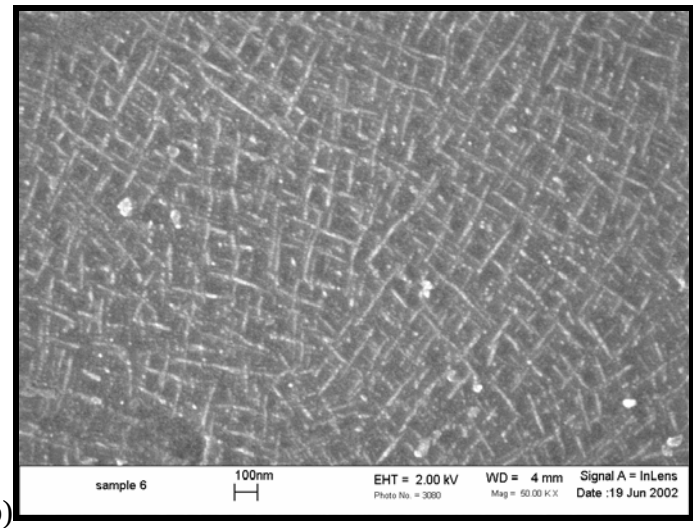

c)

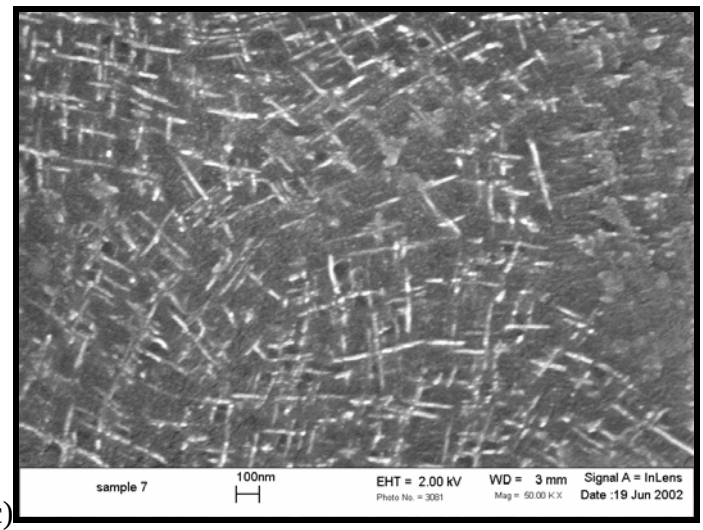

Figure 7.1.8 SEM: Effect of vanilla iPP-high MFR Level on Morphology of P/E-1(8.2,320) a) 0wt%, b) 3wt%, c) 10wt%

a)

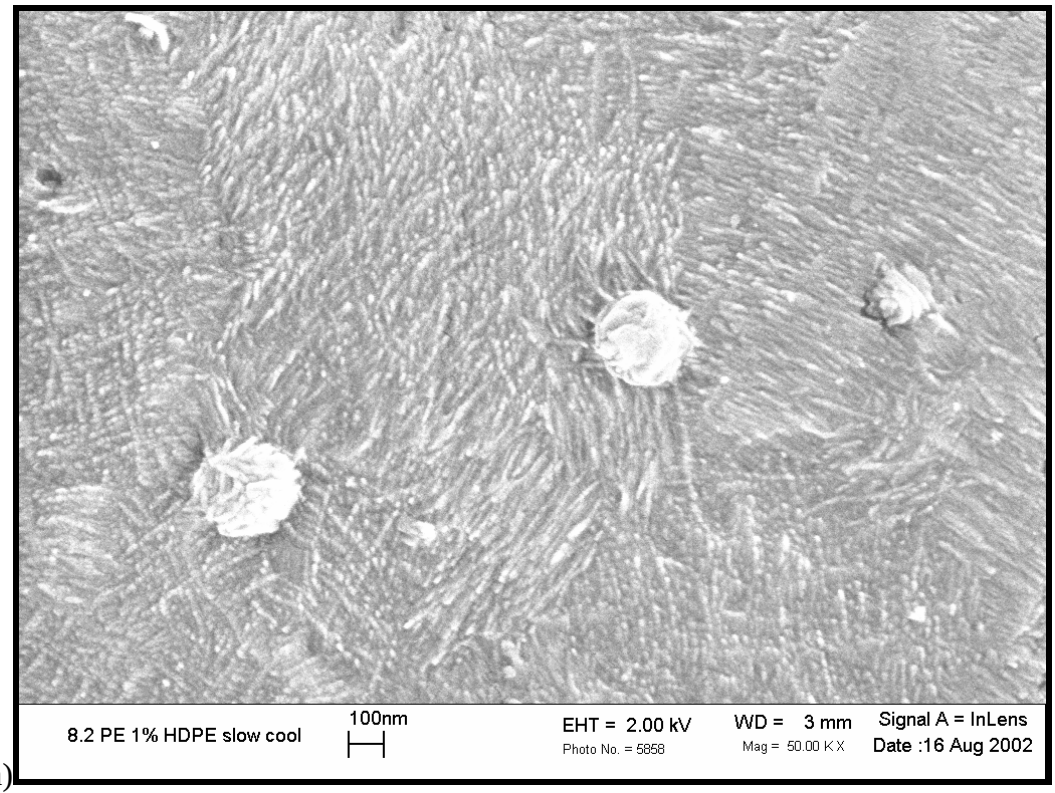

b)

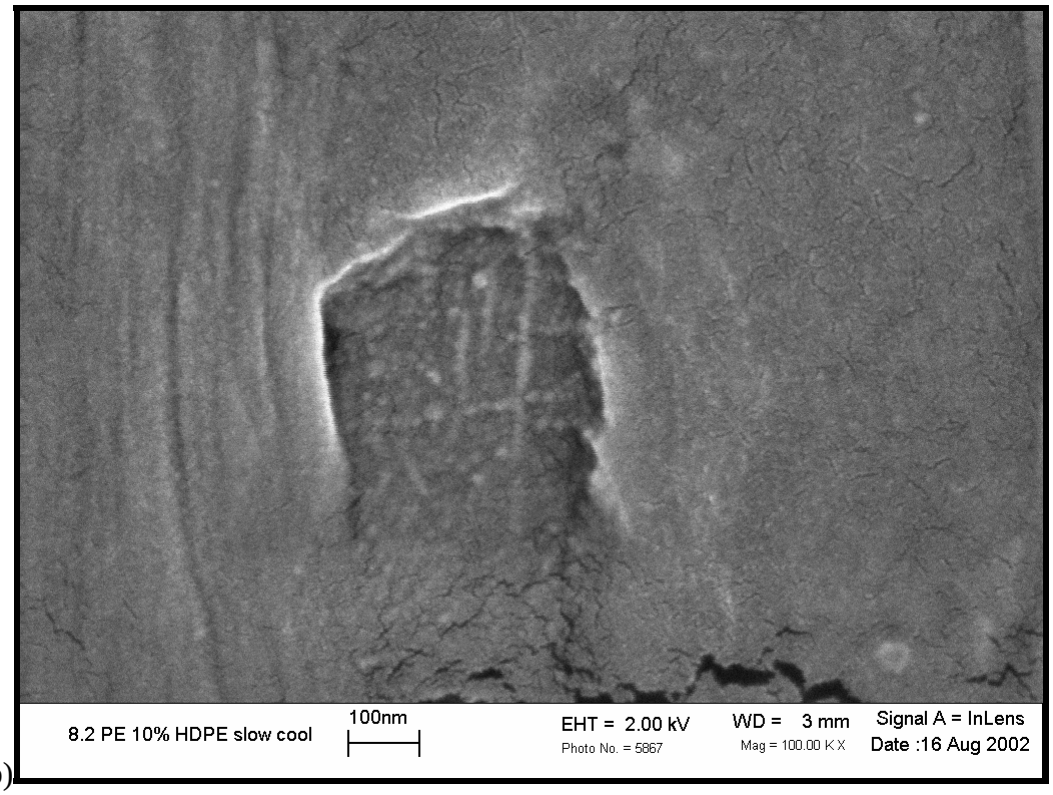

Figure 7.1.9 SEM Effect of HDPE Level on Morphology of P/E-1(8.2,320): a) 1wt%, b) 10wt %

7.2 Discussion

Commercially viable materials are required to have short processing times for the fabrication of a final product from pellets. In order to decrease the polymer solidification times, the addition of the nucleating agents is often utilized. These additives decrease the crystallization induction time by providing sites for the nuclei to form. As a result of an increase in nucleation rate, the average spherulite size usually decreases. The addition of nucleating agent also generally results in an increase in crystallization temperature.

In this study, the effect of four macromolecular nucleating agents on the properties of Dow P/E (8.2, 320) copolymer was studied. Three of these nucleating agents, vanilla iPP-low MFR, vanilla iPP-high MFR and commercial HMS iPP were miscible with the Dow propylene-ethylene copolymers. The fourth nucleating agent, HDPE, was immiscible with Dow P/E (8.2, 320) copolymer.

Since the nucleating agents crystallize at higher temperatures than does P/E (8.2, 320) copolymer, they can provide heterogeneous crystalline sites for the nucleation of the copolymer. Hence, the copolymer is able to crystallize at higher temperature, as shown in Figure 7.1.1 and Figure 7.1.2. This leads to the formation of thicker lamellae that melts at higher temperature. The nucleating efficiency increases with an increase in the temperature at which the nucleating agent crystallizes from the melt. The addition of nucleating agent also significantly broadens the melting endotherm. This result is extremely beneficial from the processing point of view, since it increases the ease and the flexibility of the final product fabrication. The addition of an immiscible nucleating agent leads to macrophase separation, as is evidenced by the double peaks in both crystallization and melting heat capacity traces.

The spherulites formed at higher temperature and at higher rate are expected to impinge earlier than they would have in the absence of the nucleating agent. Since P/E (8.2, 320) copolymer has a significant number of ethylene defects present in the chain and the crystallization is carried out at higher temperatures, the availability of long crystallizable polypropylene sequences free of the ethylene defects is limited. The result is then the preferential formation of γ-phase crystals as opposed to α-phase crystals. These argument is supported by the results of the WAXD analysis (Figure 7.1.6) showing

an increase in the γ-phase crystal content with content in nucleator. At the same time, a decrease is observed in the overall crystallinity of the copolymers as shown in Figure 7.1.5.

The crystallization mechanism of non-nucleated copolymers and copolymers modified by miscible nucleating agents, vanilla iPP-low MFR, vanilla iPP-high MFR and HMS iPP is similar, as evidenced by the SEM micrographs (Figure 7.1.7, Figure 7.1.8). All four materials exhibit cross-hatching morphology. With an increase in the concentration of nucleating agent, the length of α-phase crystals decreases while their thickness increases. This first effect is indicative of the formation of smaller radius spherulites resulting from the increased nucleation efficiency. The second effect is indicative of the presence of thicker lamellae formed as a result of crystallization at higher temperature.

In the case of nucleation by immiscible HDPE, the macrophase separation is evident for all concentrations of the nucleating agent (Figure 7.1.9). The copolymer with 1% HDPE contains drops of HDPE surrounded by cross-hatched regions of P/E (8.2, 320). As the concentration of HDPE increases, the HDPE migrates to the surface resulting in a hard skin-core around the propylene-ethylene copolymer.

8 SUMMARY AND CONCLUSIONS

The purpose of this work was to establish the property-structure relationships for novel Dow propylene-ethylene copolymers by studying the melting and crystallization behavior and morphology of these materials. It was also important to focus on the issue of ethylene inclusion into the polypropylene crystal and on the effect of inclusion on the thermodynamic heat of fusion at melting.

In Section 6.2.1, the dependence of crystallization, melting and glass transition temperatures and crystallinity on ethylene content for the propylene-ethylene copolymers was studied. A steady decrease in the peak crystallization and melting temperatures, the glass transition temperature and the crystallinity was observed with increasing ethylene content for all series of Dow copolymers. The melting offsets of Series I-III copolymers decreased with increasing ethylene concentration, while the melting offsets of Series VII and VIII showed only a weak dependence on ethylene content. These trends were explained by the effect of defect distribution on the length of isotactic polypropylene sequences. Series I-III of Dow copolymers were shown to have a more or less random defect distribution along the polypropylene chain, while Series VII and VIII exhibited blocky behavior with evidence of a high crystalline fraction.

The behavior of Dow propylene-ethylene copolymers was compared to that of the copolymers prepared with traditional metallocene and Ziegler-Natta catalysts. The catalyst system used in the polymerization of Dow copolymers was found to be close to the metallocene catalyst system. However, Dow copolymers were shown to have wider distribution of isotactic propylene sequence lengths because of the less random distribution of ethylene defects, especially in the case of series VII and VIII.

In the course of this work, the techniques of crystallinity determination were reevaluated. It was demonstrated that in order to properly evaluate the crystallinity of any semicrystalline polymer system, the precise knowledge of the behavior of crystalline and amorphous material is essential. In the case of a copolymer or a homopolymer with a substantial amount of regio and stereo defects incorporated into the chain, it is also important to correctly establish the degree of inclusion of defects into the resulting

crystal. The last point stems from the fact that, as was demonstrated by this work, if the defects are in fact incorporated into the crystal, the thermodynamic heat of fusion at melting decreases. If an overestimated heat of fusion is used in the crystallinity calculations, the resulting values of the calculated crystallinity are significantly underestimated. Since crystallinity is routinely used in material property prediction models, underestimated crystallinities can result in significant discrepancies between the models and the actual systems whose behavior they are meant to predict.

In Section 6.2.2, the linear decrease in the thermodynamic heat of fusion with increase in ethylene defect concentration was clearly demonstrated. On the basis of both the DSC work and the density measurements, it was shown that the use of an inclusion model based on the Sanchez-Eby crystallization theory is a valid approach for evaluating the crystallinities of the given propylene-ethylene system. At the same time, inadequacies in the application of the rigid amorphous fraction model to copolymers with included defects were demonstrated.

In Section 6.2.3, the dependence of the Dow copolymer morphology on the ethylene concentration was demonstrated. It was shown that due to the shortening of isotactic polypropylene sequences as a result of addition of ethylene units, the amount of α-phase crystals decreases while the amount of γ-phase crystals increases. Since γ-phase crystals form thinner lamellae, the melting temperature of γ-phase crystals was lower then that of the α-phase crystals. It was shown that both phases develop simultaneously. It was also shown that the formation of the γ-phase crystals is favored by low crystallization rates, corresponding to the crystallization at higher temperatures.

The cross-hatching morphology was present in all Dow propylene-ethylene copolymers. With an increase in ethylene concentration and a corresponding decrease in the isotactic propylene sequence lengths, the density, length and thickness of α-phase crystals were found to decrease. These results confirmed the conclusions reached earlier that an increase in ethylene concentration leads to more favorable conditions for the formation of the γ-phase crystals.

Finally, the effect of modification of P/E-I (8.2, 320) copolymer by four different nucleating agents, vanilla iPP – low MFR, vanilla iPP – high MFR, commercial HMS iPP and HDPE, was studied. It was shown that all four nucleating agents amplified the

nucleating efficiency of the Dow copolymer. The nucleation efficiency increased with an increase in the temperature at which the nucleating agent crystallized from the melt. Vanilla iPP - low MFR, vanilla iPP – high MFR, commercial HMS iPP were miscible with P/E-I (8.2, 320) copolymer system. HDPE was immiscible with P/E-I (8.2, 320). The addition of the HDPE resulted in a two-phase system for which, the nucleating agent was found to migrate to the surface when present in large concentration, resulting in a skin-core morphology.

9 FUTURE WORK

9.1 On the Crystallinity and Thermodynamic Heat of Fusion Calculations

This work demonstrated the necessity of a precise knowledge of the behavior of crystalline and amorphous phases for crystallinity determinations in semicrystalline copolymers using either the DSC or the density methods. Since many of the properties were unavailable for the calculations, the demonstrated trends showed a significant uncertainty. The accuracy of the crystallinity calculations would be greatly improved if some of the assumptions used in the calculations could removed.

It was assumed, based on the work of Alamo et al.[50], that 42% of the available ethylene units are included in the propylene crystal. This partitioning coefficient might not be representative of the Dow copolymer system. The inclusion of the ethylene into the propylene crystal partly depends on the amount of other defects present in the chain. Alamo's work did not address the issue of the partitioning coefficient of the propylene-ethylene copolymers in the presence of regio and stereo defects nor did it consider the inclusion of ethylene at the concentrations higher than 7.5 ethylene mol %. The knowledge of the exact partitioning of the ethylene and other defects between the crystal and the amorphous phase of the Dow copolymers would improve the accuracy in the crystallinities obtained from both, the density and the DSC measurements.

The same problem existed in determining the crystal and amorphous densities of these copolymers. The unit cell volumes used in the calculations were based in one case on the value of the unit cell dimensions for polypropylene with regio errors and in the second case, on the unit cell dimensions for propylene-ethylene copolymers having up to 11 ethylene mol% with different regio and stereo defect contents than the materials studied in this work. The exact knowledge of the unit cell volumes would greatly benefit the presented crystallinity calculations.

In this work, the WAXD measurements of the crystallinity development as a material is crystallized at the rate of 10°C/min were not performed. This kind of data

would complement the crystallinity development curves obtained by the DSC measurements.

While the determination of exact heat capacities for the amorphous and the crystalline materials prior to the study of each new copolymer system might not be practical, steps can be taken to improve the accuracy of the match between theoretical and experimental heat capacities in the melt and in the glass regions. If multiple heat capacity curves for each copolymer were available, their averaging could eliminate some of the errors due to the DSC instrument behavior variation from run to run.

Finally, the study of the effect of the comonomer inclusion on the thermodynamic heat of fusion of different copolymer systems would be beneficial. It would help to reinforce the concepts developed in this study.

9.2 On the Morphology

The isothermal crystallization studies performed as a part of this work, did not resolve the question of the relative rates of the formation of α- and γ-phase crystals. A more involved studies where a better deconvolution of the low and high melting endotherms were performed and the large number of the data points at short crystallization times, corresponding to primary crystallization, would help to resolve this issue.

It has been demonstrated by the results of the isothermal crystallization studies that α and γ-phases develop simultaneously. These results can be further confirmed by performing the WAXD experiments at the experimental conditions resembling those used in the DSC work. Since the positions of the peaks corresponding to α- and γ-phases are known, the exact time of the formation of each phase can be accurately determined form this kind of WAXD data.

10 REFERENCES

[1] Mangonon P.L., *The Principles of Materials Selection for Engineering Design*, Prentice-Hall, Inc., 1999, ch.15

[2] Callister W.D., *Materials Science and Engineering, an Introduction*, John Willey & Sons, Inc., 3rd ed., 1994, ch.16

[3] G.Odian, *Principles of Polymerization*, 3rded., John Wiley & Sons Inc., New York, 1991, ch.8

[4] Rempp P., Merill E.W., *Polymer Synthesis*, 2nded., John Wiley & Sons Inc., 1991, ch.8

[5] Swogger K., Poon B.C., Stephens C.H., Ansems P., Chum S., Hiltner A., Baer E., *Annual Conference – Society of Plastics Engineers*, **2003**, *61*, 1768-1774

[6] Young R.J., *Introduction to Polymers*, Chapman and Hall, Ltd., 1989, ch.2

[7] Sperling L.H., *Introduction to Physical Polymer Science*, 2nded., John Wiley & Sons Inc., New York, 1992, ch.2, pp. 23-64

[8] Sanders J.M., Komorski R.A., *Macromolecules*, **1977**, *10*, 1214-704

[9] Janimak J., Cheng S., Giusti P., Hsieh E., *Macromolecules*, **1991**, *24*, 2253-2260

[10] Keith H., Padden F., *J. Appl. Phys.*, **1963**, *34*, 2409-2421

[11] Hoffman J., Davis G., Lauritzen J., *Treatise on Solid State Chemistry*, Vol 3, *Crystalline and Noncrystalline Solids*, Hannay N., Ed. Plenum Press, New York., 1976, ch.7

[12] Keller A., Goldbeck-Wood G., *Comprehensive Polymer Science*, 2nd Supplement, Aggarual R., Ed. Elsevier, Oxford, 1996, ch.7

[13] Keith H., Padden F., Vadimsky R., *J. Appl. Phys.*, **1971**, *42*, 4585-4592

[14] Keith H., *J. Polym. Sci. A*, **1964**, *42*, 4339-4360

[15] Sperling L.H., *Introduction to Physical Polymer Science*, 2nded., John Wiley & Sons Inc., New York, 1992, ch.6, pp. 198-278

[16] Khoury F., Passaglia E., *Treatise on Solid State Chemistry*, Vol 3, *Crystalline and Noncrystalline Solids*, Hannay N., Ed. Plenum Press, New York, 1976, ch.6

[17] Keith H., *The Physics and Chemistry of the Organic Solid State*, Interscience Publishers, Inc., New York 1963

[18] Alizadeh A., Sohn S., Quinn J., Marand H., Shank L., Iler H., *Macromolecules*, **2001**, *34*, 4066-4078

[19] Sanchez I., Colson J., Eby R., *J. Appl. Phys.*, 1973, *44*, 4332-4339

[20] Marand H., Alizadeh A., Farmer R., Desai R., Velikov V., *Macromolecules*, **2000**, *33*, 3392-3403

[21] Sadler D., *Polymer*, **1983**, *24*, 1401-1409

[22] Sadler D., Gilmer G., *Polymer*, **1984**, *25*, 1446-1452

[23] Lauritzen J., Hoffman J., *J. Appl. Phys.*, **1973**, *44*, 4340-4352

[24] Clark E.J., Hoffman., *Macromolecules*, **1984**, *17*, 878-885

[25] Hoffman J., Miller R., *Polymer*, **1997**, *38* , 3151-3212

[26] Armstead J., Hoffman J., *Macromolecules*, **2002**, *35*, 3895-3913

[27] Bates F., Fredrickson G., *Physics Today*, **1999**,*52*, 32-38

[28] Evans R., Mighton H., Flory P., *J. Am. Chem. Soc.*,, **1950**, *72*, 2018-2528
[29] Flory P., Mandelkern L., Hall H., *J. Am. Chem. Soc.*, **1951**, *73*, 2532-2538
[30] Flory P., *Trans. Faraday Soc.*, **1955**, *51*, 848-857
[31] Lauritzen J., DiMarzio E., Passaglia E., *J. Chem. Phys.*, **1966**, *45*, 4444-4454
[32] Helfand E., Lauritzen J., *Macromolecules*, **1973**, *6*, 631-638
[33] Colson J., Eby R., *J. Appl. Phys.*, **1966**, *37*, 3511-3514
[34] Sanchez I., Eby R., *J. Res. Nat. Bur. Stand., Part A- Phys. Chem.*, **1973**, *77a*, 353-358
[35] Sanchez I., Eby R., *Macromolecules*, **1975**, *8*, 638-641
[36] Fischer E., Sterzel H., Wegner G ., Kolloid Z. Z. Polym., **1973**, *251*, 980-990
[37] Zimmermann H.J., *J. Macromol. Sci., Phys.*, **1993**, *B32*, 141-161
[38] Bruckner S., Phillips P., Mezghani K., Meille S.V., *Makromol. Chem.: Rapid Commun.*, **1997**, *18*, 1-7
[39] Feng Y., Hay J.N., *Polymer*, **1998**,*39*, 6589-6596
[40] Feng Y., Hay J.N., *Polymer*, **1998**, *39*, 6723-6731
[41] Laihonen S., Gedde U.W., Werner P.-E., Martinez-Salazar J., *Polymer*, **1997**, *38*, 361-369
[42] Laihonen S., Gedde U.W., Werner P.-E., Westdahl M., Jaaskelainen P., Martinez-Salazar J., *Polymer*, **1997**, *38*, 371-377
[43] De Rosa C., Auriemma F., Vinti V., Grassi A., Galimberti M., *Polymer*, **1998**, *39*, 6219-6226()
[44] De Rosa C., Auriemma F., Talarico G., Busico V., Caporaso L., Capitani D., *Macromolecules*, **2002**, *35*, 1314- 1318
[45] Auriemma F., De Rosa C., *Macromolecules*, **2002**, *35*, 9057-9068
[46] De Rosa C., Auriemma F., Fanelli E., Talarico G., Capitani D., *Macromolecules*, **2003**, *36*, 1850-1864
[47] Starkweather, Van-Catledge F., MacDonald R., *Macromolecules*, **1982**, *15*, 1600-1604
[48] Busico V., Corradini P., De Rosa C., Di Benedetto E., *Eur. Polym. J.*, **1985**, *21*, 239-244
[49] Hosier I.L, Alamo R.G., Lin J.S.., *Polymer*, **2004**, *45*, 3441-3455
[50] Alamo R.G., VanderHart D.L., Nyden M.R., Mandelkern L., *Macromolecules*, **2000**, *33*, 6094-6105
[51] Turner-Jones A., *Polymer*, **1971**, *12*, 487-508
[52] Kim M.-H., Alamo R.G., Lin J.S., *Polym. Eng. Sci.*, **1999**, *39*, 2117-2131
[53] Avella M., Martuscelli E., Della Volpe G., Segre A., Rossi E., Simonazzi T., *Makromol. Chem.*, **1986**, *187*, 1927-1943
[54] De Rosa C., Auriemma F., Capitani D., Caporaso L., Talarico G., *Polymer*, **2000**, *41*, 2141-2148
[55] De Rosa C., Talarico G., Caporaso L., Auriemma F., Galmberti M., Fusco O., *Macromolecules*, **1998**, *31*, 9109-9115
[56] Lotz B., *Eur. Polym. J. E*, **2000**, *3*, 185-194
[57] Bruckner S., Meille S.V., Petraccone V., Pirozzi B., *Prog. Polym. Sci.*, **1991**, *16*, 361-404
[58] Bruckner S., Meille S.V., Sozzani P., Torri G., *Makromol. Chem.: Rapid Commun.*, **1990**, *11*, 55-60

[59] Meille S.V., Ferro D.R., Bruckner S., Lovinger A.J., Padden F.J., *Macromolecules,* **1994**, *27*, 2615-2622
[60] Ferro D.R., Meille S.V., Bruckner S., *Macromolecules,* **1998**, *31*, 6926-6934
[61] Meille S.V., Ferro D.R., Bruckner S., *Macromol. Symp.,* **1995**, *89*, 499-511
[62] Turner-Jones A., Cobbold A.J., *J. Polym. Sci.. Part B, Polym. Letters,* **1968**, *6*, 539-546
[63] Marigo A., Marega C., Zanetii R., Fichera A., Ferrari P., *Macromol. Chem. Phys.*, **1995**, *196*, 3577-3584
[64] Lotz B., Wittmann J.C., Lovinger A.J., *Polymer,* **1996**, *37*, 4979-4992
[65] Lotz B., Wittmann J.C., *J. Polym. Sci.: Part B: Polym. Phys.*, **1986**, *24*, 1541-1558
[66] Auriemma F., de Ballesteros O.R., De Rosa C., Corradini P., *Macromolecules,* **2000**, *33*, 8764-8774
[67] De Rosa C., Guerra G., Napolitano R., Petraccone V., Pirozzi B., *Eur. Polym. J.*, **1984**, *20*, 937-941
[68] Bruckner S., Meille S.V., *Nature,* **1989**, *340*, 455-457
[69] Meille S.V., Bruckner S., Porzio W., *Macromolecules*, **1990**, *23*, 4114-4121
[70] Turner-Jones A., Aizlewood J.M., Beckett D.R., *Makromol. Chem.*, **1964**, *75*, 134-158
[71] Marigo A., Marega C., Zanetii R., Paganetto G., Canossa E., Coletta F., Gottardi F., *Makromol. Chem.*, **1989**, *190*, 2805-2813
[72] Meille S.V., Phillips P., Mezghani K., Bruckner S., *Macromolecules,* **1996**, *29*, 795-797
[73] Campbell R.A., Phillips P., Lin J.S., *Polymer,* **1993**, *34*, 4809-4816
[74] Pae K., Morrow D., Sauer J., *Nature,* **1966**, *211*, 514-515
[75] Mezghani K., Phillips P., *Polymer*, **1997**, *38*, 5725-5733
[76] Mezghani K., Phillips P., *Polymer,* **1998**, *39*, 3735-3744
[77] Mezghani K., Phillips P., *Polymer*, **1995**, *36*, 2407-2411
[78] Guidetti G.P., Busi P., Giulianelli I., Zanetti R., *Eur. Polym. J. E,* **1983**, *19*, 757-759
[79] Marigo A., Marega C., Zanetii R., Paganetto G., Schmidt S., Zachmann H.G., *Makromol. Chem.*, **1990**, *191*, 1967-1971
[80] Auriemma F., De Rosa C., Boscato T., Corradini P., *Macromolecules*, **2001**, *34*, 4815-4826
[81] Meille S.V., Ferro D.R., Bruckner S., *Macromol. Symp.,* **1995**, *89*, 499-511
[82] Alamo R.G., Kim M.-H., Galante M.J., Isasi J.R., Mandelkern L., *Macromolecules,* **1999**, *32*, 4050-4064
[83] Yamada K., Matsumoto S., Tagashira K., Hikosaka M., *Polymer*, **1998**, *22*, 5327-5333
[84] Burfield D.R., Doi Y., *Macromolecules*, **1983**, *16*, 702-704
[85] VanderHart D.L., Alamo R.G., Nyden M.R., Kim M.-H., Mandelkern L., *Macromolecules*, **2000**, *33*, 6078-6093
[86] Nyden M.R., Vandehart D.L., Alamo R.G., *Computational and Theoretical Polymer Science*, **2001**, *11*, 175-189
[87] Sperling L.H., *Introduction to Physical Polymer Science*, 2nd ed., John Wiley & Sons Inc., New York, 1992, ch.8
[88] Mandelkern L., *Physical Properties of Polymers.*, Ch 4, *The Crystalline State,* 2nd ed., ACS., Washington DC, **1993**
[89] Wunderlich B., *Prog. Polym. Sci.*, **2003**, *28*, 383-450

[90] Pak J., Pyda M., Wunderlich B., *Macromolecules*, **2003**, *36*, 495-499
[91] Grebowicz J., Lau S.-F., Wunderlich B., *J. Polym. Sci: Polym. Symp*, **1984**, *71*, 19-37
[92] Cheng S., Cao M.-Y., Wunderlich B., *Macromolecules*, **1986**, *19*, 1868-1876
[93] Suzuki H., Grebowicz J., Wunderlich B., *Br. Polym. J.*, **1985**, *17*, 1-3
[94] Suzuki H., Grebowicz J., Wunderlich B., *Makromol. Chem.*, **1985**, *186*, 1109-1119
[95] Huo P., Cebe P., *J. Polym. Sci: Part B: Polym. Phys. ed*, **1992**, *30*, 239-250
[96] Mandelkern L., *J. Phys. Chem.*, **1971**, *75*, 3909-3920
[97] Gaur U., Wunderlich B., *Macromolecules*, **1980**, *13*, 445-446
[98] Kunz M., Moller M., Heinrich U.-R., Cantow H.-J, *Makromol. Chem., Macromol. Symp*, **1988**, *20/21*, 147-158
[99] Kunz M., Moller M., Heinrich U.-R., Cantow H.-J, *Makromol. Chem., Macromol. Symp*, **1989**, *23*, 57-72
[100] Menczel J., Wunderlich B., *J. Polym. Sci: Polym. Letters Ed.*, **1981**, *19*, 261-264
[101] Huo P., Cebe P., *Colloid Polym. Sci.*, **1992**, *270*, 840-852
[102] Fischer E., Fakirov S., *J. Mat. Sci.*, **1976**, *11*, 1041-1065
[103] Bornschhlegl E., Bonart R., *Colloid Polym. Sci.*, **1980**, *258*, 319-331
[104] Wunderlich B., *Macromolecular Physics*, Ch.5, Vol 2. *Crystal Nucleation, Growth, Annealing*, Academic Press, New York, 1976
[105] Feng Y., Jin X., *J. Appl. Polym. Sci.*, **1998**, *72*, 1559-1564
[106] Basset D., *Principles of Polymer Morphology*, Ch.2, Cambridge University Press, Cambridge, 1981
[107] Gahleitner M., Wolfschwenger J., Bachner C., Bernreitner K., Neibl W., *J. Appl. Polym. Sci.*, **1996**, *61*, 649-657
[108] Wittmann J., Lotz B., *Polym. Sci.: Part B: Polym. Phys.*, **1981**, *19*, 1837-1851
[109] Wittmann J., Hodge A., Lotz B., *Polym. Sci.: Part B: Polym. Phys.*, **1983**, *21*, 2495-2509
[110] Khanna Y., *Macromolecules*, **1993**, *26*, 3639-3643
[111] Smith L., Masilamani D., Bui L., Khanna Y., Bray R., Hammond W., Curran S., Belles Jr. J., Binder-Castelli S., *Macromolecules*, **1994**, *27*, 3147-3155
[112] Carroll C., *Modern Plastics*, **1984**, *61*, 108-112
[113] Sterzynski T., Lambla M., Crozier H., *Adv. Polym, Technol.* **1994**, *13*, 25-36
[114] Kristiansen M., Werner M., Tervoort T., Smith P., Blomenhofer M., Schmidt H.-W., *Macromolecules*, **2003**, *36*, 5150-5156
[115] Martin C., Vaughan A., Sutton S., Swingler S., *J. Polym. Sci.: Part B: Polym. Phys.*, **2002**, *40*, 2178-2189
[116] Thierry A., Straupe C., Lotz B., Wittmann J., *Progr. Colloid Polym. Sci.*, **1992**, *87*, 28-31
[117] Mathot V., *Calorimetry and Thermal Analysis of Polymers*, ch.5, *Thermal Characterization of States of Matter*, Mathot V., Ed., Hanser Publishers, New York, 1994
[118] Dai P.S., Cebe P., Capel M., Alamo R.G., Mandelkern L., *J. Appl. Cryst.*, **2000**, *33*, 714-717
[119] Ditmars D., Ishihara S., Chang S., Bernstein G., West E., *J. Res. Nat. Bur. Stand.*, **1982**, *2*, 159-163

[120] Wunderlich B., *ATHAS – Table of Thermal Properties*, University of Tennessee, Knoxville, **2003**
[121] Private communication with Dr. Marek Pyda, ATHAS and Polymer Characterization Laboratory Director, University of Tennessee
[122] Isasi J.R., Mandelkern L., Galante M.J., Alamo R.G., *J. Polym. Sci.: Part B: Polym. Phys.*, **1999**, *37*, 323-334
[123] Isasi J.R., Alamo R.G., Mandelkern L., *J. Polym. Sci.: Part B: Polym. Phys.*, **1997**, *35*, 2511-2521
[124] De Rosa C., Auriemma F., Circelli T., Waymouth R., *Macromolecules,* **2002**, *35*, 3622-3629
[125]Ojeda T., Liberman S., Amorim R., *J. Polym. Eng.*, **1996/1997**, *16*, 105-120
[126] A. Kumar, M.S. Thesis, Virginia Polytechnic Institute and State University, 2001
[127] Private communication from Dow Chemical
[128] Gan S, Burfield D.R., *Macromolecules*, **1985**, *18*, 2684-2688
[129] Zhang F., Gong Y., He T., *Eur. Polym. J.*, **2003**, *39*, 2315-2322
[130] Nozaki K., Endo Y., Yamamoto T., Naiki M., *J. Macromolecular Sci.: Part B – Phys.*, **2003**, *B42*, 697-707
[131] De Rosa C., Auriemma F., Spera C., Talarico G., Tarallo O., *Macromolecules*, **2004**, *37*, 1441-1454
[132] Gaur U., Wunderlich B., *J. Phys. Chem. Ref. Data*, **1981**, *10*, 1051-1064
[133] Ferro D.R., Bruckner S., Meille S.V., Ragazzi M., *Macromolecules,* **1992,** *25*, 5231-5235
[134] Marand, H; Huang, Z., *Macromolecules*, **2004**, *37*, 6492-6497

APPENDIX 1

The algorithm of crystallinity calculations using the measured heat capacity (Cp_{app}), theoretical amorphous (Cp_l) and crystalline (Cp_c) heat capacities and the thermodynamic heat of fusion $\Delta H_f(T)$.

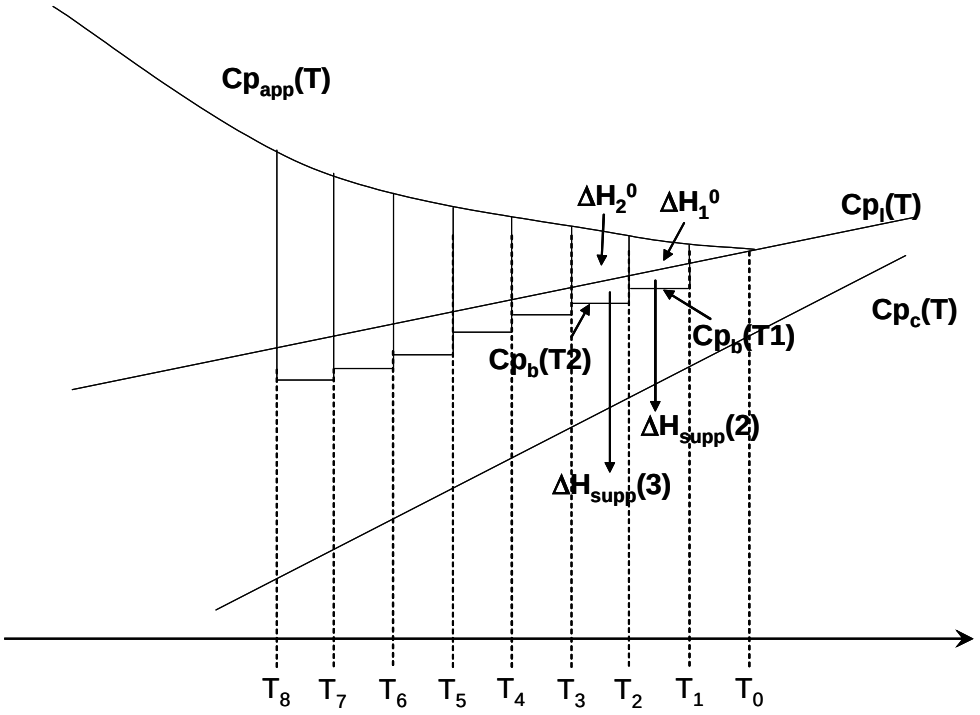

1)

$\Delta H^0(1)$ = area between Cp^b and Cp in the temperature range of $T_0 - T_1$

$\Delta C_{pb}(1)$ - change in the baseline heat capacity due to crystallization between $T_0 - T_1$

$\Delta C_{pb}(1) < 0$

$$\Delta C_{pb}(1) = C^1{}_{pb}(T_1) - C^0{}_{pb}(T_1)$$

$$C^1{}_{pb}(T_1) = C_p{}^{app}(T_1)$$

$$C^0{}_{pb}(T_1) = C_p{}^{L}(T_1)$$

$$\Delta C_{pb}(1) = \frac{\Delta H^0(1)}{\Delta H_f(T_1)} \cdot (C_p{}^{c}(T_1) - C_p{}^{L}(T_1))$$

$$\Delta H(1) = \Delta H^0(1)$$

$$X_C(1) = \frac{\Delta H^0(1)}{\Delta H_f(T_1)} \Delta H(1) = \Delta H^0(1)$$ total crystallinity at T_1

2)

$\Delta H(2) = \Delta H(1) + \Delta H^0(2) + \Delta H_{\sup p}(2)$ - total heat at crystallization at T_2

$$\Delta H_{\sup p}(2) = \Delta C_{pb}(1) \cdot (T_2 - T_1)$$

$$H_C(2) = X_c(1) + \frac{\Delta H(2) - \Delta H(1)}{\Delta H_f(T_2)}$$

$\Delta C_{pb}(2) =$ change in heat capacity from baseline (liquid C_p^L) to $C_p^{sc}(T_2)$ due to crystallization between T_0 and T_2

$$\Delta C_{pb}(2) = H_c(2) \cdot (C_p{}^c(T_2) - C_p{}^L(T_1))$$

3)

$$\Delta H(3) = \Delta H(2) + \Delta H^0(3) + \Delta H_{\sup p}(3)$$

$$\Delta H_{\sup p}(3) = \Delta C_{pb}(2) \cdot (T_3 - T_2)$$

$$H_C(3) = X_c(2) + \frac{\Delta H(3) - \Delta H(2)}{\Delta H_f(T_3)}$$

$$\Delta C_{pb}(3) = H_c(3) \cdot (C_p{}^c(T_3) - C_p{}^L(T_3))$$

VITA

Julie Uan-Zo-li, daughter of Tamara Golovach and Mikhail Dvorkin, was born on March 19, 1973 in Minsk, Belarus. She attended the city school of Minsk from 1980 to 1990 and the nursing school from 1990 to 1991. In December of 1991, Julie immigrated to the United States. In 1993 she graduated from Eagan High School in Eagan, MN after attending University of St. Thomas in St. Paul, MN as a part of the post-secondary program. In June of 1996, she graduated with a Bachelor of Science degree in Chemical Engineering from the University of Minnesota. While at the University of Minnesota Julie worked as a technical aide at 3M Science Research Laboratory. In December of 2001 Ms. Uan-Zo-li received a masters degree in Materials Science and Engineering from the Virginia Polytechnic Institute and State University. In January 2002, she joined Dr. Marand's research group at VPI & SU.